UNIVERSIDADE
BEIRA INTERIOR

CFD ANALYSIS OF THE COMBUSTION OF NATURAL GAS AND BIOGAS IN A CAN TYPE COMBUSTOR

João Miguel Cara Linda Charuto

Dissertação para obtenção do Grau de Mestre em
Engenharia Aeronáutica
(Mestrado Integrado)

Orientador: Prof. Doutor Francisco Miguel Ribeiro Proença Brójo

Janeiro 2025

Declaração de Integridade

Eu, João Miguel Cara Linda Charuto, que abaixo assino, estudante com o número de inscrição a44204 de Engenharia Aeronáutica da Faculdade de Engenharia, declaro ter desenvolvido o presente trabalho e elaborado o presente texto em total consonância com o **Código de Integridades da Universidade da Beira Interior**.

Mais concretamente afirmo não ter incorrido em qualquer das variedades de Fraude Académica, e que aqui declaro conhecer, que em particular atendi à exigida referenciação de frases, extratos, imagens e outras formas de trabalho intelectual, e assumindo assim na íntegra as responsabilidades da autoria.

Universidade da Beira Interior, Covilhã 05/01/2025

Dedication

This dissertation is dedicated to my parents and my brother for always being there for me and providing constant support throughout this journey.

Acknowledgements

I would like to express my deepest gratitude to my family for their unconditional love, encouragement, and support throughout this journey. To my parents, for always believing in me and providing the foundation upon which I could accomplish my aspirations.

I would also like to extend my heartfelt thanks to my supervisor, Prof Dr. Francisco Brójo, for his exceptional guidance, patience, and encouragement. Your mentorship has allowed me to develop this study, in its best ways. I am sincerely thankful for your support.

I am deeply grateful to my friends, I made during my time in Covilhã, and with whom I shared this journey. Your help was indispensable during the most challenging moments. Thank you for the amazing memories and laughs we had during theses 5 years.

Resumo

Neste trabalho foi realizada uma análise em CFD das emissões poluentes provenientes da combustão de gás natural e biogás numa câmara de combustão do tipo "can". Os combustíveis avaliados incluíram gás natural, utilizado como referência, uma mistura de gás natural com biogás e três tipos de biogás com composições distintas, nos quais a percentagem de CH_4 foi progressivamente reduzida, enquanto as percentagens de CO_2 e N_2 aumentaram. Adicionalmente, considerando que o biogás pode conter oxigénio na sua composição, foram também analisados dois biogases com diferentes percentagens de O_2. O estudo numérico foi realizado com o software ANSYS Fluent 2023 R2, utilizando os modelos de turbulência standard k – ε e de radiação P-1. A geometria da câmara de combustão foi desenhada no software CATIA V5. Para avaliar as emissões de espécies químicas, como CO_2, CO, UHC e NOx, foi utilizado o mecanismo detalhado de combustão GRI Mech 3.0. Os resultados mostram a variação das emissões poluentes em função da mudança de combustível, mantendo constante a potência térmica inicial. Verificou-se que a presença de uma zona de recirculação central desempenha um papel crucial na formação de poluentes, pois contribui para a estabilidade da chama e promove uma mistura mais eficiente de ar e combustível. Com o aumento das percentagens de CO_2 e N_2 no combustível, observou-se uma redução significativa nas emissões de NOx, acompanhada, no entanto, por um aumento nas emissões de CO_2. Relativamente às emissões de CO e UHC, os valores obtidos foram praticamente nulos, embora tenha sido identificada uma tendência de diminuição com o aumento de CO_2 e N_2. Quando presente O_2 no biogás, registou-se um aumento nas emissões de NOx, enquanto as emissões de CO_2 permaneceram praticamente constantes. Por outro lado, as emissões de CO e UHC mantiveram-se praticamente nulas, com uma ligeira tendência para diminuir. Concluiu-se que o biogás, apesar do aumento nas emissões de CO_2, é uma alternativa ao gás natural, apresentando não só uma formação mais sustentável e ecológica, como também menores emissões de NOx. Contudo, a presença de O_2 no biogás não se revelou vantajosa, uma vez que que as emissões de NOx aumentaram e não contribui para uma redução significativa dos restantes gases poluentes.

Palavras-chave

Câmara de Combustão; CATIA V5; ANSYS Fluent; Turbina a Gas; Gas natural; Biogás; Emissões Poluentes

Abstract

In this work, a CFD analysis was conducted on pollutant emissions from the combustion of natural gas and biogas in a can-type combustion chamber. The fuels evaluated included natural gas, used as a reference, a mixture of natural gas with biogas, and three types of biogases with distinct compositions, where the percentage of CH_4 was progressively reduced while the percentages of CO_2 and N_2 increased. Additionally, considering that biogas may contain oxygen in its composition, two biogases with different O_2 percentages were also analysed. The numerical study was performed using ANSYS Fluent 2023 R2 software, employing the standard $k-\varepsilon$ turbulence model and the P-1 radiation model. The geometry of the combustion chamber was designed using CATIA V5 software. To evaluate the emissions of chemical species such as CO_2, CO, UHC, and NOx, the detailed combustion mechanism GRI Mech 3.0 was used. The results show the variation in pollutant emissions as a function of the change in fuel, while maintaining the initial heat input constant. It was found that the presence of a central recirculation zone plays a crucial role in pollutant formation, as it contributes to flame stability and promotes a more efficient air-fuel mixture. With the increase in the percentages of CO_2 and N_2 in the fuel, a significant reduction in NOx emissions was observed, although accompanied by an increase in CO_2 emissions. Regarding CO and UHC emissions, the values obtained were nearly zero, although a decreasing trend was identified as the percentages of CO_2 and N_2 increased. When O_2 was present in the biogas, an increase in NOx emissions was recorded, while CO_2 emissions remained constant. On the other hand, CO and UHC emissions remained nearly zero, with a slight decreasing trend. It was concluded that biogas, despite the increase in CO_2 emissions, is an alternative to natural gas, as it not only has a more sustainable and ecological production process but also results in lower NOx emissions. However, the presence of O_2 in biogas did not prove to be advantageous, as NOx emissions increased and it did not contribute to a significant reduction in other pollutant gases.

Keywords

Combustor; CATIA V5; ANSYS Fluent; Gas Turbine; Natural Gas; Biogas; Pollutant Emissions

Contents

List of Figures

List of Tables

List of Acronyms

AD	Anaerobic Digestion
AFR	Air to Fuel Ratio
ASTM	American Society for Testing and Materials
CAD	Computer-Aided Design
CFD	Computational Fluid Dynamic
CPU	Central Processing Unit
CRZ	Center Recirculation Zone
CS	Combustible Species
DES	Detached Eddy Simulation
DNS	Direct Numerical Simulation
DOM	Discrete Ordinates Method
DRM	Dry Reforming Mechanism
ERZ	Edge Recirculation Zone
FAR	Fuel to Air Ratio
GHG	GreenHouse Gas
GRI	Gas Research Institute
GT	Gas Turbine
HHV	Higher Heating Value
IGS	Initial Graphic Specification
LES	Large Eddy Simulation
LFG	LandFill Gas
LHV	Lower Heating Value
LPG	Liquified Petroleum Gas
MGT	Micro Gas Turbine
MN	Methane Number
NCS	Non-Combustible Species
NG	Natural Gas
NOx	Nitrogen Oxides
NUIG	National University of Ireland Galway
PDF	Probability Density Function
PMC	Photon Monte Carlo
PRESTO!	PREssure STaggering Option
RANS	Reynolds-Averaged Navier-Stokes
RAM	Random Access Memory

RNG	Re-Normalization Group
RSM	Reynolds Stress Model
RTE	Radiative Transfer Equation
SHM	Spherical Harmonics Method
SIMPLE	Semi-Implicit Method for Pressure Linked Equations
SLFM	Steady Laminar Flamelet Model
SOx	Sulfur Oxides
STP	Standard Temperature and Pressure
UHC	Unburnt HydroCarbons
URF	Under Relaxation Factors

Nomenclature

$\%EA$	Percent excess air	[---]
AFR	Air-fuel ratio	[---]
cp_i	Specific heat at constant pressure for specie i	[J/kg. K]
D_a	Damkohler number	[---]
f	Mixture fraction	[---]
FAR	Fuel-air ratio	[---]
HHV	Higher Heating Value	[MJ/kg]
h	Absolute enthalpy	[J/kg]
$\Delta h_{f,i}^0$	Enthalpy of formation for specie i	[J/kg]
$\Delta h_{s,i}$	Sensible enthalpy changes for specie i	[J/kg]
ΔH_R	Enthalpy of combustion	[J/kg]
k	Turbulence kinetic energy	[m^2/s^2]
LHV	Lower Heating Value	[MJ/kg]
M	Molecular Weight	[kg/kmol]
m	Mass	[kg]
$\dot{m}$	Mass flow rate	[kg/s]
P	Heat Input	[kW]
p	Pressure	[Pa]
Re	Reynolds number	[---]
T	Temperature	[K]
T_{ad}	Adiabatic flame temperature	[K]
u	Velocity	[m/s]
W_0	Wobbe number	[MJ/Nm^3]
Y^+	Non-dimensional wall distance	[---]
Z	Local mass fraction	[---]

Greek letters

ε	Turbulence dissipation rate	$[m^2/s^3]$
μ_t	Turbulent viscosity	[Pa. s]
λ	Excess air coefficient	[---]
τ_c	Chemical time scale	[s]
τ_{Re}	Reynolds-stress tensor	[Pa]
τ_t	Turbulent time scale	[s]
ν	Specific gravity	[---]
ϕ	Equivalence ratio	[---]
∂	Patial differential	[---]
ρ	Density	$[kg/m^3]$
χ	Molar fraction	[---]
ω	Specific dissipation rate	$[s^{-1}]$

Subscripts

2	Combustor inlet stage
3	Combustor exit stage
a,air	Air
f,fuel	Fuel
i,j	Coordinate directions
max	Maximum value for the parameter
o	Oxidizer
prod	Products
react	Reactants
ref	Reference state
s	Stoichiometric

Chapter 1 – Introduction

1.1 Motivation

The motivation and ambition for carrying out this dissertation share the same objective that 21st century society. The world today depends on energy to meet its needs like heating, transportation, electricity etc. Among the energy resources needed by man today, electrical energy stands out the most. Electricity is a secondary energy resource due to its dependence on other primary energy sources. Primary resources are converted to electrical energy by using energy conversion machines which transforms the chemical energy in fossil fuel, such as Natural Gas (NG), coal, oil, into electricity. According to International Energy Agency, more than 51% of the electricity generated in the world today is derived from fossil fuel as a primary energy resource [1]. The Gas Turbine (GT) have been a significant part of energy production and transportation for decades and should continue indefinitely, since play a major role in power generation providing a clean, reliable and efficient means of producing electricity [2] . This device is an internal combustion engine which produces mechanical energy by combustion of a fuel. As any internal combustion engine, during the combustion is emitted harmful gaseous emissions such as, Nitrogen Oxides (NOx), carbon dioxide (CO_2), carbon monoxide (CO), Unburned HydroCarbons (UHC) and sulfur oxides (SOx), if present in the fuel. Today, there is an increased awareness of the likeliness of a global climate change associated with emissions of so-called GreenHouse Gases (GHG), which includes NOx and CO_2 [3].

Due to significant usage of fossil fuel in every sector of power generation leading to environmental pollution and depletion of conventional fuels, the world is forced to move toward alternative and cleaner sources of energy. So, in 2015, occurred the United Nations Climate Change Conference resulting the Paris agreement, setting the increase in the global average temperature to well below 2°C above pre-industrial levels and pursuing efforts to limit the temperature increase to 1.5°C above pre-industrial levels, recognizing that this would significantly reduce the risks and impacts of climate change [4]. Furthermore, emissions need to be reduced by 45% by 2030 and reach net zero by 2050 [5]. Since then, governments have increased efforts in developing their own plans to contribute towards the common goal. The GT will remain part of that solution with a variety of adaptations, while also meeting energy demand. Adapting industrial gas turbines for lower CO_2 emissions and carbon capture will be incentivized as the pricing authority on CO_2 emissions will continue to increase throughout the world. Using the

vast existing natural gas infrastructure, post combustion carbon capture to adapting to pure hydrogen or hydrogen / NG blends, will yield substantial GHG reductions could be implemented on GT's [2].

Other solution gaining more recognition is the use of biomass resources as renewable feedstock for cooking, heating, producing biofuels but primarily for electricity generation. This has been further compounded by depletion of fossil reserves, growing organic waste production, and global warming threats have combined to increase interest in Anaerobic Digestion (AD) and biogas fuel resources. With huge biomass to biogas conversion potential and many feasible biogases to electricity conversion technologies, biogas will play an extremely important role in the energy transition as a renewable energy fuel resource and in the reduction of greenhouse gas emissions. The capacity of biogas-based power has been growing rapidly for the past decade with global biogas-based electricity generation capacity increasing from 65 GW in 2010 to 120 GW in 2019 representing a 90% growth [6,7].

1.2 Objectives

1.2.1 Main Objective

Within the context mentioned in the previous section the main objective of this work is simulate the combustion and emission of pollutants from natural gas and biogas in a gas turbine can type combustor.

1.2.2 Specific Objectives

To achieve the objective described previously is necessary:

Understand the combustion process and pollutant formation in combustors;

- Select common natural gas used in gas turbines;
- Select biogas with different chemical compositions;
- Simulate the various fuels at the designated operating point;
- Conduct a comparative study of the various fuels;
- Analyse the results and estimate reasons for possible malfunction;

1.3 Document Organization

In this thesis, the work developed and presented is divided in five chapters.

In the first chapter, the current one, the motivation driving the author to take this work is expressed, furthermore, the main objective of this work as well as specific objectives are enumerated. This chapter also contains the structure of this work.

In the second chapter, concepts about combustion chambers are presented, including the types of combustion chambers and its main features. Additionally, it is presented type of fuels used in gas turbines (commons and renewables) and its properties, important aspects about the combustion process and how the pollutants are formed. Finally, some studies of other authors are presented.

The third chapter presents the CFD simulation process and all necessary steps for its execution. This chapter contains a description of the process and approaches to obtain the geometry, generation of the mesh and the numerical setup to obtain the final results. Also is presented the fuels used in the simulation and a validation of the results comparing with other study of other authors.

In the fourth chapter the results of the CFD simulation are presented and analysed, as well as discussed what is expected and what it is new. Finally, it is justified deviations.

In the fifth and last chapter is presented a conclusion about the work done, results obtained and it is made a consideration about future study.

Chapter 2 – State of the art

2.1 The Gas Turbine

A gas turbine is a continuous-flow engines that run with permanent flames once started and at stationary pressure, temperature, and flows at stabilized load, that uses a continuous stream of gases to produce mechanical power or generate electricity. It is necessary to distinguishing the terms 'aircraft gas turbine' and 'industrial gas turbine'. The first term is self-explanatory, while the second is intended to include all gas turbines not included in the first category. This broad distinction has to be made because the limitation of the size and weight of an aircraft power plant is much more important than in the case of most other applications of the gas turbine. Secondly, the aircraft power plant can make use of the kinetic energy of the gases leaving the turbine, whereas it is wasted in other types and consequently must be kept as low as possible. These two differences in the requirements can have a considerable effect on design [8].

As previously stated, the fuels tested will be natural gas and biogas, as being primarily used for electricity production, when mentioning to gas turbines is referring to industrial gas turbine. Nevertheless, the functional principles and theory applies to both categories.

Biogas powered turbines are often used for large scale power projects typically for at least 3 MW to 5 MW. Small biogas power plants generally vary in size generally between 30–75 kW as commonly available sizes in the market. The operational benefits of GT's include low maintenance requirements and higher efficiency especially for larger size plants. Micro-turbines though small can be connected in series to yield the desirable sizes based on need [7]. These units are relatively expensive, and since they rotate at very high speeds while operating at high temperatures, the gas turbine design, manufacturing, operation, and maintenance are a challenge from both engineering and engineering material point of view making their wide adoption and use in power generation limited [9]. Despite the limitations, gas turbines still have good degree of tolerance and can use wide range of fuels including raw biogas [7]. Furthermore, have an advantage over many other forms of power generation equipment in that they are able to quickly provide power during times of peak demand [10].

2.1.1 Working Cycle

The GT has three major sections, namely the compressor, combustor and turbine, illustrated in Figure 2.1. Ambient air enters the gas turbine at the compressor inlet. As the air passes through the sequential stages of compression (alternating rows of static airfoils known as compressor vanes or stators and rotating airfoils knows as compressor blades), both the pressure and the temperature increase as work is performed to decrease the volume of the air. The compressed air now passes into the combustion section where the air is further heated with the introduction and burning of fuel. In the combustor there is an increase in volume, but the pressure remains relatively constant. The gas produced during combustion is expanded through the turbine section (the turbine is similar to the compressor in that is consists of alternating rows of static vanes and rotating blades). The expanding gas performs work as it causes the turbine blades to rotate [10]. This rotation drives a rotor shaft directly coupled to an electric generator for power generation [7]. Finally, the combusted gas exits the turbine via the exhaust duct [10].

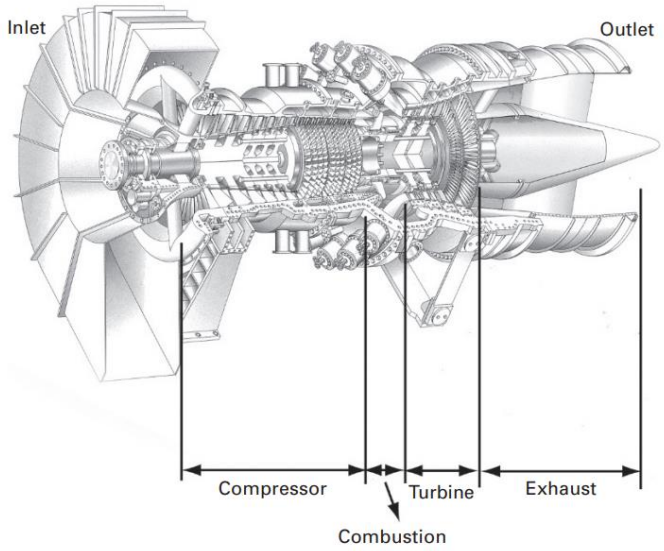

Figure 2.1: Schematic cut-away view of an industrial gas turbine [10].

The cycle just described refers to the Brayton cycle which represents the operation of a gas turbine engine. The cycle consists of four processes, as shown in Figure 2.2.

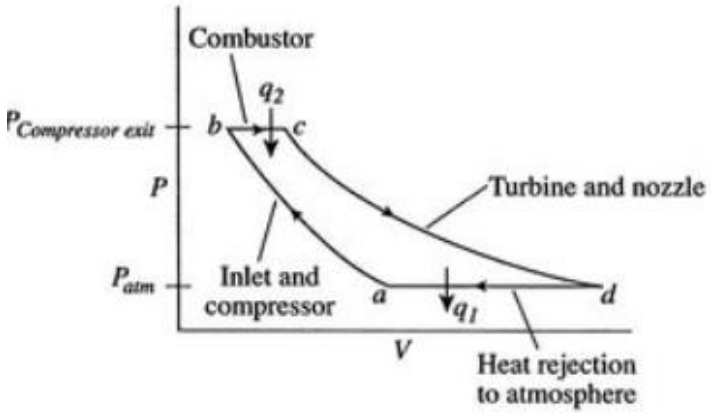

Figure 2.2: Pressure-Volume diagram of the Brayton Cycle [11]

- Process A to B: Isentropic compression in the inlet and compressor;
- Process B to C: Constant pressure fuel combustion (idealized as constant pressure heat addition);
- Process C to D: Isentropic expansion in the turbine and exhaust nozzle, where air is used into the form of mechanical energy;
- Process D to A: Cool the air at constant pressure back to its initial condition.

2.2 The Combustor

2.2.1 General Overview

The combustor in a GT serves two primary functions. First, it converts the chemical energy in the fuel into thermal energy, which is then expanded in the turbine. Second, it adjusts the temperature profile of the exhaust gases to ensure they do not exceed the material limits of the turbine. To achieve these objectives, the combustor is engineered to mix fuel with air at high pressure and temperature, thereby establishing and maintaining a stable, continuous combustion reaction. Additionally, it ensures that the combustion products are mixed to achieve the desired exhaust temperature profile. Consequently, the processes within the combustor involve a complex interplay of fluid mixing, chemical reactions, and heat transfer [12].

2.2.2 Combustor Requirements

Gas turbines must typically operate over a wide load range. Thus, the combustor should be designed to operate stably over wide range of conditions. So, there are basic requirements that combustors should ensure, not only for gas turbine but also for internal combustion engines [13]:

- High-combustion efficiency;
- Reliable and smooth ignition, both on the ground and, in the case of aircraft engines, after a flameout at high altitude;
- Wide stability limits;
- Low pressure loss;
- An outlet temperature distribution (pattern factor) that is tailored to maximize the lives of the turbine blades and nozzle guide vanes;
- Low emissions of smoke and gaseous pollutant species;
- Freedom from pressure pulsations and other manifestations of combustion-induced instability;
- Size and shape compatible with engine envelope;
- Design for minimum cost and ease of manufacturing;
- Maintainability and durability;
- Petroleum, synthetic, and biomass-based multifuel capability.

For aircraft engines, size and weight are important considerations, whereas for industrial engines more emphasis is placed on other items, such as long operating life and multifuel capability. For all types of engines, the requirements of low fuel consumption and low pollutant emissions are paramount [13].

2.2.3 Combustor Features

The design of gas turbine combustors has evolved over many decades with the final configuration based on the best of engineering judgment and intuitive reasoning. As demands have developed for efficiency and lower environmental impacts, engineering tools such as computational fluid dynamics and laser diagnostics have evolved to facilitate the design process [12].

Throughout the evolution of combustor technology, the basic requirements for combustor design have remained. In particular, the following five basic features are integral to the combustor design: a primary zone, a secondary zone, a dilution zone, various wall jets, and the management of heat transfer at the combustor boundary, as shown in Figure 2.3 [12].

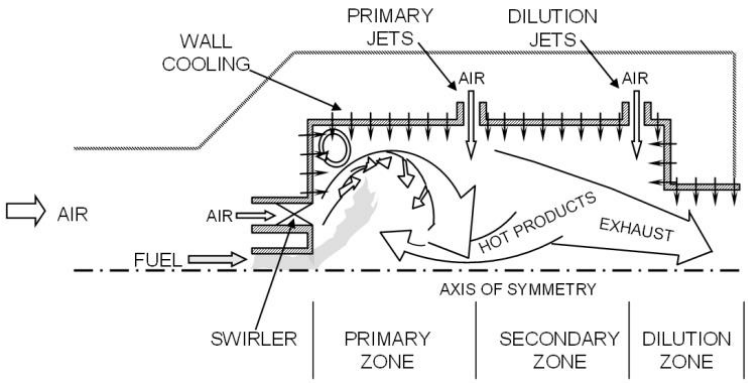

Figure 2.3: Features of a combustor [12]

2.2.3.1 Swirler

The entry point for the compressor air is through swirler vanes that are positioned at the front face of the combustor and typically surround the fuel injection port. The swirl vanes impact a circumferential velocity component to the air and thereby thrust the air radially outward as the air enters the combustor. This creates a pressure void at the centreline and induces a backflow to fill the centreline pressure deficit. This effectively creates, as a result, a recirculation flow that extends approximately one duct diameter downstream and defines the primary zone of the combustor [12].

2.2.3.2 Primary Zone

The main function of the primary zone is to anchor the flame and provide sufficient time, temperature, and turbulence to achieve essentially complete combustion of the incoming fuel–air mixture [13].

2.2.3.3 Wall Jets

Wall jets affect the mixing, stoichiometry, and structure of the flows in gas turbine combustors. In a typical combustor design, two sets of air wall jets (primary and dilution) are prescribed. The primary air jets are located approximately one duct diameter downstream from the combustor inlet and serve two major functions. First, the jets bring closure to the recirculation zone by providing a strong force against which the primary zone cannot easily penetrate. Without the set of primary air jets, the dynamics of the recirculation zone would create aerodynamic fluctuations and result in pressure oscillations, undesirable noise, and elevated pollutant emission. Secondly, the primary jets bifurcate with a substantial percentage of the flow directed upstream to mix with the recirculating fuel-air mixture, and the remainder mixing downstream into the secondary zone [12].

2.2.3.4 Secondary Zone

The role of the secondary zone is to oxidize the CO to CO_2. The principal elementary kinetic reaction that governs the oxidation is:

$$CO + OH \Rightarrow CO_2 + H \tag{2.1}$$

If the primary zone temperature is higher than around $2000\ K$, dissociation reactions will result in the appearance of significant concentrations of CO and hydrogen (H_2) in the reflux gases. Should these gases pass directly to the dilution zone and be rapidly cooled by the addition of massive amounts of air, the gas composition would be “frozen,” and CO, which is both a pollutant and a source of combustion inefficiency, would be discharged from the combustor unburned [13].

To avoid such problem a solution is dropping the temperature to an intermediate level by the addition of small amounts of air encourages the burnout of soot and allows the combustion of CO and any other UHC to proceed to completion [13]. Moreover, establishing an overall lean mixture ratio through the primary jet bifurcation, retaining the temperature at an elevated level, and providing the residence time needed to promote the oxidation it’s also a strategy to avoid the problem [12].

2.2.3.5 Dilution Zone

The role of the dilution zone is to reduce the temperature of the combustion products and mix the resultant gases in order to establish a temperature that will uphold the integrity of the turbine blades. This is accomplished by second major set of wall air jets. The dilution jet flow, approximately one-quarter of the total air flow exiting the compressor, is sufficient to reduce the overall equivalence ratio of the gases exiting the combustor to a very lean condition [12].

To protect the integrity of the turbine section, it is not sufficient to reduce the mean temperature. The radial and circumferential variation in local temperature from the mean can create hot spots and degrade, damage, and possibly destroy a turbine component (e.g., blade, stator, seal). As a result, the temperature profile at the exit plane must meet design criteria. The temperature profile is characterized by various indices including the "Pattern Factor," the "Profile Factor," and the "Turbine Profile Factor" [12].

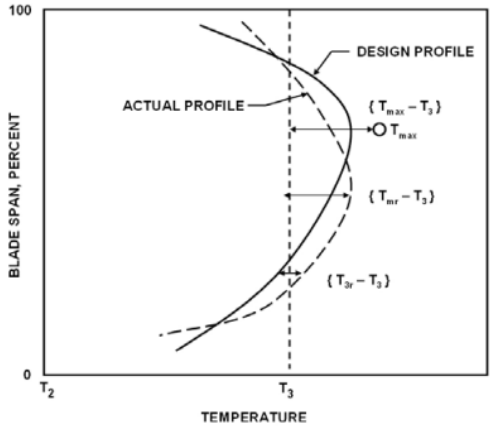

Figure 2.4: Temperature profile [12]

The Pattern Factor, represented by Equation (2.2), reflects the extent to which the maximum temperature deviates from the average temperature rise across the combustor.

$$Pattern\ Factor = \frac{T_{max} - T_{3av}}{T_{3av} - T_2} \tag{2.2}$$

Where T_{max} is the maximum recorded temperature, T_2 is the inlet combustor air temperature, and T_{3av} is the mean exit temperature.

The Profile Factor, represented by Equation (2.3), characterizes the extent to which the maximum circumferential mean temperature, T_{mr}, deviates from the average temperature rise across the combustor.

$$Profile\ Factor = \frac{T_{mr} - T_{3av}}{T_{3av} - T_2} \tag{2.3}$$

The Pattern Factor and Profile Factor, as defined above, are best suited for situations where a perfectly uniform exit-temperature distribution would be considered ideal. However, in modern high-performance engines, which employ extensive air cooling of both nozzle guide vanes and turbine blades, the desired average radial distribution of temperature at the combustor exit plane is far from flat; instead, it usually has a profile that peaks above the mid height of the blade, as illustrated in Figure 2.4 [13].

The Turbine Profile Factor, takes the design profile into account represented by Equation (2.4), addresses the maximum temperature difference by comparing the average temperature at any given radius around the circumference (T_{3r}) and the design temperature for that same radius (T_{3des}) [12].

$$Turbine\ Profile\ Factor = \frac{(T_{3r} - T_{3des})_{max}}{(T_{3av} - T_2)} \tag{2.4}$$

where $(T_{3r} - T_{3des})\ max$ is the maximum temperature difference between the average temperature at any given radius around the circumference and the design temperature for that same radius. The goal is for the actual profile to match the design profile.

2.2.3.6 Wall Cooling

The functions of the liner are to contain the combustion process and to facilitate the distribution of air to all the various combustor zones in the prescribed amounts. The liner must be structurally strong to withstand the buckling load created by the pressure differential across the liner wall. It must also have sufficient thermal resistance to withstand continuous and cyclic high-temperature operation. This is accomplished through the use of high-temperature, oxidant-resistant materials combined with the effective use of cooling air [13]. To preclude this, approximately one-quarter of the compressor air flow is allocated to liner cooling. Designs for accommodating this cooling flow are small holes in the liner with louvers on the inside wall to direct the flow along the internal boundary. New designs incorporate liner materials with hundreds of closely spaced holes that promote a diffusive flux of air at all points along the liner [12].

2.2.4 Combustors Type

The overall engine design and the requirement to make the most use of the available space influence the choice of combustor type and layout. Tubular and annular combustor types are the two main types. The "tubo-annular" or "can-annular" combustor, which consists of many equispaced tubular liners positioned inside an annular air casing, is a compromise between these two variations [13]. The three different combustor types are illustrated in Figure 2.5.

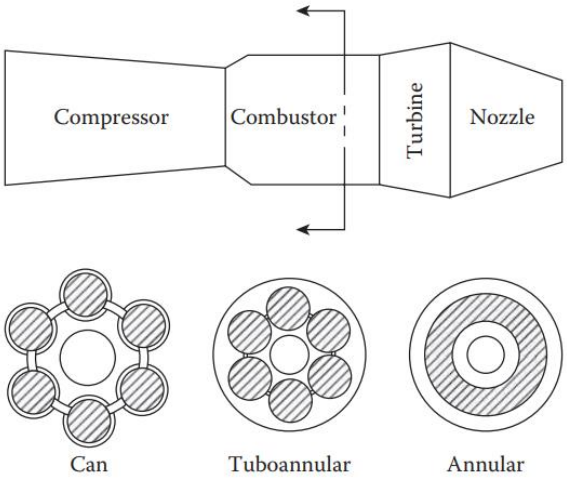

Figure 2.5: Combustors type [13]

2.2.4.1 Can Type Combustor

The earliest aircraft engines made use of can (or tubular) combustors, as shown in Figure 2.6, in which the air leaving the compressor is split into a number of separate streams, each supplying a separate chamber. These chambers are spaced around the shaft connecting the compressor and turbine, each chamber having its own fuel fed from a common supply line. This arrangement was well suited to engines with centrifugal compressors, where the flow was divided into separate streams in the diffuser [8]. The main advantage of tubular systems is that relatively little time and money is incurred in their development. Also, offer the advantages of simplicity of design, ease of maintenance, and long life due to low heat release rates [14]. However, their excessive length and weight prohibit their use in aircraft engines, and their main application is to industrial units where accessibility and ease of maintenance are prime considerations [13].

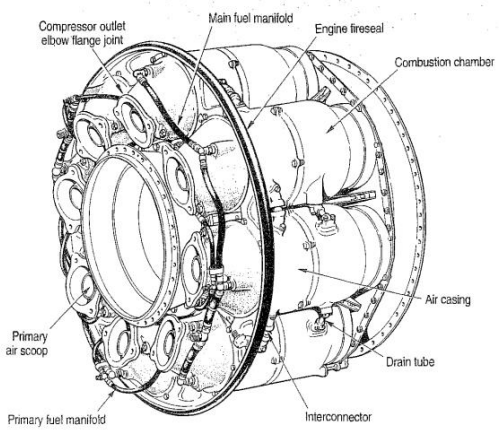

Figure 2.6: Can type combustor [13]

2.2.4.2 Annular Type Combustor

In this type, an annular liner is mounted concentrically inside an annular casing as shown in Figure 2.7. In many ways it is an ideal form of chamber, because its clean aerodynamic layout results in a compact unit of lower pressure loss than other combustor types [13]. Annular combustors presented some disadvantages, which led to the development of cannular combustors initially. Firstly, although a large number of fuel jets can be employed, it is more difficult to obtain an even fuel-air distribution and an even outlet temperature distribution. Secondly, the annular chamber is inevitably weaker structurally and it is difficult to avoid buckling of the hot flame tube walls. Thirdly, most of the development work must be carried out on the complete chamber, requiring a test facility capable of supplying the full engine air mass flow, compared with the testing of a single can in the multichambered layout. These problems were vigorously attacked and annular combustors are universally used in modern aircraft engines [8].

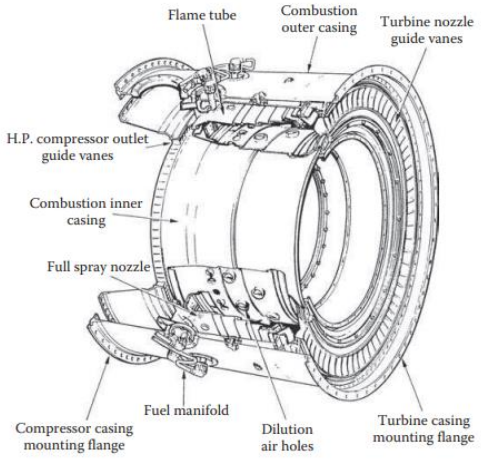

Figure 2.7: Annular type combustor [13]

2.2.4.3 Can-Annular Type Combustor

As engine pressure ratios started to climb in the late 1940s, the tubo-annular or can-annular combustor began to find increasing favour on both sides of the Atlantic. With this design, a group of tubular liners, usually from 6 to 10, is arranged inside a single annular casing, as illustrated in Figure 2.8. This concept attempts to combine the compactness of the annular chamber with the mechanical strength of the tubular chamber. Compared with the annular design, the tubo-annular chamber has an important advantage in that much useful chamber development can be carried out with very modest air supplies, using just a small segment of the total chamber containing one or more liners. Its drawbacks emerge when trying to achieve a satisfactory and consistent airflow pattern; in particular, the design of the diffuser can present serious difficulties [13].

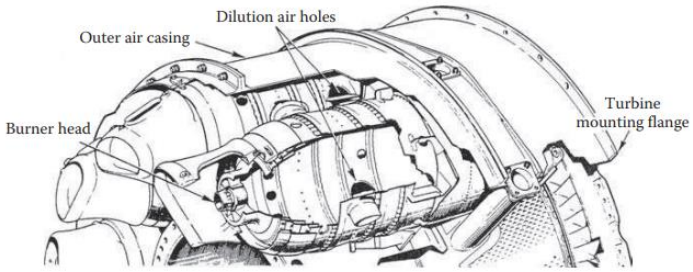

Figure 2.8: Can-annular type combustor [13]

2.3 Fuels

2.3.1 Types of Hydrocarbons

Pure hydrocarbon fuels are compounds of two elements only, carbon and hydrogen. They may be gaseous, liquid, or solid at normal pressure and temperature, depending on the number of carbon atoms and their molecular structure. Those with up to four carbon atoms are gaseous; those with twenty or more are solid, and those in between are liquid. It is usual to classify the hydrocarbons present in petroleum fuel into four main groups: alkanes, alkenes, alkynes and aromatic. The proportions in which these groups are present largely define the character of the fuel [13]. Hydrocarbons can be divided into two main groups, aliphatic and aromatic, in which, aliphatic hydrocarbons are divided into two subclasses as saturated and unsaturated hydrocarbons, as illustrated in Figure 2.9.

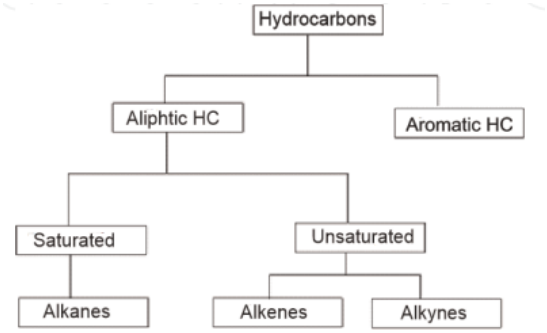

Figure 2.9: Hydrocarbons classification [15]

2.3.1.1 Alkanes (Paraffins)

Paraffins have the general formula C_nH_{2+n} ,where n =1,2... The essential characteristic of paraffins is that they have only single bonds. They are known as saturated hydrocarbons because they contain the maximum number of hydrogen atoms that can bond with the number of carbon atoms present in the molecule. The simplest paraffin (i.e., with n = 1) is methane, CH_4 as shown in Figure 2.10, a natural product resulting from the anaerobic bacterial decomposition of plant matter in water [16]. Alternative paraffin configurations, or isoparaffins, are in the form of branched chains, such as dimethyl hexane as shown in Figure 2.10 [13,16].

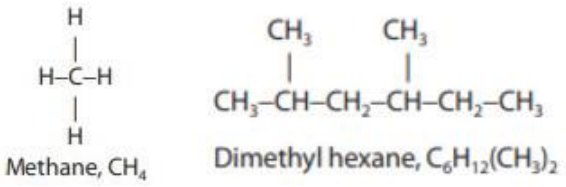

Figure 2.10: Methane and dimethyl hexane chemical formula [13]

In general, paraffins tend to have a higher hydrogen/carbon ratio, lower density, lower freeze point, and high gravimetric calorific value than other types of hydrocarbon fuels. They possess high thermal stability, and their combustion is characterized by freedom from coke deposition and exhaust smoke [13].

2.3.1.2 Naphthenes (Cycloparaffins)

Naphthenes are saturated hydrocarbons which the carbon atoms are linked to form rings instead of chains as in the case of paraffins [13,16]. They have the general formula C_nH_{2n}, where n = 3, 4, ... The simplest cycloalkane (i.e., with n = 1) is cyclopropane, C_3H_6 , as shown in Figure 2.11 [16].

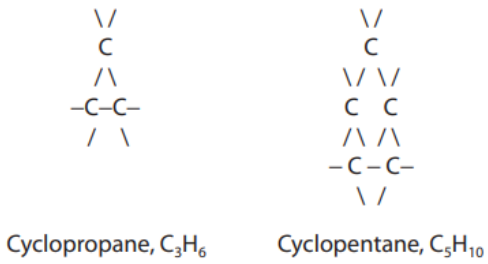

Figure 2.11: Cyclopropane and cyclopentane chemical formula [13]

They closely resemble paraffins in their chemical stability, high gravimetric heat of combustion, and low soot-forming tendencies [13].

2.3.1.3 Alkenes (Olefins)

The group of unsaturated hydrocarbons includes olefins. The term unsaturated means that these chemicals contain less hydrogens than fully saturated carbon chains as found in paraffins [17]. Olefins can be described by a molecular formula $C_nH_{2n}$where n = 2, 3 … [16]. It means that olefins and naphthenes have the same molecular formulae and thus their molecules of the same number of carbons are isomers [17]. The simplest olefin (i.e., with n = 2) is ethylene, C_2H_4, as shown in Figure 2.12.

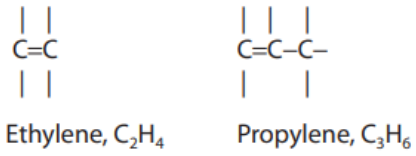

Figure 2.12: Ethylene and propylene chemical formula [13]

They are very active chemically and readily react with a great many compounds to form resinous gums and rubberlike materials. For this reason, olefins are very undesirable in gas turbine fuels, and are found only in trace quantities [13].

2.3.1.4 Aromatics

The group of aromatic hydrocarbons is a special kind of unsaturated hydrocarbons. They are classified separately because their properties differ from those of unsaturated hydrocarbons [17]. The characteristic formula for the aromatics is C_nH_{2n-6} , the simplest aromatic is benzene, C_6H_6, as shown in Figure 2.13. Benzene is a colourless, flammable liquid obtained mainly from petroleum and coal [16].

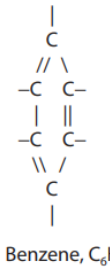

Figure 2.13: Benzene chemical formula [13]

Aromatics contain less hydrogen and, in consequence, their specific energy is appreciably lower. The disadvantages of aromatic compounds include a marked tendency to soot formation and a high hygroscopicity that can lead to precipitation of ice crystals when the fuel is subjected to low temperatures. Aromatics also have a strong solvent action on rubber that can cause trouble in fuel [13].

2.3.2 Gaseous Fuels in Gas Turbines

The potential fuels to be utilized on high efficiency GT's are very large, and in this changing energy landscape, there is a growing interest in turning to non-traditional fuels, capitalizing on the experience gained during the past five decades. As continuous flow machines with robust designs and universal combustion systems, gas turbines have demonstrated distinctive capabilities to accept a wide variety of fuels. Gas turbines, in particular, have been operating with a variety of fuels [18]. The most common fuels used in gas turbines are gaseous fuels. Gaseous fuels are simpler to ignite, handle and control than liquid or solid fuels. The molecular mixing of gaseous fuels and oxygen is very fast, especially when compared to the time of mass transport needed for the heterogeneous reactions of solid fuels. The combustion process of gaseous fuels is only limited by the velocity of mixing and the kinetics of the combustion reactions allowing for compact and intense burning [19]. According to Lackner [19], gaseous fuels can be classified by their origin. The first category is gases found in their final form in nature such as the natural gas. The second category is gases produced directly from various sources, such as the biogas and syngas[1]. There is still a third category, not that important for this work, which is by-product gases, where the primary aim of the process is not the generation of the

[1] Syngas is a mixture of hydrogen and carbon monoxide produced from the gasification of carbonaceous feedstocks

gaseous fuel in question, such as coke oven gas. An emphasis will be placed on natural gas and biogas, as these are the fuels that will be used in this work.

2.3.2.1 Natural Gas

Natural gas, in itself, might be considered a very uninteresting gas - it is colourless, shapeless, and odourless in its pure form. Quite uninteresting - except that natural gas is combustible, and when burned it gives off a great deal of energy [20]. Unlike other fossil fuels, natural gas is clean burning and emits lower levels of potentially harmful emissions into the air [21]. The society requires energy constantly, to heat homes, cook food, and generate electricity. It is this need for energy that has elevated natural gas to such a level of importance in society, and in people's lives [20].

Natural gas is a combustible mixture of hydrocarbons with non-combustible species that exists in a gaseous state at standard temperature and pressure [21]. It is formed primarily by CH_4, it can also include C_2H_6, propane (C_3H_8), butane (C_4H_{10}), pentane (C_5H_{12}), and the Non-Combustible Species (NCS), such as, nitrogen (N_2), oxygen (O_2) and CO_2 [20].

The formation of conventional natural gas is a multifaceted process influenced by geological and chemical variables [22]. Millions of years ago, the remains of plants and animals decayed and built up in thick layers. This decayed matter from plants and animals is called organic material –a compound that capable of decay or sometime refers as a compound consists mainly carbon. Over time, the mud and soil changed to rock, covered the organic material and trapped it beneath the rock. Pressure and heat changed some of this organic material into coal, some into oil (petroleum), and some into natural gas. After oil and natural gas were formed, they tended to migrate through tiny pores in the surrounding rock. Some oil and natural gas migrated all the way to the surface and escaped. Other oil and natural gas deposits migrated until they were caught under impermeable layers of rock or clay where they were trapped. These trapped deposits are where we find oil and natural gas wells today where drilling process are conducted to obtain the gas [20]. Gas companies generally pump natural gas straight from the well to a processing plant, avoiding the need for storage facilities at the wellhead and reducing the potential for leakage [21]. Natural gas is normally produced far away from the consumption regions; therefore, they require an extensive and elaborate transportation system to reach its point of use. The transportation system for natural gas consists of a complex network of pipeline, designed to quickly and efficiently transport natural gas from the origin to areas of high natural gas demand. Transportation of natural gas is

closely linked with its storage since the demand of the gas is dependent on the season [20].

2.3.2.2 Biogas

The most important issue facing humanity in the 21st century is the issue of energy and fuel. Because on the one hand, the number of energy consuming industries is increasing, and on the other hand, fossil fuels (the most important energy consumed by these industries) are running out. Meanwhile, the pollution caused by these fuels has caused problems in the world, and international unions are passing laws to eliminate or minimize the consumption of these fuels in the coming decades [23]. Also, the challenges of heat and electricity generation, the desire for sustainability, the high cost of power generation, and related environmental challenges have created interest in alternative sources of energy and technology globally. Biogas has a significant potential has a low-cost energy carrier. With huge biomass to biogas conversion potential and many feasible biogases to electricity conversion technologies, biogas will play an extremely important role in the energy transition as a renewable energy fuel resource [6]. Moreover, the easy scalability of biogas technology makes it capable to mitigate energy security concerns. Biogas technology offers fewer infrastructures and production cost advantages over other renewable technologies such as solar and wind [24]. In addition, its production prevents uncontrolled production and emission of methane to the atmosphere. Methane is a powerful GHG having the ability to remain in the atmosphere for up to 15 years and is close to 20 times more potent in trapping heat in the atmosphere than carbon dioxide for a timescale of 20 years [6].

Biogas is a mixture of gases with CH_4 and CO_2 being the main constituents. Other than CH_4 and CO_2 as the main constituents of biogas, common contaminants present as trace elements include ammonia (NH_3), moisture, hydrogen sulfide (H_2S), N_2, methyl siloxanes, O_2, halogenated volatile organic compounds and CO. Some of the trace elements significantly affect biogas as fuel and must be removed for quality purpose. Biogas has got thermodynamic properties comparable with other known fuels. Although biogas has slightly inferior thermal properties compared to fossil fuels, it is an attractive fuel because of its environmental benefits. The main determinant of the heating value of biogas is the composition of methane in biogas. The composition of CH_4 in biogas varies from 45% to 75% by volume [6]. Furthermore, high concentrations of CO_2 and high inert gas ratio decrease the heating value [24]. In biogas production, various factors are of

great importance, however the type of organic substrate used has been found to play a significant role in the yield and composition of the biogas [25].

Feedstocks and Production

Biogas production from locally available renewable organic resources can be a good alternative because it contributes to the reduction of GHG emissions. Biogas technology provides an attractive route for the utilization of different categories of biomass for meeting energy needs. This technology offers a unique set of benefits, some of which include good waste management technique, enhancement in the ecology of rural areas, decrease in pathogenic diseases, optimization of the energy consumption of rural communities and promotion in agricultural structure [25]. Mainly, biogas is generated from different organic matter (biomass made of fats, proteins, carbohydrates, cellulose, and hemicellulose which are necessary ingredients for biogas generation) through AD. Anaerobic digestion is a process through a systematic breakdown of large organic polymers by the anaerobic action of different microorganisms into smaller molecules in the absence of oxygen [6,26]. AD for biogas production takes place in a sealed vessel called a reactor, which is designed and constructed in various shapes and sizes specific to the site and feedstock conditions. These reactors contain complex microbial communities that break down (or digest) the waste and produce resultant biogas and digestate (the solid and liquid material end-products of the AD process) which is discharged from the digester [26].

To use biomass in biogas production, the feedstock can be liquid as concentrated or diluted or as solid or slurry form. The composition of the feedstock as well as process control influences the quality and composition of the products of anaerobic digestion in terms of biogas yield, biogas quality, state of digestate, and stability of biogas plants and operations. There are great variety of organic material can be used in anaerobic digesters as a feedstock for generating biogas [6]:

- Agriculture waste – These wastes include manure from livestock such as cows, pigs, chickens and crop residues such as livestock waste inedible food, straw, corn stalks, and other plant residues left after harvesting;
- Sewage and Wastewater Sludge[2] – Sludge collected from the treatment of municipal and industrial wastewater

[2] Sludge are solids separated during the wastewater treatment process

- Landfill[3] Waste – Solid waste collected from residential, industrial, and commercial entities.

Both agriculture waste and wastewater sludge are put in a reactor for the anaerobic digestion, in contrast, landfill waste digestion process takes place in the ground rather than in an anaerobic digester [27]. Landfills contain the same anaerobic bacteria present in a digester that break down organic materials to produce biogas, in this case LandFill Gas (LFG). Instead of allowing LFG to escape into the atmosphere, it can be collected and used as energy. Landfills must have a certain size to install and operate a LFG collection and control system [28].

2.3.3 Liquid Fuels

Natural gas has been shown to be the primary source of fuels for gas turbine applications mainly due to its widespread availability and low cost. However, there are many other fuels which are used or considered, especially where pipeline gas is either not available or of insufficient quantity [29]. An alternative is the use of liquid fuels, which occupies a large proportion of the total energy production in the world, where the fuel is of two types, heavy fuel and light fuel [30]. Liquid fuels are combustible substances that exist in a liquid state at standard temperature and pressure conditions. Moreover, are those combustible or energy-generating molecules that can be harnessed to create mechanical energy [31]. Gas turbines typically operate on a range of liquid fuels such as diesel, kerosene, and specialized heavy fuels, each chosen based on availability, cost, and specific operational requirements. Liquid fuels are particularly advantageous for gas turbines due to their high energy density, which allows for efficient combustion and reliable power output. In contrast, liquid fuels require specialized storage tanks and containers to keep them in their liquid state. This can be costly and requires careful handling to prevent leaks, spills, or accidents during transportation [32].

[3] Landfill is a facility for the disposal of solid waste

2.3.3.1 Light Distillate fuels

Light distillates are classified as “middle distillates” by the oil business. Light distillate consists of kerosene and diesel, their use in GT’s does not require the additives package that is necessary for aircraft and diesel cars. Kerosene’s and diesel are “straight-run” refinery products that originate from the atmospheric distillation of crudes at the top of the distillation tower, above the middle distillates. They are prime-quality, expensive GT fuels. While diesel is the conventional liquid fuel for heavy-duty GT’s, kerosene is the preferred one for aeroderivative in consideration of its still-higher purity [33].

2.3.3.2 Heavy oil Fuel

There are cases where neither diesel nor gaseous fuels are available and the only suitable “fuel” is heavy oil fuel. This creates challenges that have to be handled through fuel pre-treatment and fuel injection system functionality. Heavy oil fuels need to be treated in order to meet industrial gas turbine limits on metallic and other contaminants in the fuel. Crude oil often contains high amounts of alkaline metals (sodium, potassium) and heavy metals (vanadium, nickel, etc.) which if introduced into the combustion system can result in accelerated deposit formation and high temperature corrosion in gas turbine hot gas path components. Also, viscosity is one of the key parameters used when evaluating liquid fuels for use in industrial GT’s. Therefore, there are some gas turbine models that are able to operate on liquid fuels with much higher viscosities, and can, by using fuel heating or blending [29].

2.3.3.3 Liquified Petroleum Gas (LPG)

Less used, but still viable, gas turbine fuels include those containing higher hydrocarbon species. These require specific assessment and consideration within both the fuel system and combustor injector [29].

LPG is formed as a byproduct during the extraction of natural gas and the refining of crude oil. It primarily consists of hydrocarbons, mainly C_3H_8 and C_4H_{10}, and can include small amounts of other gases [34]. LPG can be used either in vaporized or liquid form. When vaporized and maintained in gaseous form, the gas should be supplied at elevated temperatures due to the use of the higher hydrocarbons usually associated with LPG, butane and propane. Special injectors will be required to ensure the metered fuel is correctly controlled. When supplied in liquid form special consideration must be made

to the fuel system. LPG has a very low viscosity and special pumps are required to overcome the problem of low lubricity associated with LPG. Storage of such fuels needs particular attention. Having a lower viscosity in liquid form and being heavier than air when in gaseous form means special precautions have to be adopted [29].

2.3.4 Fuel Properties

Before combustion can take place in a combustion chamber, the fuel needs to be injected, evaporated, and combined with air. The physical characteristics of the fuel have a major impact on how limiting these processes are for burning [13]. The properties indicate the quality of the fuel. Engine performance and emission are also directly related to these [35].

2.3.4.1 Relative Density

Fuel density is very important because it defines the energy content in the fuel tank with a mixed volume. The relative density of a fuel is usually defined as the ratio of the mass of a given volume of fuel at a temperature T_{fuel} to the mass of an equal volume of pure water at a temperature T_1 . A reference temperature of T_{fuel} = 289 K is often used, with T_1 set at 277 K, where the density of water is highest [13]. The relation is shown by the Equation (2.5).

$$Relative\ Density = \frac{Fuel\ Density\ at\ T_{fuel}}{Water\ Density\ at\ T_1} \tag{2.5}$$

2.3.4.2 Vapor Pressure

The vapor pressure of a liquid is the pressure exerted by the vapor above its surface at a given temperature. A high vapor pressure is desirable from a combustion viewpoint, because it ensures rapid evaporation of fuel in the primary combustion zone. On the other hand, low vapor pressure has advantages in terms of reduced pressure in unvented fuel tanks, lower fuel losses due to evaporation at high altitudes in vented tanks, and reduced fire hazard [13].

2.3.4.3 Distillation Range

The distillation range of a fuel is important because it largely determines the physical and combustion characteristics of the fuel and has a dominating influence on availability. Since practical fuels are a mixture of many compounds, each having its own boiling point, these fuels have no single boiling point, but rather a distillation range defined by the temperature vs. percentage fuel evaporated relationship [13].

2.3.4.4 Volatility Point

Volatility is a fuel's tendency to vaporize. Two physical properties are used to characterize fuel volatility: vapor pressure and distillation range. A more volatile fuel has a higher vapor pressure and lower initial distillation temperatures. It is important because a fuel must vaporize before it can burn. However, too high volatility can result in evaporative losses or fuel system vapor lock [36].

2.3.4.5 Flash Point

Flash point is one of the most important properties of fuel. The flash point is the lowest temperature at which the vapours above a flammable liquid will ignite on the application of an ignition source. At the flash point temperature, just enough liquid has evaporated to bring the vapor-air space over the liquid above the lower flammability limit [36]. Higher flash point makes fuel safer for handling and storage and prevent unexpected ignition of fuel during combustion [18]. As might be expected, the flash point is directly related to vapor pressure; the higher the vapor pressure, the lower the lash point [13].

2.3.4.6 Viscosity

Viscosity is a measure of the resistance to flow and is important in the design of fuel pumping systems [14]. Higher viscosity increases fuel pump power consumption and causes poor spray and atomization and also increases fuel consumption. In these respects, lower viscosity is desired [35]. The viscosity of gas turbine fuels depends greatly on temperature [14].

2.3.4.7 Freezing Point

The freezing point of the jet fuel is defined as the temperature at which the last wax crystals melt when warming the solidified fuel [13]. Freezing point also increases with carbon number for compounds in the same class but is strongly influenced by molecular shape. Molecules such as normal paraffins and unsubstituted aromatics freeze (crystallize) at much higher temperatures than other compounds with the same carbon number because they have a compact geometry that allows them to pack together easily into a crystalline structure [36].

2.3.4.8 Boiling Point

The boiling point of a liquid is the temperature at which its vapor pressure is equal to the local atmospheric pressure. However, atmospheric pressure decreases exponentially with increasing altitude. At 3000 meters atmospheric pressure is only about 69 % as great as at sea level, and at 6000 meters, it drops to 46 percent of the sea-level value. Thus, liquids boil at lower temperatures at higher altitudes. Boiling point increases with carbon number for compounds in the same class. For a given carbon number, iso-paraffins have the lowest boiling points, followed by normal paraffins, naphthenes, and aromatics [36].

2.3.4.9 Specific Heat

The specific heat of a substance is the amount of heat required to raise it by one degree celsius [16]. Paraffinic fuels are the most attractive in this regard because they have considerably higher specific heats than either naphthenic or aromatic fuels [13].

2.3.5 Ignitability and Interchangeability Properties Gaseous Fuels

Several technical parameters are used to define the ignition tendency of different fuels in combustion engines. For gaseous fuels, the Methane Number is commonly used to assess this ignition tendency. Regarding the interchangeability of fuels, which is more prevalent with gaseous fuels, the Wobbe number (W_o) is the key parameter for evaluating this capability.

2.3.5.1 Methane Number (MN)

The one of main quality requirements of NG as an engine fuel is the Methane Number (MN). This parameter indicates the fuel's capability to avoid knocking in the engine which is one of the reasons for engine power decreases. A higher MN value indicates a better gas fuel quality for gas engines. NG with higher methane content tends to have higher MN value [37]. Pure Methane is assigned a Methane Number of 100 and pure Hydrogen is assigned a Methane Number of zero [38]. Methane Number is not a gas thermodynamic property, this means that the methane number determination methods are based on empirical experiments. The results obtained with individual methods may vary significantly. It should also be noted that some of these calculation methods do not include components heavier than butane. Usually, the content of components heavier than butane should be small [37].

2.3.5.2 Wobbe Number

It is essential that the various fuels used in a specific burner be similar in nature. The Wobbe number is the main indicator of the interchangeability of fuel gases such as NG. It is calculated from the fuel's Higher Heating Value (HHV) in and its specific gravity (v) with respect to air is used instead of density, the W_o, is defined by Equation (2.6):

$$W_o = \frac{HHV}{\sqrt{v}} \tag{2.6}$$

The Wobbe number is used to compare the combustion energy output of different composition fuel gases in an appliance. If two fuels have identical Wobbe numbers then for given pressure and valve settings the energy output will also be identical. Typically, variations of up to 5% are allowed as these would not be noticeable [39].

2.4 The Combustion Process

2.4.1 General Overview

The subject of combustion embraces a wide variety of processes and phenomena. Combustion is perhaps described most simply as an exothermic reaction of a fuel and an oxidant. In gas turbine applications, combustion of a liquid fuel involves the mixing of a fine spray of droplets with air, vaporization of the droplets, the breaking down of heavy

hydrocarbons into lighter fractions, the intimate mixing of molecules of these hydrocarbons with oxygen molecules, and finally the chemical reactions themselves [8].

This is a fast process that requires less than 1 ms for 80% completion. It is characterized by the presence of a flame that propagates through the unburned mixture. A flame may be defined as a rapid chemical change occurring in a very thin fluid layer, involving steep gradients of temperature and species concentrations, and accompanied by luminescence. From a macroscopic viewpoint, the flame front can be viewed as an interface between the burned gases and the unburned mixture. Compared with the unburned mixture, the burned gases are much higher in volume and temperature, and much lower in density. Deflagration waves in hydrocarbon fuel-air mixtures normally propagate at velocities below 1 m/s. All the flame processes that occur in gas turbine combustors fall within this category [13].

2.4.2 Combustion Fuel Properties

The combustion properties of most interest are those that govern the flame temperature, the rate of chemical reaction, the burning range, and the tendency to form soot [9].

2.4.2.1 Calorific Value

The calorific value of a fuel is defined as the amount of heat released during combustion when a unit quantity of the fuel is burnt [18]. Higher calorific value for fuel is desired because it facilitates the heat release during combustion and improves engine performance. The amount of heat release from combustion of the fuel will depend on the phase of water in the products. If water is in the gas phase in the products, the value of total heat release is denoted as the Lower Heating Value (LHV) [40]. For gas turbine fuels, the lower calorific value is most relevant, since it pertains to complete combustion to $CO_2$and water (H_2O) vapor [13]. When the water vapor is condensed to liquid, additional energy (equal to the latent heat of vaporization) can be extracted and the total energy release is called the Higher Heating Value [40].

2.4.2.2 Enthalpy

The enthalpy of a fuel is a measure of its capacity to absorb heat; the enthalpy also indicates the amount of heat required to accomplish a given change in the temperature or state of a fuel [13].

2.4.2.3 Spontaneous-Ignition Temperature

An important factor affecting aircraft fire and explosion hazards is the tendency of the fuel toward spontaneous ignition. When an aircraft crashes, a common cause of ire is the spontaneous ignition of fuel coming into contact with hot surfaces, especially near engines. The spontaneous-ignition temperature depends greatly on molecular structure, since the oxidation reactions leading to spontaneous ignition can occur only when the chemical bonds within the fuel are broken by thermal agitation. Consequently, the spontaneous-ignition temperature is lower for fuels with higher relative density, whose molecules are less compact [13].

2.4.2.4 Limits of Flammability

Not all fuel air mixtures will burn or explode; flames can propagate through fuel air mixtures only within certain limits of composition. If small amounts of combustible fuel gas or vapor are gradually added to air, a point will be reached at which the mixture just becomes flammable. The percentage of fuel gas at this point is called the lower flammable limit. If more fuel is added, another point will eventually be reached at which the mixture will no longer burn. The percentage of fuel gas at this point is called the upper flammable limit [13]. Overall, these limits represent the maximum and minimum fuel concentrations that produce combustible mixtures.

2.4.2.5 Smoke Point

Probably, the most widely used index of soot-forming tendency is the smoke point (ASTM D 1322). It is determined experimentally by burning the fuel under test in a special wick lamp and slowly increasing the height of the flame until it begins to smoke. The maximum height of smokeless lame in millimetres is the smoke point; the higher this is, the tendency of the fuel to soot formation is lower. This applies to kerosene or kerosene-based fuels.

2.4.3 Stoichiometric Combustion

To balance a chemical reaction, the number of atoms on the reactant side must be equal to the number on the product side. A stoichiometric mixture contains the precise amount of fuel and oxidizer needed so that, after combustion, all the fuel and oxidizer are fully

consumed, resulting in the formation of products. This ideal mixture typically produces the highest flame temperature because all the energy released during combustion is used to heat the products. In this case, combustion of hydrocarbon fuel requires sufficient amount of air to convert the fuel completely to CO_2 and H_2O vapor [41]. The equation of a stochiometric reaction is represented by Equation (2.7):

$$C_xH_y + \left(x + \frac{y}{4}\right)(O_2 + 3.76N_2) \Rightarrow xCO_2 + \frac{y}{2}H_2O + \left(x + \frac{y}{4}\right)3.76N_2 \tag{2.7}$$

where air is approximately 20.9% O_2 and 79.1% N_2 by volume (air also has argon, CO_2 and trace amounts of many other species).

Analysing Equation (2.7), it can be verified that for every mole of fuel burned, $4.76(x + \frac{y}{4})$ mol of air is required and $4.76(x + \frac{y}{4}) + \frac{y}{4}$ mol of combustion products are generated. The gas compositions are usually reported in terms of mole fraction, due to the fact this last does not vary with temperature nor pressure, as does the molar concentration. Thus, the product mole fraction (χ) of CO_2, H_2O and N_2, is represented by Equation (2.8), Equation (2.9), Equation (2.10), respectively:

$$\chi(CO2) = \frac{x}{4.76\left(x + \frac{y}{4}\right) + \frac{y}{4}} \tag{2.8}$$

$$\chi(H2O) = \frac{\frac{y}{2}}{4.76\left(x + \frac{y}{4}\right) + \frac{y}{4}} \tag{2.9}$$

$$\chi(N2) = \frac{x + \frac{y}{4}}{4.76\left(x + \frac{y}{4}\right) + \frac{y}{4}} \tag{2.10}$$

Stoichiometric mixture contains sufficient amount of oxygen for complete combustion but the combustion process can also take place when there is excess (fuel lean) or deficiency of the oxygen (fuel rich). The deficiency of the oxygen result in incomplete combustion because there is insufficient amount of oxygen to fully oxidize the fuel ingredients carbon (C) and hydrogen (H) to CO_2 and H_2O. During incomplete combustion are formed such components as CO and UHC. In general, the combustion process in gas turbines continues with the excess of air, thus the exhaust gases consist primarily of such combustion product as CO_2, H_2O, O_2 and N_2 [42].

For example, the stoichiometric combustion of the main combustible of natural gas (methane) takes place according to the Equation (2.11):

$$CH_4 + 2(O_2 + 3.76N_2) \Rightarrow 1CO_2 + 2H_2O + 3.76N_2 \tag{2.11}$$

So, on a stoichiometric combustion of 1 mol of methane the amount of combustion air needed is 2 moles of O_2 plus 2 x 3.76 moles of N_2. Furthermore, it is produced from the combustion 1 mol of CO_2, 2 mol of H_2O and 3.76 mol of N_2 [43].

2.4.4 Methods of Quantifying Fuel and Air Content of Combustible Mixtures

In practice, fuels are often combusted with an amount of air different from the stoichiometric ratio. If less air than the stoichiometric amount is used, the mixture is described as fuel rich. If excess air is used, the mixture is described as fuel lean. For this reason, it is convenient to quantify the combustible mixture using one of the following commonly used methods [44].

2.4.4.1 Fuel-Air Ratio (FAR)

The fuel-air ratio is given by the Equation (2.12):

$$FAR = \frac{m_f}{m_a} \tag{2.12}$$

where m_f and m_a are the respective masses of the fuel and ir. For a stoichiometric mixture, Eq. 2.13 becomes:

$$FAR_s = \frac{M_f}{\left(x + \frac{y}{4}\right) 4.76\, M_a} \tag{2.13}$$

where M_f and M_a are the molecular weight of fuel and air, respectively. The range of FAR is bounded by zero and infinite. Most hydrocarbon fuels have a stoichiometric FAR in the range of 0.05–0.07. The air-fuel ratio (AFR) is also used to describe a combustible mixture and is simply the reciprocal of FAR, as $AFR = \frac{1}{FAR}$ [27].

2.4.4.2 Equivalence Ratio (ϕ)

The equivalence ratio is the actual fuel-air ratio divided by the stoichiometric fuel-air ratio, given by Equation (2.14):

$$\phi = \frac{FAR}{FAR_s} \tag{2.14}$$

Thus, for all fuels, ϕ = 1 denotes a stoichiometric mixture. Also, for all fuels, a value of ϕ < 1 indicates a lean mixture, whereas a value of ϕ > 1 indicates a rich mixture [13]. Similar to FAR, the range of ϕ is bounded by zero and infinite corresponding to the limits of pure air and fuel respectively [44].

An alternative variable based on AFR is frequently used and is called excess air coefficient (λ). λ is the ratio of the actual air-fuel ratio to the stoichiometric air-fuel ratio defined as:

$$\lambda = \frac{AFR}{AFR_s} = \frac{1}{\phi} \tag{2.15}$$

λ of stoichiometric mixtures is 1. For rich mixtures, λ is less than 1; for lean mixtures, λ is greater than 1 [44].

2.4.4.3 Percent Excess Air (%EA)

The amount of air in excess of the stoichiometric amount is called excess air. The percent excess air, %EA, is defined as:

$$\%\text{EA} = \frac{AFR - AFR_s}{AFR_s} \times 100 = \frac{1-\phi}{\phi} \times 100 \tag{2.16}$$

For example, a mixture with %EA equal to 50 contains 150% of the theoretical (stoichiometric) amount of air.

2.4.5 Enthalpy of Formation, Absolute Enthalpy, and Enthalpy of Combustion

In combustion processes, reactants are consumed to form products and energy is released. This energy comes from a rearrangement of chemical bonds in the reactants to form the products. The standard enthalpy of formation, $\Delta h_{f,i}^0$, quantifies the chemical bond energy of a chemical species at standard conditions. The enthalpy of formation of a substance is the energy needed for the formation of that substance from its constituent elements at Standard Temperature and Pressure (STP) conditions ($25^{\circ}C$ and 1 atm) [44]. The enthalpy of formation of chemical elements in their natural state is conventionally defined as zero. The enthalpy of formation of a substance is negative when the reaction forming that substance from its elements in their natural state releases energy [45].

The sensible enthalpy, $\Delta h_{s,i}$, is defined as the heat evolved in the change between the standard state (T=25ºC , P=1 atm) and the intended state (T, P). The sensible enthalpy at a T temperature is represented by Equation (2.17):

$$\Delta h_{s,i}(T)\left[\frac{J}{K_g}\right] = \int_{T_{ref}}^{T} c_{p,i(T^*)}\, dT^* \tag{2.17}$$

The absolute enthalpy of a substance at a given temperature T can be defined as the sum of the enthalpy of formation, $\Delta h^0_{f,i}$, at STP conditions with the change in sensible enthalpy, $\Delta h_{s,i}$, between the reference temperature and temperature T. The absolute enthalpy is represented by Equation (2.18):

$$h_i(T)\left[\frac{J}{K_g}\right] = \Delta h^0_{f,i}\left(T_{ref}\right) + \Delta h_{s,i}(T) \tag{2.18}$$

Once defined the absolute enthalpy of a substance, it is possible to define the absolute enthalpy of the reactants (h_{react}) and the absolute enthalpy of the products (h_{prod}). It is calculated by the sum of the absolute enthalpy values of all reactants and of all products, respectively [46].

The enthalpy of reaction, ΔH_R, or combustion enthalpy in case of combustion reactions, consists in the heat released when a fuel (usually a hydrocarbon) reacts with an oxidant to yield the combustion products. This amount of heat can be calculated relating the absolute enthalpies of the reactants and products as shown by Equation 2.19:

$$\Delta H_R(\mathrm{T}) = h_{prod}(T) - h_{react}(T) \tag{2.19}$$

2.4.6 Adiabatic Flame Temperature

Flame temperature is perhaps the most important property in combustion because it has a controlling effect on the rate of chemical reaction [13]. For a combustion process that takes place adiabatically with no shaft work, the temperature of the products is referred to as the adiabatic flame temperature. The adiabatic flame temperature is a measure of the maximum temperature that could occur in a combustion process. In the absence of dissociation, the maximum adiabatic flame temperature for a given fuel and oxidizer combination occurs with a stoichiometric mixture. The adiabatic flame temperature is a strong function of the air-fuel ratio and of the temperature of the reactants. The amount of excess air can be tailored as part of the design to control the adiabatic flame temperature [40]. In gas turbines, where the maximum permissible temperature is defined by metallurgical considerations in the turbine, close control of the temperature of the products is essential [47].

In combustion studies, two types of adiabatic flame temperature can be used, depending on how the process is completed. These are constant volume and constant pressure.

However, in this work, only the combustion at constant pressure is relevant, as gas turbine combustors operate in this condition [46].

To calculate the adiabatic flame temperature of a combustion reaction, since it's an adiabatic process, ΔH_R is zero. So, the adiabatic flame temperature can be determined by equating the absolute enthalpy of the products at the adiabatic temperature, T_{ad}, to the absolute enthalpy of the reactants at temperature before being burnt T_1,considering the same pressure for both, as shown by Equation (2.20):

$$h_{prod}(T_{ad}, P_1) = h_{prod}(T_1, P_1) \tag{2.20}$$

In a practical situation, the temperature of the combustion products is generally lower than the adiabatic flame temperature due to heat losses by conduction, convection, or radiation to the surroundings of the reactive system [46].

2.5 Emissions

Pollutant emissions from combustion processes have become of great public concern due to their impact on health and the environment. The past decade has witnessed rapid changes both in the regulations for controlling gas turbine emissions and in the technologies used to meet these regulations. Gas turbines have become firmly established as prime movers in the gas and oil industry, and have acquired new ranges of application in combined cycle plants and in many areas of utility power generation. All these developments have been accompanied by continuous and increasing pressure on the combustion engineer to reduce pollutant emissions [13].

2.5.1 Pollutant Species

The concentration levels of pollutants in gas turbine exhausts can be related directly to the temperature, time, and concentration histories of the combustion process. These vary from one combustor to another and, for any given combustor, with changes in operating conditions [13]. There are two distinct categories. The major species (CO_2) are present in percent concentrations. The minor species such as CO, UHC, NOx, SOx, and particulate matter are present in parts per million concentrations [48]. The effects of these pollutant species are presented in Table 2.1. For the large number of engines burning natural gas, the emissions of UHC, particulate matter, and SOx are negligibly small, and most of the drive toward more stringent regulations for stationary gas turbines has been directed at

NOx [13]. The nature of pollutant formation is such that the concentrations of CO and UHC are highest at low power conditions (relative low temperature and pressure) and diminish with an increase in power [9]. By contrast, NOx and smoke are fairly insignificant at low-power settings and attain maximum values at the highest power condition [13].

Table 2.1: Principal Pollutants Emitted by Gas Turbines [13]

Pollutant	Effect
Carbon monoxide (CO)	Toxic
Unburned hydrocarbons (UHC)	Toxic
Particulate matter (C)	Visible
Oxides of nitrogen (NO_x)	Toxic, precursor of chemical smog, depletion of ozone in stratosphere
Oxides of sulfur (SO_x)	Toxic, corrosive

2.5.1.1 Carbon Monoxide

In hydrocarbon combustion, CO is the major intermediate species before CO_2 is formed. As such, a substantial amount of CO is formed once the fuel and intermediate hydrocarbon fragments are consumed. Oxidation of CO to CO_2occurs in the late stages of a combustion process, and it produces a large amount of heat [44].

The CO oxidation mechanism is really basic and consists of, represented by Equation (2.21) and Equation (2.22):

$$CO + O + M \Rightarrow CO_2 + M \quad (2.21)$$

$$CO + O_2 \Rightarrow CO_2 + O \quad (2.22)$$

When a combustion zone is operating fuel-rich, large amounts of CO are formed owing to the lack of suficient O_2 to complete the reaction to CO_2 [13].

The rate of both these CO oxidation reactions are quite small at normal combustion temperartures. Thus, CO oxidation rate in hydrogen-free environments is very slow. However, if H atoms are present, even in small amounts, the CO oxidation mechanism becomes stronglyreactive, through the following reactions [47]:

$$CO + OH \Rightarrow CO_2 + H \quad (2.23)$$

$$CO + HO_2 \Rightarrow CO_2 + OH \quad (2.24)$$

The reaction represented by Equation (2.24) is rarely as important as reaction represented by Equation (2.23), although at very high pressures or in the initial stage of

hydrocarbon oxidation, the high hydroperoxyl radical (HO_2) concentration can make it competitive. All hydrocarbon oxidation eventually involves H_2 and CO oxidation kinetics and most of the CO_2 produced results from Equation (2.23) [47].

In practice, CO emissions are found to be much higher than predicted from equilibrium calculations and to be highest at low-power conditions, where burning rates and peak temperatures are relatively low. This is in conflict with the predictions of equilibrium theory, and it suggests that much of the CO arises from incomplete combustion of the fuel [13].

2.5.1.2 Unburned Hydrocarbons

UHC include fuel that is released in the form of vapor or droplets from the combustor, as well as the products of the parent fuel's thermal breakdown into species with a lower molecular weight. They are typically linked to insufficient burning rates, poor atomization, the chilling effects of film-cooling air, or any combination of these. The dynamics of UHC development are more intricate than those of CO formation, but generally speaking, the same factors that affect CO emissions also affect UHC emissions [13].

2.5.1.3 Oxides of Nitrogen

Formation mechanism of oxides of nitrogen has been a topic of intensive research for many decades. The importance of this mechanism stems from the fact that nitrogen oxides are one of the principal contaminants emitted by combustion processes [47].

Most of the nitric oxide (NO) formed in combustion subsequently oxidizes to nitrogen dioxide (NO_2) in the cold regions of a combustor [13,28]. For that reason, the term NOx, refers to the sum NO and NO_2 [49]. NOx is produced through four main pathways: thermal NO (Zel'dovich Mechanism), prompt NO (Fenimore Mechanism), N_2O route and Fuel NO [45]. Only the first three mechanisms will be explained, since are the most relevant for this work.

Thermal NO (Zel'dovich Mechanism)

This is produced by the oxidation of atmospheric nitrogen in high-temperature regions of the flame and in the post flame gases. The process is endothermic and it proceeds at a significant rate only at temperatures above around 1850 K, being a strong function of the

temperature. Most of the proposed reaction schemes for thermal NO utilize the extended Zel'dovich mechanism (A. N. Hayhurst and I. M. Vince [50]) [13]:

$$O_2 \leftrightharpoons 2O, \tag{2.25}$$

$$N_2 + O \leftrightharpoons NO + N, \tag{2.26}$$

$$N + O_2 \leftrightharpoons NO + O, \tag{2.27}$$

$$N + OH \leftrightharpoons NO + H \tag{2.28}$$

NO formation is found to peak on the fuel-lean side of stoichiometric. This is a consequence of the competition between fuel and nitrogen for the available oxygen. Although the combustion temperature is higher on the slightly rich side of stoichiometric, the available oxygen is then consumed preferentially by the fuel [13].

Prompt NO (Fenimore)

C. P. Fenimore [51] discovered that some NO was promptly produced at the flame front by the presence of CH radicals, an intermediate species produced only at the flame front at relatively low temperature [44]. Numerous studies have shown that prompt NO in hydricarbon flames is formed primarily by a reaction sequence that is indicated by the rapid reaction of hydrocarbon radicals (CH, CH_2, C_2, C) with molecular nitrogen, leading to formation of amines of hydrocyanic acid (HCN) that subsequently reacts to form NO [47]. The following reactions are considered principal reactions, although there migh also be other reactions:

$$CH + N_2 \Rightarrow HCN + N \tag{2.29}$$

$$CH_2 + N_2 \Rightarrow HCN + NH \tag{2.30}$$

$$CH_2 + N_2 \Rightarrow H_2CN + N \tag{2.31}$$

$$HCN + N \Rightarrow \cdots \Rightarrow NO \tag{2.32}$$

Also, N atoms generated from Equations (2.29) (2.31) can react with O_2 to produce NO or can react further with hydrocyanic acid (HCN) leading to NO via a series of intermediate steps [44].

N_2O Route

When the engine is running in fuel lean mixture, nitrogen oxides like N_2O are crucial. Research shows that N_2O is a very short-lived species in hot combustion gasses [44]. In

the presence of a third body, Z, O atoms attacks N_2 forming N_2O, as described by Equation (2.33):

$$N_2 + O + Z \Rightarrow N_2O + Z \tag{2.33}$$

Then N_2O may subsequently react with O atoms to form NO, as described by Equation (2.34):

$$N_2O + O \Rightarrow NO + NO \tag{2.34}$$

2.5.1.4 Soot formation (Smoke)

In fuel-rich areas of the flame which are, in typical combustors, always near the fuel spray inlet split soot particles are what produce exhaust smoke. These are the regions in which recirculating burned products move upstream toward the fuel injector, and local pockets of fuel vapor become enveloped in oxygen-deficient gases at high temperature. In these fuel-rich zones, soot may be produced in considerable quantities [1]. Soot deposits affect an engine's mechanical and thermal performance. The soot distribution has a direct impact on a flame's temperature field and heat radiation [44].

Agglomerates with sizes as large as several hundred nanometres constitute soot. Their main particles are round and have a fine structure. The decomposition of fuel molecules in the rich area of flames results in the synthesis of polycyclic aromatic hydrocarbons, which is the first step in the formation of soot [44]. Exhaust gas soot is mostly composed of carbon (96%) and a combination of hydrogen, oxygen, and other components, according to analysis. Except at mixture strengths far richer than those used in the main zones of gas turbines, soot is not an equilibrium result of combustion. Thus, it is impossible to predict its rate of formation and final concentration from kinetic and thermodynamics data [13].

Soot creation in internal combustion engines is significantly more complex and difficult to study, unlike the formation of nitric oxides is widely understood. The process of soot particle generation in diesel sprays is so quick and complex that it is still not fully understood [44].

2.5.1.5 Oxides of sulfur

Oxides of sulfur, primarily sulfur dioxide (SO_2) and sulfur trioxide (SO_3), are another pollution of concern when stationary engines use residual fuels. These pollutants are created when sulfur-containing compounds in the fuel react with oxygen in the

combustion air. They are corrosive and dangerous, and they cause sulfuric acid to develop in the atmosphere. The only practical limitation technique is to remove sulfur from fuel before combustion occurs since almost all of the sulfur in fuel is converted to SOx [13].

2.6 Chemical Kinetics

Chemical kinetics deals with the quantitative study of the rates of chemical reactions and of the factors (such as temperature, pressure, concentrations of chemical species) upon which they depend. It also deals with the interpretation of the empirical kinetic laws in terms of reaction mechanisms, describing the governing chemical pathways from reactants to products. In order to develop a model, both experimental studies of reaction rates and theorical models are taken into account to predict the outcome [47]. The fuel combustion kinetics are essential to create a model that enables an accurate emission projection from the combustion. The large-scale utilization of biogas in burning facilities necessitates a much better understanding of its kinetic behaviour which is a necessary condition for generating trustworthy predictions [1].

There are several natural gas/biogas kinetic models available and some conditions must be applied during the processing of choosing the kinetic model. The approach of utilizing CFD simulation to predict gas turbine emissions, and more especially NOx, requires first determining a natural gas/biogas kinetic mechanism that permits simulating the combustion process and then one that accurately predicts the creation of NOx. Because kinetic model CFD requires expensive computing resources, additionally, there must be a limit on the number of species in the kinetic scheme. As there are many models, which fulfil the conditions, the choice of the model was based on the study done by Fischer et al [52]. This study focused on evaluating the ignition delay times of biogas combustion through simulations, where CO and NO emissons were evaluated, as well. To achieve this, the authors tested five different chemical reaction mechanisms: GRI 3.0 (G. Smith et al [53]), DRM 22 (A. Kazakov et al [54]), Heghes mechanism (C. I. Heghes[55]), Frenklach mechanism (M. Frenklach et al [56]), and the NUIG mechanism (S. Martinez et al. [57]) Each of these mechanisms has been developed to model the combustion of hydrocarbons, with a particular emphasis on methane, the main component of biogas. It was concluded that the GRI 3.0 mechanism is the most reliable for modelling biogas combustion overall, particularly when hydrogen is not significantly present in the biogas. Since the biogas composition used in this study does not contain hydrogen, the GRI 3.0

reaction mechanism can be confidently applied to simulate biogas combustion. The Gri 3.0 contains 325 reactions and 53 species [53]. Furthermore, provides sub-mechanisms to cover all the relevant NOx pollutant species and its different pathways, mentioned in section 2.5.1.3.

2.7 Bibliographic Review

This review aims to synthesize existing research on the natural gas/biogas combustion in gas turbines. It covers the thermodynamic performance of biogas-fuelled turbines, emissions profiles, and the implications for efficiency and power output. Furthermore, the review examines advancements in gas turbine technology that enhance compatibility with biogas. By assessing these developments, the review provides insights into the feasibility of biogas as a sustainable fuel for gas turbines and its potential role in the future energy landscape.

Experimental studies

A study conducted by A. Wresta and A. Saepudin [58] presented significant findings regarding the combustion characteristics of biogas, particularly focusing on the effects of varying methane content and air equivalence ratios. The simulation was done in the possibly range of methane content for biogas from 20 to 100% and air equivalence ratio from 1 to 3. The results indicated that the maximum temperature of the combustion products is highly dependent on the methane concentration in the biogas. Specifically, when the methane content is at 20%, the maximum temperature can exceed 700 °C, while at 100% methane content, it can reach more than 1900 °C. This demonstrates a clear correlation between higher methane levels and increased combustion temperatures, which is crucial for optimizing energy output from biogas. Furthermore, the study reveals that the air biogas equivalence ratio plays a critical role in determining the combustion efficiency and temperature. As the equivalence ratio increases, the amount of excess oxygen and inert nitrogen in the combustion products also rises, which subsequently leads to a decrease in the maximum temperature achieved. For instance, at a methane content of 50% and an equivalence ratio of 1, the maximum temperature can reach up to 1700 °C, but this temperature significantly drops to below 1195 °C when the equivalence ratio is increased to 2. This finding underscores the importance of balancing the air-fuel mixture to achieve optimal combustion conditions. The findings suggest that

careful management of these parameters can enhance the efficiency of biogas combustion, making it a more viable renewable energy source.

Other study done by H. Seliger-Ost et al [59] revealed significant insights into the performance and emissions characteristics when utilizing biogas as a fuel source. The experimental investigation focused on the fuel flexibility of a 3 kW electrical micro gas turbine combined heat and power system, specifically examining the impact of biogas, which consists of natural gas mixed with up to 50 vol.-% carbon dioxide. The study was conducted under atmospheric conditions. The results indicated that the combustor could be stably operated across all stationary load points with both natural gas and biogas mixtures, demonstrating its adaptability to varying fuel compositions. The research highlights that the combustor maintained low emissions, with NOx levels in the single-digit range. While an increase in CO_2 content in the fuel led to slightly higher CO emissions, it also resulted in a significant reduction in NOx emissions, particularly at high adiabatic flame temperatures. This finding suggests that the addition of CO_2 can enhance the environmental performance of the combustor. Overall, the study confirms the combustor's capability to operate efficiently with biogas, emphasizing its potential for use in sustainable energy systems.

The study performed by I. Sivri et al [60] focused on the combustion and emission characteristics of biogas mixtures. Three mixtures of biogas were used in this study BG1, BG2 and BG3, respectively with 70%, 55%, 45% of CH_4 and 30% 45% and 55% of CO_2. The key factor influencing these biogases was the varying concentration of CO_2 in the biogas mixtures. Biogas mixtures with higher CO_2 content, such as the BG3 mixture, demonstrated significantly lower combustion temperatures. This occurred because CO_2 acts as an inert gas during combustion, absorbing heat and inhibiting the flame. As a result, the overall temperature within the combustion chamber was reduced. In contrast, biogas mixtures with a higher concentration of CH_4 , like the BG1 mixture, achieved much higher flame temperatures. This highlighted the importance of methane in maintaining higher combustion temperatures and improving the efficiency of the combustion process. The study also found that CO_2 emissions varied depending on the biogas composition. Surprisingly, the BG3 mixture, despite having the highest CO_2 content, emitted less CO2 during combustion compared to other mixtures. This outcome was attributed to the lower combustion temperature of BG3, which slowed down the conversion of CO to CO_2, leading to lower overall CO_2 emissions. Conversely, the biogas mixtures with higher combustion temperatures, such as BG1, emitted more CO_2 due to the more complete oxidation of CO. In terms of carbon monoxide emissions, the study found that biogas mixtures with lower methane content, like BG2 and BG3, produced

higher levels of CO. This was a result of the lower combustion temperatures and less efficient combustion processes in these mixtures, which led to incomplete oxidation of carbon atoms. The CO emissions were particularly high in the flame region, where incomplete combustion was most prevalent.

Numerical studies

CFD has been verified and validated over past decades to be a powerful design tool in industries where experimental work can be costly, hazardous and time consuming, to support the design and development process. With recent developments in processor speeds and solver improvements, CFD has been successfully validated and used as a tool for optimizing combustor technology.

N. Ghenai and N. Janajreh [61], aimed to investigate numerically the combustion of natural gas and biogas in a gas turbine can combustor. Natural gas, anaerobic digester biogas, landfill biogas and natural gas/biogas fuels combustion in gas turbine can combustor are presented in this study. The effect of the biogas fuel composition, and fuel heating values on flame shape, flame temperature, CO_2, CO and NOx emissions was determined in this study. The turbulence in the combustion process is modeled using the standart $k-\varepsilon$ model, for non-premixed gas combustion it was utilized the chemical equilibrium with the Probability Density Function (PDF) model and the P-1 radiation model is employed to simulate radiation effects from the flame during combustion. The results showed lower flame temperatures for the biogas and biogas/natural gas mixtures compared to the adiabatic flame temperature of natural gas. The flame temperature for biogas fuel combustion depends on the carbon dioxide to methane ratio. The peak flame temperature decreases by 37% and 22%, respectively for the biogas-landfill (CO_2/CH_4 = 0.89) and biogas anaerobic digester (CO_2/CH_4 = 0.54) compared to natural gas fuel. The presence of inert gas (CO_2) with methane cools down the reaction by absorbing energy from the combustion and modifies the reaction zone by reducing the burning velocity of the flame and the burning rate. The emissions from biogas combustion vary with the composition of biogas. The higher CO_2 percentage in the biogas fuel, the lower is the NOx emissions and the higher is the CO_2 emissions at the exit of the combustor. The CO emissions also decrease by increasing the CO_2/CH_4 ratio of the biogas fuel.

A study conducted by X. Chen et al [62] focused on a numerical analysis of combustion in a micro gas turbine (MGT) annular type combustor using methane/biogas fuels, focusing on the effects of CO_2 content in the fuel and the excess air coefficient (1.5 to 3) on combustion performance. To model the turbulence was used the Re-Normalization

Group (RNG) k – ε model. The results indicated that as the CO_2 proportion in the fuel increased, there was a reduction in the overall temperature within the combustion chamber, which led to a decrease in NO and CO emissions. However, this also resulted in an increase in fuel flow rate and pressure drop within the combustion chamber, which requires stronger materials to maintain the thermal load of the MGT. Additionally, the analysis of the excess air coefficient revealed that an increase in this parameter leads to a decrease in average outlet temperature. The emissions of pollutants such as CO and NO showed different trends, with CO concentration first decreasing and then increasing as the excess air coefficient increased, while NO concentration continuously decreased.

Chapter 3 - Methodology, Modelling and Computation

The study of systems involving fluid flow, heat transport, and related phenomena including chemical reactions using computer-based simulation is known as computational fluid dynamics, or CFD. The method is quite effective and covers a broad spectrum of both industrial and non-industrial use cases [63].

In this work, it was used ANSYS Fluent 2023 R2 to model the flow of fluids, heat transport, and fluid-structure interactions. Many sectors, including the aerospace, automotive, chemical, and many more, utilize ANSYS Fluent extensively. The finite volume approach is used by ANSYS Fluent to solve the fluid flow and heat transfer governing equations. To achieve this, the simulation's domain is divided into a number of tiny, linked control volumes, or cells. At the centroids of these cells, the values of the variables (such as temperature and velocity) are then computed. Iterative techniques are used by ANSYS Fluent to solve these equations and produce a convergent solution [64].

To properly set up and solve a case of study, it will be needed to follow a few steps to achieve a solution. The process includes:

- Design and model the geometry;
- Generate a mesh;
- Set up the solver and physical models (turbulence models, material properties, boundary conditions);
- Compute and monitor the solution;
- Analyse the solution and consider revisions to the numerical or physical model parameters, if necessary.

3.1 Numerical Modelling

3.1.1 Turbulence Modelling

Almost all fluid flow which we encounter in daily life is turbulent. Airplanes, automobiles, and buildings are examples of bluff bodies that create turbulent boundary layers and wakes. Also, the combustion in piston engines, gas turbines and combustors are a highly turbulent process. There is no definition on turbulent flow, but it has a number of characteristic features, such as [65]:

- Irregularity – The turbulent flow is irregular and chaotic;
- Diffusivity - The diffusivity increases in turbulent flow. The momentum exchange increases by the turbulence. In internal flows, such those in pipes and channels, the higher diffusivity also results in an increase in heat transmission and resistance (wall friction);
- Large Reynolds Numbers - When the Reynolds number is high, turbulent flow happens. For instance, a transition to turbulent flow happens in boundary layers at $Re_x \simeq$ 500 000 and in pipes at $Re_D \simeq$ 2300;
- Three Dimensional - Turbulent flow is always three-dimensional and unsteady;
- Dissipation - Because of the dissipative nature of turbulent flow, the kinetic energy contained in the small eddies is converted to thermal energy. Slightly bigger eddies provide the kinetic energy to the smaller eddies. Larger eddies receive energy from slightly larger eddies, and so on. The mean flow provides the energy source for the largest eddies. The term "cascade process" refers to this flow of energy from the biggest turbulent scales (eddies) to the tiniest.

Turbulent flows are characterized by fluctuating velocity fields. These fluctuations mix transported quantities such as momentum, energy, and species concentration, and cause the transported quantities to fluctuate as well [64]. Eddies with a wide range of length and time scales that interact in a dynamically complicated manner develop in the flow due to turbulence [63]. Since these fluctuations can be of small scale and high frequency, they are too computationally expensive to simulate directly in practical engineering calculations [64].

Given the importance of the avoidance or promotion of turbulence in engineering applications, it is no surprise that a substantial amount of research effort is dedicated to the development of numerical methods to capture the important effects due to turbulence [63]. Through these numerical methods there are three main approaches.

Direct Numerical Simulation (DNS) compute the mean flow and all turbulent velocity fluctuations. The unsteady Navier–Stokes equations are solved on spatial grids that are sufficiently fine that they can resolve the Kolmogorov length scales at which energy dissipation takes place and with time steps sufficiently small to resolve the period of the fastest fluctuations. These calculations are highly costly in terms of computing resources, so the method is not used for industrial flow computations [63]. For the current computational capacities, DNS is applicable only to relatively simple flow problems at low Reynolds numbers [66].

Instead of DNS, two alternative methods can be employed to render the Navier-Stokes equations tractable so that the small-scale turbulent fluctuations do not have to be directly simulated: Reynolds-averaging (or ensemble-averaging) and filtering. Both methods introduce additional terms in the governing equations that need to be modelled in order to achieve a "closure" for the unknowns [64]. The two alternatives' models referred are the Reynolds Average Navier-Stokes (RANS) simulation and the Large Eddy Simulation (LES). A comparison of all models referred is shown by the Figure 3.1.

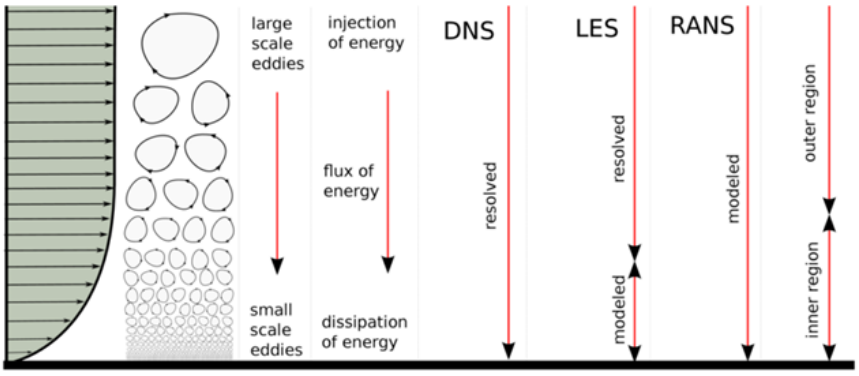

Figure 3.1: Turbulent models approach [67]

It is not essential to resolve the specifics of the turbulent fluctuations for the majority of engineering objectives. Users of CFD are generally satisfied with the information provided on the flow's time-averaged characteristics. As a result, the Reynolds-averaged Navier-Stokes (RANS) equations have formed the basis for the great majority of turbulent flow computations [63]. The RANS approaches consist of solving the governing equations in terms of mean variables and by modelling the turbulent quantities. Depending on the degree of approximation of these quantities, there are algebraic models, models with one equation, for example Spalart-Allmaras), models with two equations (for example $k-\varepsilon$, $k-\omega$, etc.), four equation models ($v2-f$), seven-equation models (RSM). They have the advantage of being more economical from the point of view of computing resources, but less precise than the DNS, because all of them have certain terms modelled [67].

LES provides an alternative approach in which large eddies are explicitly computed (resolved) in a time-dependent simulation using the "filtered" Navier-Stokes equations. The rationale behind LES is that by modelling less of turbulence (and resolving more), the error introduced by turbulence modelling can be reduced. It is also believed to be easier to find a "universal" model for the small scales, since they tend to be more isotropic

and less affected by the macroscopic features like boundary conditions, than the large eddies. Filtering is essentially a mathematical manipulation of the exact Navier-Stokes equations to remove the eddies that are smaller than the size of the filter, which is usually taken as the mesh size when spatial filtering is employed as in Ansys Fluent. Like Reynolds-averaging, the filtering process creates additional unknown terms that must be modelled to achieve closure. LES for high Reynolds number industrial flows requires a significant number of computational resources [64].

There is no perfect turbulence model, so as an attempt to unite the supremacies of RANS modelling approach and DNS or LES into a single solution strategy was created the hybrid RANS/LES method (Detached Eddy Simulation (DES) approach), which takes into account the computational accuracy and resource consumption, has been favoured. DES model combines the advantages of RANS and LES, using RANS to calculate the laminar flow area near the wall and LES to calculate the separated flow area on the far wall [68]. The LES region is normally associated with the core turbulent region where large unsteady turbulence scales play a dominant role. In this region, the DES models recover LES like subgrid models. In the near-wall region, the respective RANS models are recovered. The application of DES, however, may still require significant CPU resources and therefore, as a general guideline, it is recommended that the conventional turbulence models employing the Reynolds-averaged approach be used for practical calculations [64].

Taking in account the previous information, it was possible to conclude that it would be chosen a RANS model. Among the RANS models, the $k-\varepsilon$ model was the one chosen. It requires low memory, shows a good convergence and perform well in swirling flows, which is the case. Furthermore, among RANS models it is one of the least computationally expensive. Different variations of the $k-\varepsilon$ model exist such as Standard, Realizable, RNG, each with certain modifications to perform better under certain fluid flow conditions.

3.1.1.1 k-ε Turbulence Models

In order, to assess which variation of the $k-\varepsilon$ model perform better under swirling flows was made some reviews about the performance of the models.

O. A. Marzoukand et al [69] performed a computational study of turbulent swirling flows in a vertical cylindrical combustion chamber. The combustion chamber had a diameter of 198 mm, a primary jet with a diameter of 32 mm and a swirling secondary jet with a

diameter of 64 mm. The primary objective was to simulate and compare the mean velocity components (axial and radial), streamline patterns and recirculation bubble length. The key findings indicated that the standard $k-\varepsilon$ model provides the best agreement with experimental data, especially in predicting the recirculation bubble length, demonstrating the shortest recirculation bubble among the models. The RNG $k-\varepsilon$ model predicted additional tertiary recirculation zones not observed in experiments, indicating a potential over-prediction of flow complexity, offering more detailed flow dynamics but with some discrepancies from experimental data. The realizable $k-\varepsilon$ model produced a longer recirculation bubble with a similar qualitative structure to the standard model, showing good qualitative agreement but differing in the quantitative prediction of the recirculation zone length. Regarding the velocity profiles the standard model had the best overall performance based on the mean gas-phase velocities. The RNG model showed considerable deviations from the measurements in some regions. The main drawback of the realizable model was its erroneous prediction of the radial velocity. The main differences in the predicted velocity profiles were related to the different flow structures and mean streamlines. The authors conclude that the standard k-ε model had the best performance and compliance with the experimental data. Another author, Norwazan, A.R [70] conducted a numerical analysis of isothermal swirling turbulent flows within a combustion chamber, focusing on the effects of flow axial and tangential velocities to obtain the centre recirculation zone. This combustion chamber had an axial swirler with an outer diameter of 280 mm, the swirler diameter with 73 mm and the length of the combustion chamber was 1000 mm. The swirler adopted into had swirl vane angle of 50^{0}. Regarding the Center Recirculation Zone (CRZ), the standard $k-\varepsilon$ model predicted the smaller CRZ volume compared to RNG $k-\varepsilon$ model provides slightly improved prediction of CRZ. In addition, the realizable k-ε model presented the small of CRZ compared to the standard $k-\varepsilon$ and RNG $k-\varepsilon$ models. Based on overall performances of the $k-\varepsilon$ models, the author concluded that the standard $k-\varepsilon$ model gives more appropriate results and reasonably priced. Since the center recirculation zone was presentend in a good and reasonable shape, which is wide and shorter than others.

In both studies, it was concluded that the standard $k-\varepsilon$ model was the model with the best performance. Even if other $k-\varepsilon$ model had a similar performance, the standart $k-\varepsilon$ model has the least CPU demanding. Taking in account the previous information, the standard $k-\varepsilon$ model was the one chosen among the $k-\varepsilon$ models.

3.1.1.2 Governing equations

The RANS equations govern the transport of the averaged flow quantities, with the whole range of the scales of turbulence being modelled [64]. The flow properties are decomposed the instantaneous variables (for example the velocity components and the pressure) into a mean value and a fluctuating value [65]. The mean value is obtained by time-averaging the variable over a sufficiently long period of time, while the fluctuating component represents the deviation from the mean at any given instant.

The Reynolds Averaged Navier-Stokes equations can be written in cartesian tensor form as [71]:

- Continuity:

$$\frac{\partial \bar{p}}{\partial t} + \frac{\partial}{\partial x_i}(\bar{p}\tilde{u}_i) = 0 \tag{3.1}$$

- Momentum:

$$\frac{\partial}{\partial t}(\bar{p}\tilde{u}_i) + \frac{\partial}{\partial x_j}(\bar{p}\tilde{u}_i\tilde{u}_j) - \frac{\partial}{\partial x_j}(\overline{pu_i''u_j''}) - \frac{\partial}{\partial x_j}\left[\mu\left(\frac{\partial \tilde{u}_i}{\partial x_j} + \frac{\partial \tilde{u}_j}{\partial x_i} - \frac{2}{3}\delta_{ij}\frac{\partial \tilde{u}_i}{\partial x_i}\right)\right] = -\frac{\partial \bar{p}}{\partial x_i} \tag{3.2}$$

- Scalar Transport:

$$\frac{\partial}{\partial t}(\bar{p}\tilde{Y}_\alpha) + \frac{\partial}{\partial x_i}(\bar{p}\tilde{u}_i\tilde{Y}_\alpha) + \frac{\partial}{\partial x_i}(\overline{pu_i''Y_\alpha''}) - \frac{\partial}{\partial x_i}\left(\Gamma_\alpha\frac{\partial \tilde{Y}_\alpha}{\partial x_i}\right) = \widetilde{\omega}_\alpha \tag{3.3}$$

These equations are formally identical to the Navier-Stokes equations with the exception of the additional term:

$$\tau_{Re} = -(\overline{pu_i''u_j''}) \tag{3.4}$$

which constitutes the so-called Reynolds-stress tensor. It represents the transfer of momentum due to turbulent fluctuations [66].

In laminar flow, the fluid stress is proportional to the rate of strain with the viscosity being a constant of proportionality [71]. In turbulent flow, the Reynolds stress is related to the mean rate of strain through turbulent viscosity (μ_T). This is the so called Boussinesq's hypothesis, and is represented in Equation (3.5):

$$-(\overline{pu_i''u_j''}) = \mu_T\left(\frac{\partial \tilde{u}_i}{\partial x_j} + \frac{\partial \tilde{u}_j}{\partial x_i}\right) - \frac{2}{3}\delta_{ij}\left(\bar{\rho}k + \mu_T\frac{\partial \tilde{u}_k}{\partial x_k}\right) \tag{3.5}$$

The Boussinesq hypothesis is used in the $k-\varepsilon$ models. The advantage of this approach is the relatively low computational cost associated with the computation of the turbulent

viscosity, μ_T. In the case $k-\varepsilon$ models, two additional transport equations (for the turbulence kinetic energy, k, and either the turbulence dissipation rate, ε, are solved, and μ_T is computed as a function of k and ε. The disadvantage of the Boussinesq hypothesis as presented is that it assumes μ_T is an isotropic scalar quantity, which is not strictly true [64].

3.1.1.3 Regime of Turbulent Combustion

In order to derive models for turbulent combustion, a physical approach is required. This approach is based on the comparison of the various time scales present in turbulent combustion [71]. The Damköhler number is used in turbulent combustion and corresponds to the ratio of turbulent time scale τ_t and chemical time scale τ_c, through Equation (3.6).

$$D_a = \frac{\tau_t}{\tau_c} \tag{3.6}$$

Damköhler number measures how important is the interaction between chemistry and turbulence. Most combustion models are placed in the extremes of Damköhler [72]. When the Damköhler number is very large ($Da \gg 1$), the flame front is thin and its inner structure is not affected by turbulence, which at most can wrinkle the flame surface. This occurs when the Kolmogorov scales, which are the smallest turbulence scales, have a τ_t greater than τ_c, which means that the turbulent motions are too slow to affect the flame structure [73].

3.1.2 Heat Transfer Modelling

The flow of thermal energy from matter occupying one region in space to matter occupying a different region in space is known as heat transfer. Heat transfer can occur by three main methods: conduction, convection, and radiation. Physical models involving conduction and/or convection only are the simplest and radiation models are more complex [64]. Radiative heat transfer is often neglected in CFD calculations, because the majority of engineering problems are dominated by high rates of convective heat transfer. There are, however, several practically important categories of problems where radiative heat transfer should be considered, there is usually vigorous convection in combustors, but the chemical reactions generate operating temperatures that are sufficiently high for radiative heat fluxes to be of similar order of magnitude [63].

Over the years many methods have been developed for the solution of radiative heat transfer. These include various analytical approximation techniques and a suite of numerical methods [63]. The main types of Radiative Transfer Equation (RTE) solution are Discrete Ordinates Method (DOM), Spherical Harmonics Method (SHM), and the Photon Monte Carlo (PMC) method [74]. Depending on the problem, ANSYS Fluent can solve a variation of the energy equation that takes into account the specified heat transfer methods. The P-1 method is one of the SHM methods, the RTE a diffusion equation, which is easy to solve with little CPU demand. The model includes the effect of scattering. For combustion applications where the optical thickness is large, the P-1 model works reasonably well. In addition, the P-1 model can easily be applied to complicated geometries with curvilinear coordinates. The DOM spans the entire range of optical thicknesses, and allows you to solve problems ranging from surface-to-surface radiation to participating radiation in combustion problems. It also allows the solution of radiation at semi-transparent walls. Computational cost is moderate for typical angular discretization, and memory requirements are modest. The current implementation is restricted to either gray radiation or non-gray radiation using a gray band model. Solving a problem with a fine angular discretization may be CPU-intensive. The PMC model can solve problems ranging from optically thin (transparent) regions to optically thick (diffusion) regions, like combustion. It allows you to calculate quasi-exact solutions. While it is more accurate compared to other available models, it has a higher computational cost [64].

Taking in account all it has been mentioned before, the fact the case in study is a combustion and due to the requirement to decrease the CPU demand, it was decided to use the P-1 model.

3.1.3 Species Modelling

In this work, it will be used the non-premixed combustion model as fuel and oxidizer enter the reaction zone in distinct stream. This is in contrast to premixed systems, in which reactants are mixed at the molecular level before burning. The basis of the non-premixed modelling approach is that under a certain set of simplifying assumptions, the instantaneous thermochemical state of the fluid is related to a conserved scalar quantity known as the mixture fraction, f. The mixture fraction is the mass fraction that originated from the fuel stream. In other words, it is the local mass fraction of burnt and unburnt fuel stream elements (C, H, etc.) in all the species (CO_2 , H_2O, O , etc.) [64]. The mixture fraction can be written in terms of the atomic as shown in Equation (3.7):

$$f = \frac{Z_i - Z_{i,o}}{Z_{i,fuel} - Z_{i,o}} \tag{3.7}$$

Simply put, non-premixed modelling relies on solving the transport equation for mixture fraction(s) (for one or two conserved scalars). Species mass fractions, temperature and density are distinctively dependent upon mixture fraction(s). This combustion modelling method uses pre-processed calculations for chemistry and turbulence interaction by virtue of PDF model (S. Pope [75]) [76]. This model does not involve the solution for individual species (computationally efficient) rather uses predicted mixture fraction fields to deduce species concentrations. In other words, this model simplifies the combustion to a mixing problem. Once mixed, the chemistry can be modelled as being in chemical equilibrium with the Equilibrium model, being near chemical equilibrium with the Steady Laminar Flamelet model (SLFM), or significantly departing from chemical equilibrium with the Unsteady Laminar Flamelet model [64].

3.1.3.1 Steady Laminar Flamelet Model

As a consequence of turbulence, flame experiences stretch and an aerodynamic strain which results in augmented temperature gradients. This leads to higher diffusion rate (heat and radical species leave the flame zone faster) in comparison with reaction rate. Because of this condition, species are left with minimal time to achieve chemical equilibrium (which increases local non equilibrium). In order to predict such moderate chemical non-equilibrium in turbulent flames, steady laminar flamelet model (H. Pitsch and N. Peters [77]) is used [76]. The advantage of the laminar flamelet approach is that realistic chemical kinetic effects can be incorporated into turbulent flames. The chemistry can then be pre-processed and tabulated, offering tremendous computational savings. The steady laminar flamelet approach models a turbulent flame brush as an ensemble of discrete, steady laminar flames, called flamelets. The flamelet concept views the turbulent flame as an ensemble of thin, laminar, locally one-dimensional flamelet structures embedded within the turbulent flow field, as shown in Figure 3.2.

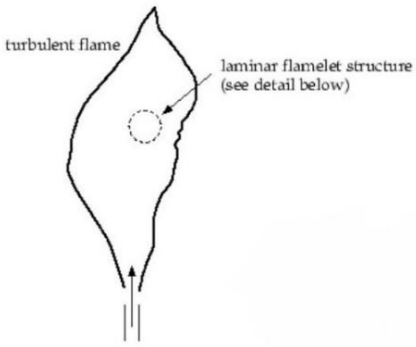

Figure 3.2: Flamelet structure [64]

The individual flamelets are assumed to have the same structure as laminar flames in simple configurations, and are obtained by experiments or calculations. Using detailed chemical mechanisms, ANSYS Fluent can calculate laminar opposed-flow diffusion flamelets for non-premixed combustion. The laminar flamelets are then embedded in a turbulent flame using statistical PDF methods [64]. When selecting the non-premixed model, there are a few options on how the chemical equilibrium will be modelled (state relation option). The SLFM was the one chosen for using in the simulations, as was described earlier.

3.2 Geometry Model

The geometry used is the combustion chamber employed by N. Ghenai and N. Janajreh [61]. Some data regarding the geometry dimensions were not found, so it had to be estimated. Therefore, there may be slight differences in the dimensions. The CAD model of the gas turbine can combustor, as shown in Figure 3.3, was designed using the software CATIA V5. All features of the combustion chamber were designed as surfaces.

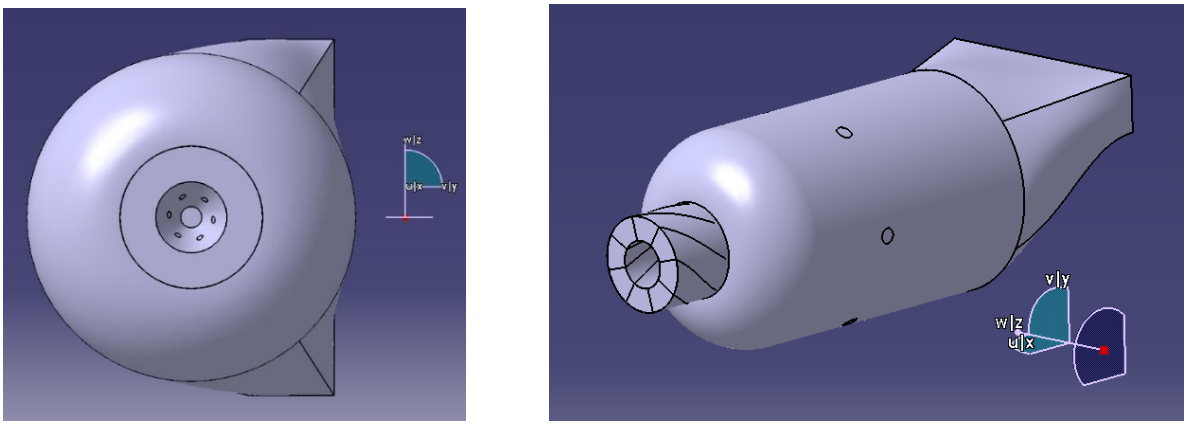

Figure 3.3: Geometry Front view (left) and Isometric view (right)

The size of the combustor is 590 mm in the X direction, 250 mm in the Z direction, and 230 mm in the Y direction. More views of the geometry can be found in Appendix A.

The primary air inlet is guided by vanes with an angle of 60º to give the air a swirling velocity component and it has a diameter of 100 mm. The fuel is injected through six fuel inlets in the swirling primary air flow each with a diameter of 4.2 mm. The secondary air or dilution air is injected at 100 mm from the fuel injector to control the flame temperature and NOx emissions and is injected in the combustion chamber through six side air inlets each with a diameter of 16 mm. The can combustor outlet has a rectangular shape with an area of 0.0150 m^2 (250mm × 60 mm). It's possible to observe the detail of the gas turbine can combustor fuel injectors and swirler in Figure 3.4.

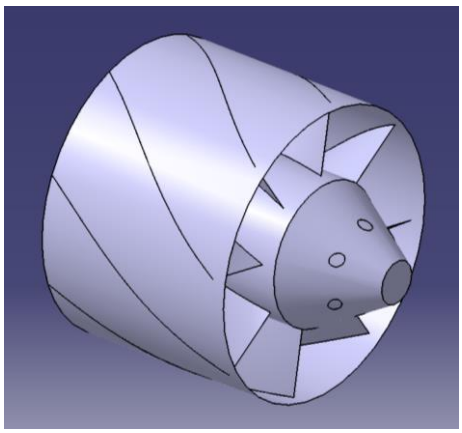

Figure 3.4: Detailed view of the fuel injectors and swirler

As previously mentioned, some dimensions had to be estimated namely:

- Length of the swirler (X direction) (75 mm);
- Length of the vanes (X direction) (70 mm);
- Inner diameter of the primary inlet air (50 mm);
- Length of the fuel injectors cone (30 mm).

3.3 Generation of the Numerical Mesh

During the meshing process the object that has to be simulated is divided into smaller cells, which may precisely determine the object's shape. It is possible to correlate the governing equation with each cell, which facilitates the flow simulation in that discrete area. For that reason, the generation of the model mesh is one of the most important steps in a CFD simulation.

3.3.1 Software choice

In this work, the chosen meshing software among many was the *Fluent Meshing*, because of the following reasons. *Fluent Meshing* uses built-in intelligence and automation to create a high quality CFD mesh using its sophisticated meshing technology, which includes the innovative poly-hexacore meshing (mosaic meshing technology) algorithm, tools for high quality boundary layer mesh generation and parallel meshing. By simplifying the process of mesh generation, the Watertight Geometry workflow enables all users to complete all stages of a CFD simulation, from meshing through to post-processing, entirely within the same software session, in the same single window user environment. Furthermore, *Fluent Meshing* is a friendly user software which allows a quicker learning and navigation into the software [78]. In addition, ANSYS provides advices on best practices for gas turbine combustor meshing using *Fluent Meshing* [79].

3.3.2 Mesh Independence Analysis

A mesh independence study is a study to determine the dependence of the results on the mesh density. In a CFD simulation, a mesh independence study is a mandatory step to obtain an independent mesh, so that the results obtained are the most accurate and correct.

Firstly, it was created the coarser mesh possible that could represent all the features of the geometry and meet the requirements for Y^+ (Standard $k-\varepsilon$ is only valid for fully turbulent flow). Then, this mesh was refined obtaining the intermediate mesh and, finally repeating the previous process from the intermediate mesh obtaining the finer mesh. The meshing process followed to obtain these meshes is described in Appendix B The study was performed with a coarse, intermediate and a fine mesh with 122388 cells, 284059 cells and 479954 cells, respectively, see Table 3.1. The internal structure obtained for the three meshes (in cut view) is shown in the Figure C.1, in Appendix C. For the independence test the fuel used was methane, the boundary conditions and operating conditions were the same used by N. Ghenai and N. Janajreh [61]. The parameters used to analyse the independence of the mesh were:

- The average static temperature of the combustion chamber in the outlet;
- The average velocity magnitude in a defined plane (Plane XY Z=0).

Table 3.1: Values obtained in the mesh independence test

Mesh	Static Temperature [K]	Relative error [%]	Velocity Magnitude [m/s]	Relative error [%]
Coarse	916.41		5.6736	
		0.618		0.282
Intermediate	910.75		5.6576	
		0.0198		0.184
Fine	910.57		5.6472	

Note: The fuel used in the independence tests will not be used in the simulations, since the objective of the independence test is to evaluate the error between the values and not the discussion of the results obtained.

To analyse the independence of the meshes, the relative error between meshes is used in the obtained values. The relative error for two consecutive meshes is obtained by dividing the absolute error of each parameter in study by the value obtained with the finer mesh of these two meshes, as shown in the Equation (3.8).

$$Relative\ Error\ [\%] = \frac{|Value_{\ Coarser\ Mesh} - Value_{Finer\ Mesh}|}{Value_{\ Coarser\ Mesh}} \times 100 \qquad (3.8)$$

Looking at the Table 3.1, it is possible to verify the maximum error occurred to average static temperature of the combustion chamber in the outlet, value of 0.6%, between the values of the coarse and intermediate mesh. Also, the maximum error regarding the velocity magnitude in a defined plane (Plane XY Z=0), value of 0.3%, occurred between the same meshes. Between the intermediate mesh and fine mesh occurred the lowest error for both average static temperature of the combustion chamber in the outlet and average velocity magnitude in a defined plane (Plane XY Z=0) obtaining a value of 0.02% and 0.2% respectively. After analysing these values, the results demonstrate that there is no significant difference between the intermediate and fine mesh results, so it was opted to use the intermediate mesh in this work to save computer power and time.

3.3.3 Mesh quality

The quality of the mesh plays a significant role in the accuracy and stability of the numerical computation. In *Fluent Meshing* it is possible to check the mesh quality using a set of quality metrics, such as skewness cell, orthogonal quality and aspect ratio.

Skewness is defined as the difference between the shape of the cell and the shape of an equilateral cell of equivalent volume. Highly skewed cells can decrease accuracy and destabilize the solution [64]. This parameter has a range from 0 to 1, with 1 being the

worst and 0 being the best, and it is recommended to achieve a maximum skewness below 0.95 [79]. Table 3.2 shows the spectrum of the cell skewness.

Table 3.2: Mesh skewness metrics spectrum [80]

Excellent	Very good	Good	Acceptable	Bad	Unacceptable
0-0.25	0.25-0.50	0.50-0.80	0.80-0.94	0.95-0.97	0.98-1.00

The cell orthogonal quality for cells is computed using the face normal vector, for each face, the vector from the cell centroid to the centroid of each of the adjacent cells, and the vector from the cell centroid to each of the faces. The range for orthogonal quality is from 0 to 1, where a value of 0 is worst and a value of 1 is best, and it is usually recommended to achieve an orthogonal quality higher than 0.1 [79]. Table 3.3 shows the spectrum of the cell orthogonal quality.

Table 3.3: Mesh orthogonal quality metrics spectrum [80]

Unacceptable	Bad	Acceptable	Good	Very good	Excellent
0-0.001	0.001-0.14	0.15-0.20	0.20-0.69	0.70-0.95	0.95-1.00

The aspect ratio is a measure of the stretching of a cell. It is computed as the ratio of the maximum value to the minimum value of any of the following distances: the distances between the cell centroid and face centroids, and the distances between the cell centroid and nodes [64]. It remains best to avoid sudden and large changes in the cell aspect ratio in areas where the flow field exhibits large changes or strong gradients. While meshing a combustion chamber is recommended to target a maximum aspect ratio less than 100 [79].

In this work, in the end of the meshing process, was made a quality mesh check in *Fluent Meshing* getting the following values (for the intermediate mesh):

- Regarding the orthogonal quality was obtained a minimum value of 0.25 presented by the cell with the lowest value and an average value of 0.9567, which according to Table 3.3 it is excellent. The orthogonal quality of the cells is distributed as shown in Figure 3.5.
- Regarding the skewness was obtained a maximum value of 0.749 and an average value of 0.392, which according to Table 3.2 it is very good.
- Regarding the aspect ratio was obtained a maximum value of 33.57 presented by the cell with the highest value, which is excellent as it is well below 100.

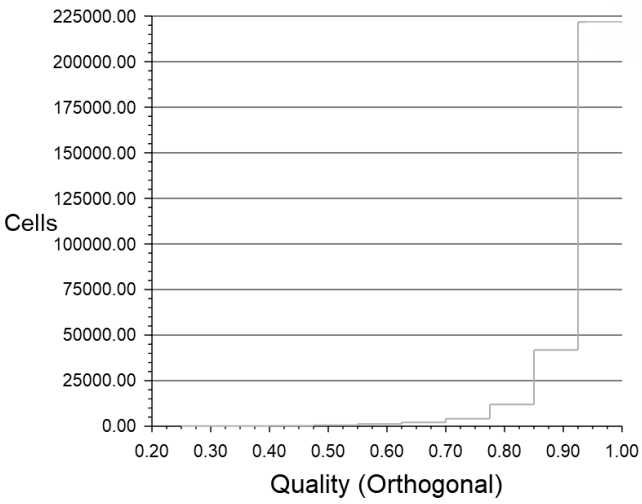

Figure 3.5: Histogram of mesh orthogonal quality by percentage of cells, obtained with ANSYS Fluent software

Lastly, a mesh check was performed at the end of the meshing process to make sure that there were no errors in the mesh, no errors were found. In the Figure C.2 (in Appendix C) shows the reports displayed for the mesh quality and the mesh check. The final intermediate mesh created is shown in Figure 3.6.

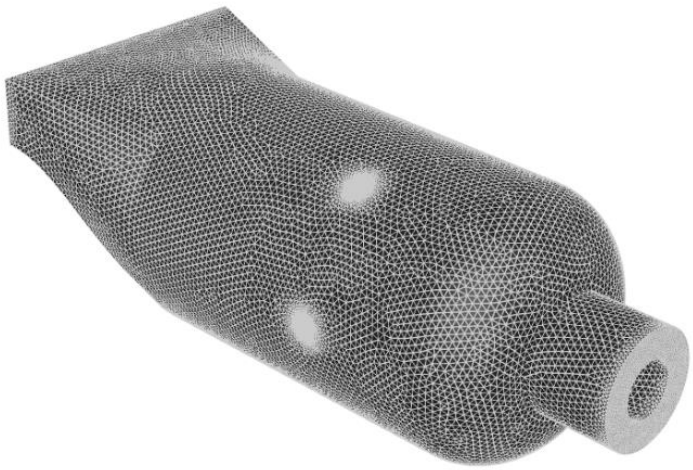

Figure 3.6: Intermediate mesh obtained with Fluent Meshing software

3.4 Chosen Fuels

The chosen fuels to use in the simulations are NG and biogas, with different chemical compositions to better understand the influence of the species in the combustion process, as shown in the Table 3.4. The natural gas will be used for the validation of the setup model with the work done by N. Ghenai and N. Janajreh [61].

Different biomass sources produce biogas with different chemical composition. In general, biogas from waste water treatment digesters usually contains from 55% to 65% methane, from 35% to 45% carbon dioxide and 0 to 1% nitrogen, biogas from organic waste digesters usually contains from 60% to 70% methane, from 30% to 40% carbon dioxide and 0 to 1% nitrogen while in landfills methane content is usually from 45% to 55%, carbon dioxide from 30% to 40% and nitrogen from 5% to 15% [81]. These values were taken into account when choosing the chemical composition of the different biogas. Additionally, Biogas 4 and Biogas 5 were derivate from Biogas 3 with an O_2 enrichment, in order to understand the influence of O_2 in the combustion process, since biogas may contain small amounts of O_2 in its composition. Finally, to better compare the different fuels, it is used a parameter, the ratio of non-combustible and Combustible Species (CS), such as N_2, CO_2, O_2 and CH_4, C_2H_6, respectively.

Table 3.4: Chemical composition of the chosen fuels

Fuel	Natural Gas (NG)	50%Natural Gas + 50% Biogas 1 (NB_1)	Biogas 1 (B_1)	Biogas 2 (B_2)	Biogas 3 (B_3)	Biogas 4 (B_4)	Biogas 5 (B_5)
CH4 (%v)	95	80	65	55	45	45	45
CO2 (%v)	0	17.5	35	35	35	30	30
N2 (%v)	2	1	0	10	20	20	17.5
O2 (%v)	0	0	0	0	0	5	7.5
C2H6 (%v)	3	1.5	0	0	0	0	0
NCS/CS	0.02	0.21	0.54	0.82	1.22	1.22	1.22
LHV (MJ/ kg)	48.20	31.25	20.25	16.38	12.83	13.10	13.05

To calculate the LHV of the fuels was used the following Equation (3,9):

$$\mathrm{LHV}\left(\frac{\mathrm{MJ}}{\mathrm{m}^3}\right) = \left(\mathrm{CH_4}\% \times \mathrm{LHV_{CH_4}}\right) + \left(\mathrm{C_2H_6}\% \times \mathrm{LHV_{c_2H_6}}\right) \tag{3.9}$$

with the $\mathrm{LHV_{CH_4}} = 35.8\ \mathrm{MJ/m^3}$ and $\mathrm{LHV_{c_2H_6}} = 64\ \mathrm{MJ/m^3}$.

After using the Equation 3.9 the density of the fuel was calculated to convert the units to MJ/kg.

3.5 Problem Setup

Once the mesh is chosen form the independence test, the problem setup can start. As mentioned before, the software used to perform this simulation was ANSYS Fluent 2023 R2.

When initiating ANSYS Fluent, a window named Fluent Launcher is displayed. Here it is necessary to ensure that the 3D model is enabled and it gives the possibility to use single or double precision in the simulation. Double precision option offers more accurate results, but requires a more CPU effort and a longer time to get the solution. Despite the negative aspects of enabling double precision, it was the chosen one due to the fact that a small error can largely influence the results of the models.

Once Ansys Fluent is launched, it is best practice to check mesh immediately after reading in the mesh, to ensure that there is no problem to the mesh itself since any problem with it can greatly affect the solution's convergence and results. Also, it is advised to check again the quality of the mesh, even if it was checked in the meshing process. In this case, as it was expected, no error or problem was found during the mesh check. After the previous steps are done, it is necessary to define the models.

3.5.1 Models

There are many different models in ANSYS Fluent that may be selected based on the requirements of each simulation. For this simulation five models were selected and presented below.

1 - Energy Model

This model must be activated as this regards the energy related to the temperature change within the combustion process or heat transfer [71].

2 - Viscous Model

The Viscous Model allows to set parameters for inviscid, laminar, and turbulent flow. As discussed in section 3.1.1.1, the model chosen for the final simulations was the standard

$k-\varepsilon$. All constants were kept default and the near wall treatment chosen was the Standard Wall Function.

3 - Radiation Model

As discussed in section 3.1.2, the P-1 model was chosen to simulate the heat transfers by radiation for all simulations.

4 - Species Model

ANSYS Fluent can model the mixing, transport and combustion of chemical species, so it is necessary to enable the species model. As mentioned in section 3.1.3, fuel and oxidizer enter the reaction zone in distinct stream, so non-premixed combustion is selected. Regarding the PDF creation, it was selected the inlet diffusion. The inlet diffusion option includes the diffusion flux of species at the flow inlet. In the chemistry tab, the energy treatment selected was non-adiabatic so that the model considers any loss or gain due to chemical reactions and heat transfers by radiation. In the state relation was selected the SLDF, as described in section 3.1.3.1. To create the flamelet file it was necessary to import the chemical kinetics mechanism and thermodynamic data. The files imported had to agree with CHEMKIN format, otherwise ANSYS Fluent will not be able to read it. In this case, it was used the GRI 3.0 detailed mechanism, mentioned in the section 2.6.

The specification of the fuel species name and concentration (see Table 3.1) is done in the boundary tab. In the present tab, the oxidizer species and concentration, as well as the temperatures of the oxidizer and the fuel have to be introduced. The oxidizer was considered composed only by nitrogen and oxygen with concentrations of 0.78992 and 0.21008, respectively. In the flamelet tab, all values were kept default except for the maximum number of grid points in flamelet, which was changed from 32 to 64.

After the previous steps being performed, the last step in the species model is the calculation of the PDF table in the table tab. Here all of the table default parameters were maintained except the maximum number of species which was increased to 53 so all the species of the GRI 3.0 were included, and the Automatic Grid Refinement was enabled. Finally, the PDF table can be calculated, and as a result the quantity of species created can be checked in Materials.

5 - NOx Model

ANSYS Fluent NOx model provides the capability to model thermal, prompt, and fuel NOx formation as well as NOx consumption due to reburning in combustion systems [64]. Despite this capability of the software, to assess the NOx emissions in this work, it was used the sub-mechanisms provided in the detailed mechanisms GRI 3.0, since it covers all the relevant pollutant species and its pathways, as mentioned in section 2.5.1.

3.5.2 Boundary Conditions

The boundary conditions used in this work were based on the work of N. Ghenai and N. Janajreh [61].

All simulations were performed at atmospheric pressure. As mentioned before, the oxidizer is composed only by N_2 and O_2 with concentrations of 0.78992 and 0.21008, respectively. The boundary conditions regarding both oxidizer (primary and secondary air inlet) and fuel species are the following:

- The temperature is 300 K;
- The turbulent intensity is set to 10%;
- The primary air velocity is 10 m/s;
- The secondary air velocity is 6 m/s;

For the fuel the mean mixture is f = 1 and for the oxidizer is f = 0. The wall boundaries were remained at default settings and the exit gauge pressure, regarding the pressure-outlet, was set to zero as this considers the system pressure at the exit to be the operating pressure, which is 101325 Pa.

It is noted that the heat input from NG combustion is 48.2 kW with a fuel mass flow rate of 0.001 kg/s. The heat input is calculated using the Equation (3.10).

$$P\ (\text{kW}) = LHV_{Fuel} \times \dot{m}_f \times 10^3 \tag{3.10}$$

In order to assess which fuel produces less gaseous emissions from the combustion process is important all simulations are performed under the same operating conditions and mostly important under the same heat input. For the remaining fuels, the fuel mass flow rate varies in order with the LHV due to the change in the fuel composition such that heat input is equal to 48.20 kW.

For example, the B_1 has a LHV of 20.25 MJ/kg , which with a a fuel mass flow rate of 0.001 kg/s would get a heat input of 24.8 kW. In order to generate a heat input of 48.2 kW it is necessary to have a fuel mass flow rate of 0.00238 kg/s (2.38 times greater).

By using a primary air velocity of 10 m/s and a secondary air velocity of 6 m/s the AFR is 77.54 meaning there is an excess of air, which is a standard practice for combustion in gas turbines. In Table 3.5, it is possible to check the boundary conditions and air-fuel mixtures of each simulation.

Table 3.5: Boundary conditions

Parameters	Natural Gas	50% NG + 50% B_1	Biogas 1	Biogas 2	Biogas 3	Biogas 4	Biogas 5
Fuel mass flow rate (kg/s)	0.001	0.00154	0.00238	0.00294	0.00376	0.00368	0.00369
Velocity of primary air (m/s)	10	10	10	10	10	10	10
Velocity of secondary air (m/s)	6	6	6	6	6	6	6
AFR_{st}	16.49	10.63	6,91	5.59	4.38	4.23	4.09
AFR	77.56	50.36	32.59	26.38	20.63	21.07	21.02
Equivalence ratio	0.21	0.21	0.21	0.21	0.21	0.2	0.19
Lower Heating value (MJ/kg)	48.20	31.25	20.25	16.38	12.83	13.10	13.05
Heat Input (kW)	48.20	48.20	48.20	48.20	48.20	48.20	48.20

3.5.3 Solution Methods, Solution Controls and Monitors

After setting the boundary conditions, it is necessary to choose the spatial discretization schemes, solution controls, monitors and convergence criteria. These steps are very important and greatly influence the final solution.

3.5.3.1 Solution Methods

In this study, a first approach was made which the schemes selected in the Solution Methods task page for Pressure Velocity Coupling and Spatial Discretization were the SIMPLE scheme and the Green-Gauss Node Based Gradient method, respectively. Regarding the Spatial Discretization, on unstructured meshes the accuracy of the least-square cell based gradient method is comparable to that of the Green-Gauss node-based gradient method and both are much more superior compared to the Green-Gauss cell-based gradient method. However, it is less expensive to compute the least-square cell

based gradient method than the Green-Gauss Node Based gradient method [64]. After a few attempts using Least-Square Cell Based Gradient method was noticed that the solution was not converging, so was switched to the Green-Gauss Node Based Gradient method which, finally, made the solution convergence smoothly. As referred before, the only disadvantage of using Green-Gauss Node Based method is the extra computational effort needed and consequently a much higher time to get a converged solution. The Pressure Discretization scheme selected was PRESTO! since this scheme is recommended for flows with high swirl numbers, high-Rayleigh-number natural convections, high-speed rotating flows, flows involving porous media, and flows in strongly curved domains [64]. For all the other equations, the First Order Upwind scheme was selected.

The results obtained from the First Order Upwind are normally not that accurate as a higher order scheme. So, after the First Order Upwind solution converged, the Second Order Upwind scheme was selected. The Pressure Velocity Coupling, the Spatial Discretization and the pressure discretization scheme were kept the same. The schemes used for each step of the simulations are identified in Table D.1 (in Appendix D).

3.5.3.2 Solution Controls

In the Solution Controls task page, it is possible to find the Under-Relaxation Factors (URF) section, which contains the under-relaxation factors for all equations that are being solved with the pressure-based solver [64]. Regarding the First Order Upwind approach all the URF were kept default, as the solution converged smoothly. For the Second Order Upwind approach, the URF default values are considered too aggressive, as they led to convergence problems. In order to obtain URF values capable of getting a converged solution a trial-and-error approach was made. Only after several attempts was possible to find the URF values to get the solution converged. Thus, most of URF values had to be initially reduced, more specifically the parameters of momentum, pressure, energy, density, turbulent dissipation rate and turbulent kinetic energy. The Table D.2 (in Appendix D) presents the values used for the URF in each approach.

3.5.3.3 Monitors

ANSYS Fluent allows to set up tools for monitoring the convergence of your solution dynamically by checking residuals, statistics, force values, surface integrals, and volume integrals. The purpose of the monitors is to set a value for a certain parameter and then check if each equation is converging to the defined value. Additionally, allows to print reports or display plots of the variation of several variables of the flow (such as temperature, pressure, velocities, etc.), or even surface/volume integrations and residuals for the variables of interest [64]. The monitors by their-self should not be regarded as the unique factor to obtain good results, however it is important that these user defined values are achieved. By default, the values of the convergence criteria are E^{-3} for all equations except P-1 and Energy which are E^{-6}. It is possible that if the initial guess is very bad, the initial residuals are so large that a three-order drop in residual does not guarantee convergence. This is especially true for k and ε equations where good initial guesses are difficult [64]. So, to ensure that the convergence process is smooth all values were set to E^{-6}. The absolute convergence criteria were the one applied.

3.5.3.4 Solution initialization and Calculation

After set up the simulation case, and prior to solving it, it is of good practice to check case. By checking case the simulation case will be checked for compliance in the mesh, models, boundary and cell zone conditions, material properties, and solver categories, as this ensures that there are no errors within the case [64]. After that, the simulation is ready to initialize the solution.

To initialize the solution is necessary providing ANSYS Fluent with an initial "guess" for the solution flow field. There are two methods for that by using the standard Initialization or the hybrid Initialization. Standard initialization takes the values defined by the user for the solution variables and initializes the flow field to these values. Hybrid initialization is an initialization process done by the computer by calculating the variable field. In most cases, ANSYS Fluent hybrid initialization option provides a good initialization. However, in this case, it was not good enough. After a few trials, these initial values were inadequate since the solution did not converge. Thus, standard initialization was employed and it proved to be an excellent option because the solution converged smoothly and rapidly.

3.6 Results Validation

In order to validate the numerical model, as mentioned in section 3.4, the results obtained from the NG simulation will be validated with available data of the research done by N. Ghenai and N. Janajreh [61]. Those results are the average static temperature of the combustor in the outlet, the maximum static temperature in the combustion chamber, the average CO_2 mole fraction of the combustion chamber in the outlet and the average NOx mole fraction of the combustion chamber in the outlet. It is important to mention that N. Ghenai and N. Janajreh, in their work, used the First Order Upwind approach and selected the chemical equilibrium on the state relation option. Differently, in this work was selected the Steady Laminar Flamelet Model on the state relation option. Additionally, it will be compared the results obtained from the First Order Upwind approach and Second Order Upwind approach.

The results obtained from N. Ghenai and N. Janajreh work using NG are the following presented in the Table 3.6.

Table 3.6:Values obtained by N. Ghenai and N. Janajreh [61]

Parameter	Value
Maximum static temperature [K]	2109
Average static temperature in the outlet [K]	869
Average CO_2 mole fraction in the outlet	0.022
Average NOx mole fraction in the outlet	0.0000113

3.6.1 First Order Upwind Approach

The results obtained using the First Order Upwind approach are the following presented in the Table 3.7.

Table 3.7: Values obtained using First Order Upwind approach while burning Natural Gas

Parameter	Value	Relative Error [%]
Maximum static temperature [K]	2111.5	0.119
Average static temperature in the outlet [K]	885	1.84
Average CO_2 mole fraction in the outlet	0.0228	0.08
Average NOx mole fraction in the outlet	0.000144	1174

To analyse the results validation, the relative error is used in the obtained values. The relative error is obtained by dividing the absolute error of each parameter by the value obtained by N. Ghenai and N. Janajreh [64], as shown in the Equation (3.11).

$$Relative\ Error\ [\%] = \frac{|Value_{\ Ghenai} - Value_{Obtained}|}{Value_{\ Ghenai}} \times 100 \qquad (3.11)$$

Looking at the Table 3.7, it is verified that the values of the maximum static temperature, static temperature in the outlet and average CO_2 mole fraction in the outlet are in accordance with those of N. Ghenai and N. Janajreh, with a relative error of 0.119%, 1.84% and 0.08%, respectively. The most probable cause for the little differences is the estimated distances in the can type combustor geometry, mentioned in section 3.2. Regarding the average NOx mole fraction in the outlet, the value obtained is much higher than N. Ghenai and N. Janajreh's value, therefore is the parameter with the highest relative error, 1174%. This was expected by using the kinetic model GRI 3.0 for modelling the combustion. As mentioned in section 2.6, the GRI 3.0 mechanism calculates the NOx emissions from different pathways, such as the Thermal NO, the Prompt NO, the N_2O mechanism and, additionally, has reburn chemistry. In contrast, N. Ghenai and N. Janajreh only took in consideration Thermal NO and Prompt NO, so the value obtained by N. Ghenai and N. Janajreh would expect to be much lower, by only considering two different pathways. It is possible to conclude that the present data result is in excellent agreement with N. Ghenai and N. Janajreh results.

3.6.2 First Order Upwind Approach vs Second Order Upwind Approach

The first and second order upwind schemes are based on different approaches. When using the first order upwind scheme quantities at cell faces are determined by assuming that the cell-centre values of any field variable represent a cell-average value and hold throughout the entire cell, the face quantities are identical to the cell quantities. If the second order upwind is used quantities at cell faces are computed using a multidimensional linear reconstruction approach. In this approach, higher-order accuracy is achieved at cell faces through a Taylor series expansion of the cell-cantered solution about the cell centroid [64]. Therefore, this scheme provides a higher accurate result than the First Order Upwind scheme. So, it is important to assess the difference in the results from both approaches, and determine if it is worth using the Second Order Upwind scheme, given that take a much longer time and higher difficulty to converge.

The results obtained using the First and Second Order Upwind approach are the following presented in the Table 3.8.

Table 3.8: Values obtained using the First and Second Order Upwind approach while burning Natural Gas

Parameter	First Order	Second Order
Maximum static temperature [K]	2111.5	1977.5
Average static temperature in the outlet [K]	885	880
Average CO_2 mole fraction in the outlet	0.0228	0.0226
Average NOx mole fraction in the outlet	0.000142	0.000141

Looking at the Table 3.8, it is verified that the average static temperature in the outlet, the average CO_2 mole fraction in the outlet and the avarage NOx mole fraction in the outlet from both approaches are very similar, with a very little gap between the values. The major difference is in the maximum static temperature with a gap of 134 K. In a combustor simulation, capturing the sharp gradients in the flame front and the temperature field is crucial. The First Order Upwind approach overly smooth these gradients, leading to an over prediction of peak temperatures. The Second Order scheme, by better resolving these gradients, provides a more physically accurate representation of the flame shape and combustion process. This is confirmed when comparing the static temperature contours of both approaches. In Figure 3.7, looking at the contour of the First order Upwind approach there is an elongated smooth flame shape with no sharp edges and a width without sudden variations. In contrast, at the contour of the Second Order Upwind approach there is a shorter flame shape with sharp edges and sudden width variations.

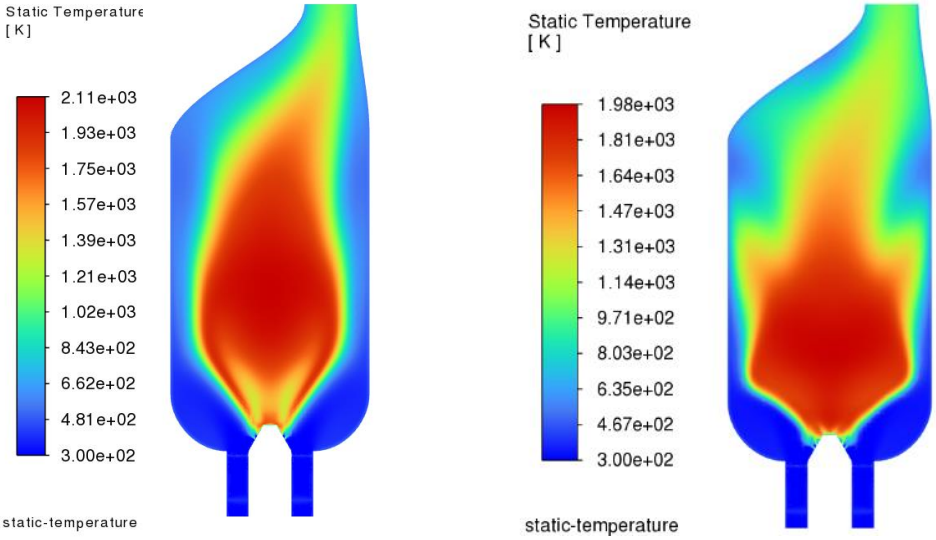

Figure 3.7: Contours of static temperature while burning Natural Gas using the First Order Upwind order (left) and Second Order Upwind approach (right) (view of plane XY Z=0), obtained with ANSYS Fluent software

Besides the difference between the flame shape, the results of both approaches are quite similar. Therefore, in order to save computational power and time was chosen the First Order Upwind approach.

Chapter 4 – Results and Discussion

In the present chapter, the results for the parameters that were intended to simulate for the combustion of natural gas and biogas with a total of 7 simulations compose the final results. Thus, this chapter will start with an evaluation of convergence, regarding the quality of the numerical solution followed by the recirculation zone analysis and then by the temperature distribution across the combustor. Finally, the emissions, which are the primary goal of this study, are finally presented separately for each fuel. In order to evaluate the fuels, it will be compared, firstly the fuels without O_2 in its composition and, secondly the fuels with O_2 enrichment will be compared to assess the differences with the B_3 as they derive from it. To conclude this chapter, the conclusions obtained from the results are discussed.

In order to perform the simulations, it was used a computer with 16 GB of RAM, a CPU Intel Core I7 with 8 cores. Each simulation took about three hours to get the results.

4.1 Convergence Analysis

The convergence analysis is an important step before checking the results, to make sure the solution obtained is the correct and accurate one. By ANSYS there are three indicators that convergence has been reached:

- The residuals have decreased to a sufficient degree, which means the convergence criterion for each variable has been reached. In this case, the converge criteria was set to E^{-6} to all residuals;
- The solution no longer changes with more iterations, so it is important not only examining the residuals plot, but also monitoring relevant integrated quantities, such as temperature and species mole fractions;
- The overall mass, momentum, energy, and scalar balances are obtained. The net imbalance should be less than 0.2 % of the net flux through the domain when the solution has converged.

In order to examine the convergence of the solution, firstly, the residuals plot was analysed concluding that all residuals achieved the converge criteria settled previously at around 575 iterations, as illustrated in Figure 4.1. Also, it verifies that the residuals converged smoothly and fast.

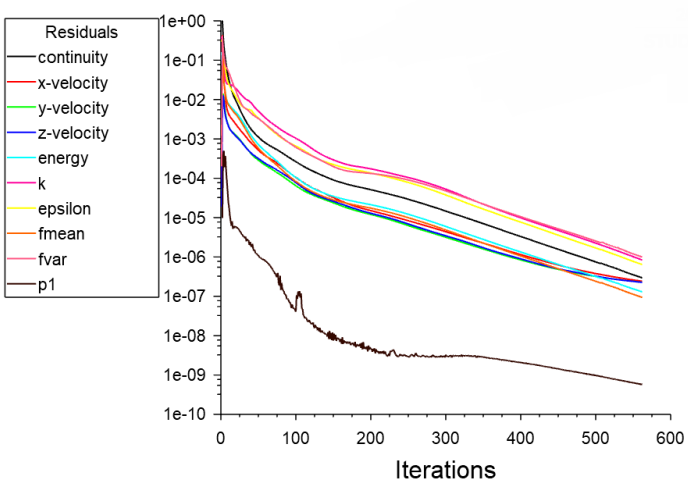

Figure 4.1: Residuals plot obtained with ANSYS Fluent software

Secondly, during the convergence process, a few quantities were selected to be monotonized, namely, the average volume static temperature and the average CO_2 mole fraction in the outlet, illustrated in Figure 4.2. This helps, evaluating the convergence of the solution where it is possible to assess if the quantities are constant despite the increase of iterations. These plots reveal regions where the studied parameters remain constant and areas where they fluctuate. As previously discussed, a solution is considered converged when all relevant parameters have constant values.

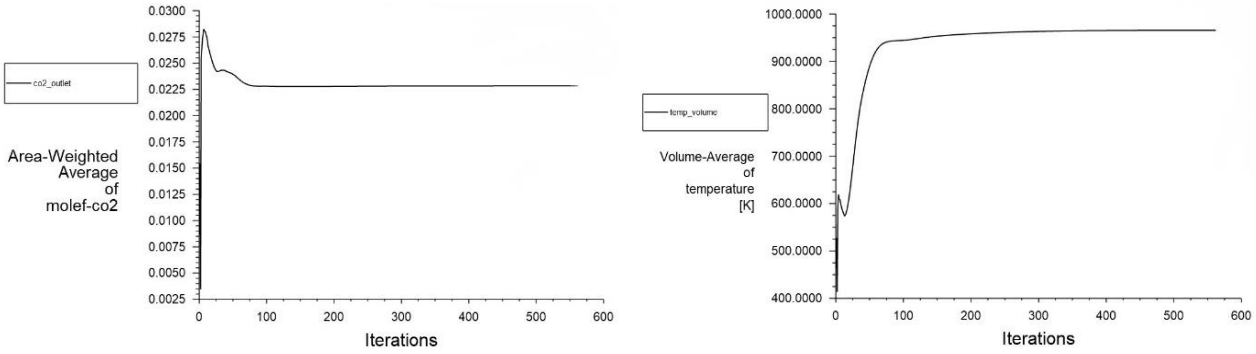

Figure 4.2: Plots of the average CO_2 mole fraction in the outlet (left) and volume average static temperature (right) obtained for simulation with Natural Gas obtained with ANSYS Fluent software

Therefore, the iterations where values remain practically constant in both plots can be linked to converged solutions for the simulation steps. The presence of constant values at the end of the plots strongly indicates that the solution is converged.

Finally, the mass imbalance in this case was $-1.1718775E^{-9}$ (≈ 0), which is another proof that the solution is completely converged and therefore correct for the problem setup. It is important to note that, although the plots are not included in this work, the convergence analysis for each of the other 6 simulations was conducted in the exact same manner as demonstrated in this example.

4.2 Recirculation Zone

The design and performance of a combustor is strongly affected by aerodynamic processes. The achievement of aerodynamically efficient designs, characterized by good mixing and stable flow patterns with minimal parasitic losses, is one of the primary design objectives [82].

As mentioned in section 2.2.3.1, the swirl vanes impart a circumferential velocity to the incoming air, pushing it radially outward as it enters the combustor. This outward motion creates a low-pressure region along the centreline, inducing a backflow to balance the centreline pressure deficit. The result is the formation of a recirculation flow. The goal of swirler design is to maximize the benefits of recirculation by imparting sufficient swirl to the flow while minimizing the incurred pressure losses [82].

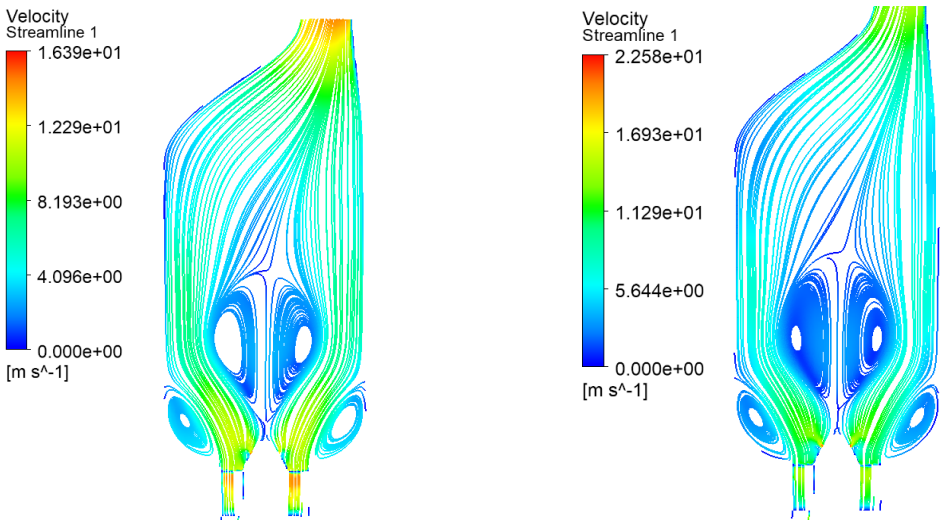

Figure 4.3: Velocity Streamline Contour, in the view plane XY Z=0, while burning Natural Gas (left) and Biogas 1 (Right)

In Figure 4.3, in primary zone, the negative axial velocities in the centre of the combustion chamber indicate the existence of an CRZ. This hot gas helps stabilize the flame by providing a continual source of ignition to the incoming fuel. It also serves as a zone of intense mixing within the combustion by promoting turbulence through high levels of shear between the forward and reverse flows. Flame stability, combustion intensity, and performance are directly associated with the size and shape of this recirculation vortex. Negative axial velocities in corner regions indicate the existence of two Edges Recirculation Zones (ERZ) resulting from sudden expansion. ERZ takes it shape from the neighbouring boundary walls. In this study, the primary inlet air has an initial velocity of 10 m/s and, after passing through the swirler, enters the combustion chamber at 16 m/s. For all tested fuels, the CRZ and ERZ maintain a similar shape and

size, as the swirled air velocity remains the same. The velocity streamlines contours of the remaining simulations can be found in Appendix E.

4.3 Temperature Distribution Across the Combustor

The temperature greatly influences the combustion process, and consequently the formation of pollutant emissions. So, it is important to understand how the temperature is distributed across the combustor. In a first step, the temperature along the combustor centreline is analysed, as seen in Figure 4.4.

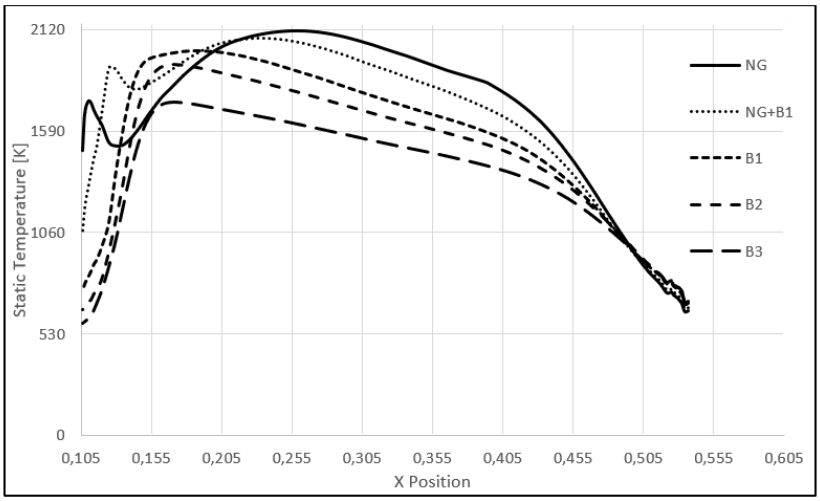

Figure 4.4: Static temperature plot along the combustor centreline

Looking at the Figure 4.4, it is possible to verify that exist two static temperature profiles on the combustor centreline.

- The first profile, verified in the NG and NB_1 fuels, characterized by an initial temperature peak near the injection zone, followed by a drop in temperature, and then a second rise leading to a maximum temperature further downstream. After reaching the peak, the temperature drops until the outlet;
- The second profile, verified in the remaining fuels, characterized by a slower increasing of the temperature reaching the maximum peak temperature in the primary zone. After reaching the peak, the temperature drops until the outlet.

This can be explained by the interactions between fuel injection velocity, gas recirculation, and the air-fuel mixing process along the centreline.

For the first profile, as the fuel injection velocities are the lowest in the NG and NB_1, the fuel disperses more slowly, meaning that a higher concentration of fuel remains near the injection points (richer mixture). The swirling air introduced by the swirler creates a strong recirculation zone along the centreline. Hot combustion products become trapped in the recirculating mass and are returned to the combustor dome inlet, preheating the incoming fuel and air. As a result, near the centreline, the fuel ignites quickly due to the heat from the recirculated gases. This leads to an initial temperature peak near the injection zone, as the combustion begins almost immediately along the centreline, fuelled by both the fresh air-fuel mixture and the recirculated hot gases. After this initial peak, the temperature decreases along the centreline. This drop occurs because, after the initial combustion, the burned gases are diluted by the recirculating gases and the incoming air, leading to a temporary cooling effect. Additionally, due to the lower fuel injection velocity, the air-fuel mixing is not yet fully efficient along the centreline immediately after injection. This results in a partial combustion, where not all the fuel is burning optimally, leading to a lower heat release rate, and thus, a dip in temperature. Further downstream, the air-fuel mixture becomes more homogeneous, and the combustion process becomes more efficient. The recirculated hot gases along the centreline continue to preheat the mixture, stabilizing the combustion process. After reaching the maximum temperature, the mixture flows axially and it diffuses away from the centre to ensure entrainment of more air (secondary air) along the centreline of the secondary zone of the combustor thereby reducing the temperature in this region.

For the second profile as the increasing CO_2 and N_2 content slows the combustion process, reducing the burning velocity of the flame and the burning rate, which shifts the combustion to a point further downstream. So, the mixture requires more time to reach ignition conditions. This means that the combustion process starts later and occurs more gradually, rather than having an initial burst of combustion near the injection zone, therefore the combustion develops more slowly and steadily, leading to just one peak further downstream. Additionally, the higher injection velocity spreads the fuel-air mixture more widely and at a faster rate, further delaying the ignition. As the fuel is injected with greater momentum, it moves further downstream before it can ignite, causing the peak temperature to shift away from the injectors. The recirculated hot gases along the centreline continue to pre-heat the mixture, stabilizing the combustion process. Furthermore, the combustion mixture begins to move to colder and more diluted regions of the chamber. Also, with the introduction of the secondary air helps to reduce the temperature of the combustion gases.

A parameter, which is critical to assess, as it significantly influences the formation of emissions, especially NOx, is the maximum temperature reached inside the combustion chamber.

Table 4.1: Maximum temperature reached inside the combustor while burning Natural Gas, 50% Natural Gas + 50% Biogas 1, Biogas 1, Biogas 2 and Biogas 3

Fuel	Maximum Temperature [K]
NG	2111.5
NB_1	2076.8
B_1	2014.6
B_2	1984
B_3	1947.1

As seen in Table 4.1, the maximum temperature reached decreases as the ratio of NCS to CS increases through the different fuels. This happens due to the increasing CO_2 and N_2 content in the fuel. First, both CO_2 and N_2 are inert gases in the combustion process, meaning they do not actively contribute to the chemical reaction that generates heat. Additionally, CO_2 and N_2 have higher specific heat capacities compared to gases like methane and oxygen. This means they absorb more heat without undergoing a significant increase in temperature. As a result, more energy is expended in heating these gases rather than in raising the overall temperature of the combustion process. For these reasons, increasning the content in CO_2 and N_2 decreases the overall temperature of the combustion process, and consequently the maximum temperature.

To get a better view of the process explained previously, the contours of the static temperature of the NG, $B_1$and B_3 fuels are illustrated in Figure 4.5, the contours of the static temperature of the remaining simulations can be found in Appendix F. As the ratio of NCS to CS increases, it is possible to verify that the temperature in the CRZ drops and the ignition point keeps further delaying from the injection point. As mentioned previously, this happens due to the increasing content of CO_2 and N_2, which decreases the overall temperature of the combustion process, reduces the burning velocity of the flame and the burning rate. Due to these features, a notable change of the flame shape is visible as the flame shape begins with a conical shape and ends up with a “V” shape. The

data shows that the length decreases and thickness of the flame increase with an increase of the ratio of NCS to CS.

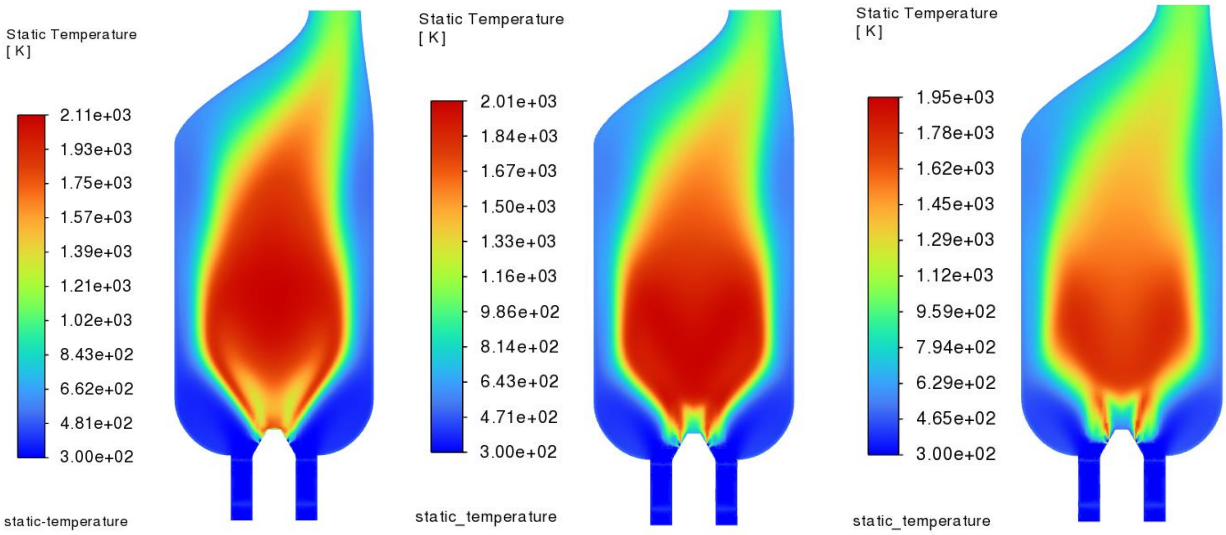

Figure 4.5: Contours of static temperature while burning Natural Gas (left), Biogas 1 (middle) and Biogas 3 (right) (view of plane XY Z=0), obtained with ANSYS Fluent software

4.3.1 Influence of O_2 Enrichment in the Temperature Distribution Across the Combustor

The presence of O_2 in the fuel can greatly influence the overall temperature of the combustion process and its maximum temperature reached. The Figure 4.6, shows that the static temperature profile is very similar among the three different fuels. This would be expected, as the variation of the fuels is minimal since the main difference is the addition of a small percentage in O_2 and a decrease of the same percentage in N_2.

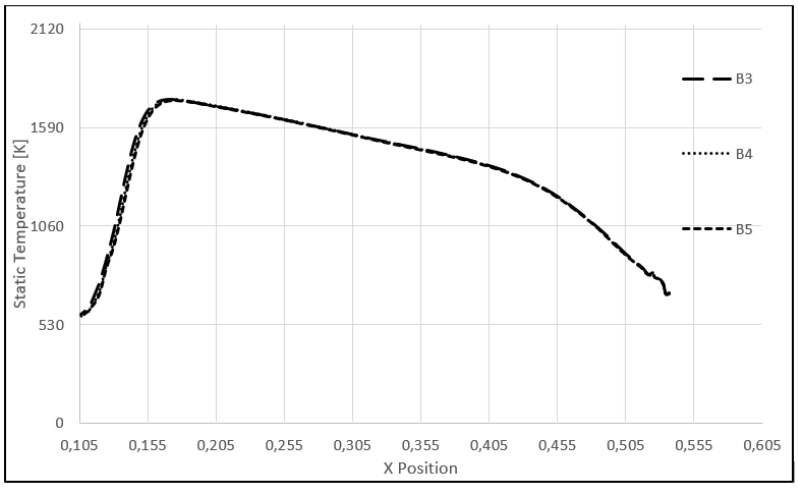

Figure 4.6: Static Temperature Plot along the combustor centreline

When it comes to the maximum temperature reached there is a notable difference, as seen in Table 4.2. The addition of oxygen to the fuel makes the mixture more reactive, as part of the oxygen required for combustion is already present in the fuel stream. This increases the intensity and efficiency of burning, resulting in a higher flame temperature. Also, with less content in N_2 helps reducing the energy expended in heating the inert gases, which contributes to a higher temperature. It is possible to conclude that increasing the percentage of O_2, the maximum temperature reached increases, as well.

Table 4.2: Maximum temperature reached inside the combustor while burning Biogas 3, Biogas 4 and Biogas 5

Fuel	Maximum Temperature [K]
B_3	1947.1
B_4	2020.8
B_5	2053.7

An interesting occurrence worth to mention when comparing the maximum temperature reached in Table 4.2 with the Figure 4.6 is the maximum temperature reached during the combustion of the fuels with O_2 enrichment does not occur along the centerline, unlike the fuels without O_2 enrichment. In the previous cases, without O_2 in the fuel, the main source of oxygen was the air introduced through the swirler. This meant that combustion occurred where fuel and air mixed most efficiently, which typically happens near the centerline of the combustor. In these cases, the highest temperature would be near the centerline, where the fuel and air streams interact the most. When O_2 is added to the fuel, oxygen is now distributed throughout the fuel stream, meaning combustion is no longer confined to regions where the air-fuel mixture is optimal. This allows for more combustion away from the centerline, where fresh oxygen from the fuel is available, spreading the combustion reactions more evenly throughout the chamber. The result is that the hottest regions of the flame are no longer limited to the centerline, as oxygen is already available everywhere in the fuel stream. This leads to peak temperatures being recorded outside the centreline. To better visualize it, the static temperature contours of the combustion of the B_3, B_4 and B_5 are shown in Appendix F.

4.4 Carbon Dioxide Emission Analysis

Carbon dioxide is the primary GHG emitted through human activities. While CO_2 emissions come from a variety of natural sources, human-related emissions are responsible for the increase that has occurred in the atmosphere since the industrial revolution. The main human activity that emits CO_2 is the combustion of fossil fuels (coal, natural gas, and oil) for energy and transportation. CO_2 emissions are an inevitable result of complete combustion of fuels, therefore the most effective way to reduce CO_2 emissions are to reduce fossil fuel consumption [83]. In this case, despite being tested different fuels with varying CH_4 and C_2H_6 contents, to keep the same combustion conditions it was necessary to adjust the fuel mass flow rate leading to a similar fossil fuel consumption. Besides that, being CO_2 one of the main components of biogas, directly contributes to the CO_2 emissions, as it does not directly participate in the combustion reactions. Carrying out a prior prediction, it is expected that CO_2 emissions will increase along the fuels. In order to assess the CO_2 emissions, the average CO_2 mole fraction in the outlet are shown in the Table 4.3.

Table 4.3: Average CO_2 mole fraction in the outlet while burning Natural Gas, 50% Natural Gas + 50% Biogas 1, Biogas 1, Biogas 2 and Biogas 3

Fuel	Average CO_2 mole fraction in the outlet
NG	0.0228
NB_1	0.0272
B_1	0.0339
B_2	0.0361
B_3	0.0388

The results in Table 4.3 show that the average CO_2 mole fraction in the outlet increase along the different fuels, as expected. The two main factors contributing to the increase in CO_2 emissions are the CO_2 content in the fuel composition and the fuel mass flow rate. The CO_2 content in NG, NB_1, and B_1 is 0%, 17.5%, and 35%, respectively. With similar fossil fuel consumption across these cases, the increase in CO_2 content in the fuel leads to a corresponding rise in CO_2 emissions. Although B_1, B_2, and B_3 have the same CO_2 content, there is an increase in the ratio of NCS to CS, which requires a higher fuel mass flow rate to maintain the same heat input. This higher fuel mass flow rate results in greater CO_2 emissions.

4.4.1 Influence of O_2 Enrichment in the Carbon Dioxide Emission

As said previously, CO_2 is a natural byproduct of complete combustion, where carbon-containing fuels, such as CH_4 in biogas, react fully with O_2 to produce CO_2 and water H_2O. In a general way, the presence of additional O_2 in biogas can enhance the combustion efficiency by promoting more complete oxidation of the fuel. As a result, this increased combustion efficiency can lead to higher CO_2 production. In order to assess the CO_2 emissions, the average CO_2 mole fraction in the outlet are shown in the Table 4.4.

Table 4.4: Average CO_2 mole fraction in the outlet while burning Biogas 3, Biogas 4 and Biogas 5

Fuel	Average CO_2 mole fraction in the outlet
B_3	0.0388
B_4	0.0363
B_5	0.0364

The results obtained do not follow the expected behaviour, but certain factors may explain these outcomes. Firstly, the CO_2 content in B_3 is 35%, whereas in B_4 and B_5 it is 30%. This difference in CO_2 percentage has a significant impact on the CO_2 emissions, leading to a higher average CO_2 mole fraction at the outlet for B_3 compared to the other fuels. The results for B_4 and B_5 show an interesting behaviour, as both have identical CO_2 mole fractions despite B_5 containing 2.5% more O_2 than B_4. Since both fuels have similar fuel mass flow rates and the same CO_2 content, these results suggest that this additional O_2 in B_5 does not significantly improve combustion efficiency. This indicates that the combustion of B_4 already achieved a near maximum efficiency not promoting more complete combustion. Moreover, in the Table 4.2, the difference in the maximum temperature reached by the fuels is small (33 K), which aligns with the observation that the increase in combustion efficiency due to the additional O_2 in B_5 is minimal. This further supports the conclusion that the combustion process in B_4 is already highly efficient.

4.5 Carbon Monoxide and Unburned Hydrocarbons Emission Analysis

Like CO_2, CO and UHC are produced from the combustion of fossil fuels. CO_2 is formed when the carbon in the fuel is fully oxidized. In contrast, CO and UHC are the result of incomplete combustion, which happens when there are areas with insufficient air supply during the burning process. UHC come out of the combustor as droplets or vapor. Conducting a prior analysis, based on the static temperature of the combustor centreline in section 4.3, it is expected that lower overall combustion temperatures will increase CO and UHC emissions. In order to assess the CO and UHC emissions, the average CO and UHC mole fractions in the outlet are show in Table 4.5.

Table 4.5: Average CO and UHC mole fraction in the outlet while burning Natural Gas, 50% Natural Gas + 50% Biogas 1, Biogas 1, Biogas 2 and Biogas 3

Fuel	Average CO mole fraction in the outlet	Average UHC mole fraction in the outlet
NG	8.55 E-06	2.22E-08
NB_1	6.85E-06	4.78E-09
B_1	2.96E-06	4.60E-09
B_2	1.39E-06	2.03E-09
B_3	4.33E-07	4.33E-10

Table 4.5 shows that the average CO and UHC mole fractions at the outlet decrease across the different fuels, which was initially unexpected. The values are virtually zero but they still provide useful insights for analysis.

Although the overall combustion temperature decreases, this reduction is not directly due to a less completed combustion (which would typically increase CO and UHC emissions). Instead, it is primarily due to the presence of N_2 and CO_2 in the fuel, which absorb some of the heat released during the combustion of CH_4 and C_2H_6, as explained in section 4.2. This reduction in CO and UHC emissions could be influenced by several factors, including the quality of the air-fuel mixture. As noted in Section 4.2, NG and NB_1 initially exhibit a fuel-rich mixture near the injection zone, which contributes to higher CO and UHC emissions. Additionally, lower fuel injection velocities in these cases may lead to less efficient air-fuel mixing. Moreover, along fuels B_1, B_2, and B_3, the ratio of NCS to CS increases, which reduces the flame burning velocity and the rate of combustion. This shift delays the combustion zone further downstream, allowing more time for air-fuel mixing. Combined with the higher injection velocities, these fuels promote a more homogeneous air-fuel mixture, ultimately resulting in lower CO and

UHC emissions. Furthermore, the results from Table 11 indicate that combustion gets more completed across the different fuels, resulting in lower CO and UHC emissions.

4.5.1 Influence of O_2 Enrichment in the Carbon Monoxide and Unburned Hydrocarbons Emission

The presence of O_2 in the fuel composition can significantly influence the formation of UHC and CO emissions in combustion processes. Oxygen within the fuel itself provides an additional source of oxidizing agents, which enhances the oxidation reactions of hydrocarbons during combustion. This intrinsic oxygen presence can lead to more complete combustion, thereby reducing the amount of UHC and CO produced. In order to assess the CO and UHC emissions, the average CO and UHC mole fractions in the outlet are show in Table 4.6.

Table 4.6: Average CO and UHC mole fraction in the outlet while burning Biogas 3, Biogas 4 and Biogas 5

Fuel	Average CO mole fraction in the outlet	Average UHC mole fraction in the outlet
B_3	4.33E-07	4.33E-10
B_4	2.97E-07	3.81E-11
B_5	2.51E-07	8.45E-12

The results in Table 4.6 show that the average CO and UHC mole fraction in the outlet decreases as the O_2 content is increased. Similar to the data in Table 4.5, the values are virtually zero but they still provide useful insights for analysis. As previously explained, when oxygen is already embedded within the fuel molecules, it acts as an internal oxidizing agent. The added oxygen from the fuel can sustain oxidation reactions that would otherwise be incomplete, leading to a more through conversion of fuel molecules into CO_2, thus reducing CO emissions. In addition, the oxygen within the fuel supports improved combustion efficiency by enabling the oxidation of hydrocarbons in areas that might not receive optimal air-fuel mixing. When combustion is more efficient, fewer fuel molecules remain unburned, leading to a reduction in UHC emissions.

As noted in Section 4.4.1, it was concluded that the combustion of B_4 had already reached near maximum efficiency, so the additional O_2 in B_5 does not lead to a significant improvement. This conclusion is further supported by the minimal decrease in the average CO and UHC mole fractions at the outlet between B_4 and B_5, which are only 0.46E-07 and 2.97E-11, respectively.

4.5 Oxides of Nitrogen Emissions Analysis

Nitrogen oxides are among the most significant pollutants produced in combustion processes, where their formation is highly dependent on factors such as temperature, fuel composition. The term NOx refers to the sum NO and NO_2, so in order to analyse the NO_x emisions the average NO and NO_2 mole fraction in the outlet is presented in Table 4.7.

Table 4.7: Average NO and NO_2 mole fraction in the outlet while burning Natural Gas, 50% Natural Gas + 50% Biogas 1, Biogas 1, Biogas 2 and Biogas 3

Fuel	Average NO mole fraction in the outlet	Average NO_2 mole fraction in the outlet
NG	1.42E-04	2.73E-06
NB_1	1.39E-04	2.05E-06
B_1	1.10E-04	1.46E-06
B_2	9.11E-05	1.25E-06
B_3	6.67E-05	9.87E-07

Regarding NO emissions, the results in Table 4.7 show that the average NO mole fraction at the outlet decreases across the different fuels. As outlined in Section 2.5.1.3, the leading mechanism of thermal formation NOx is governed by the Zel'dovich mechanism, which describes how NOx is formed from atmospheric nitrogen at sufficiently high temperatures. In Figure 4.7, it can be seen that besides these high peak temperatures are located within the flame zone, the oxidation occurs mainly in the recirculation zone and post flame zone area, in which the concentration of the radicals O and OH are sufficient for the process to occur. The remaining contours of the NO mole fraction can be found in Appendix G. This mechanism is highly temperature-dependent, meaning that the peak temperature achieved during combustion has a substantial impact on NO_x formation. In Section 4.2, it was shown that the peak combustion temperature decreases as the ratio of NCS to CS increases across the different fuels. Consequently, as the peak temperature drops, the average NO mole fraction at the outlet also decreases. Biogas is a great alternative for NO emissions reduction, the presence of N_2 and CO_2 in biogas plays a significant role in absorbing the heat release from combustion, which reduces the combustion temperature decreasing the NO emissions.

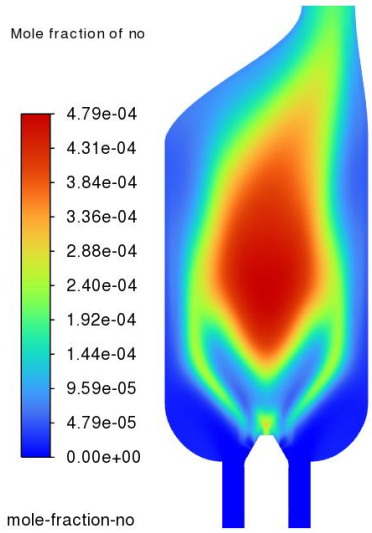

Figure 4.7: Contour of NO mole fraction, in the view plane XY Z=0, while burning 50% Natural gas + 50% Biogas 1

Regarding NO_2 emissions, the results in Table 4.7 show that the that the average NO_2 mole fraction at the outlet decreases across the different fuels, similarly to the NO emissions. As mentioned in section 2.5.1.3, part of the NO formed in combustion subsequently oxidizes to NO_2 in the cold regions of a combustor. This statement can be proved by analysing the Figure 4.8, it can be seen that the major concentrations of NO_2 are located outside of the flame, where exist the coldest regions. The remaining contours of the NO_2 mole fraction can be found in Appendix H. Being the NO_2 emissions dependents on the formation of NO, as the NO formation decreases the average NO_2 mole fraction in the outlet also decreases.

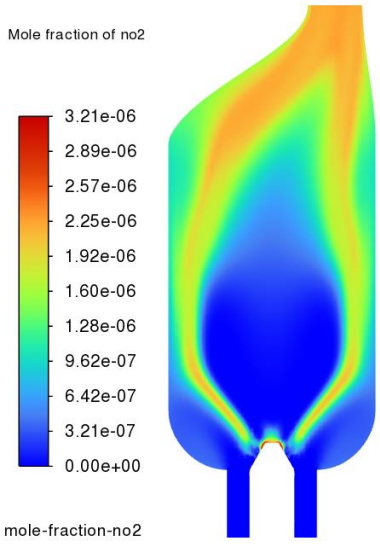

Figure 4.8: Contour of NO_2 mole fraction, in the view plane XY Z=0, while burning 50% Natural gas + 50% Biogas 1

It can be then concluded from the NOx emissions analyses, that biogas have the potential to decrease these types of emissions. The fuel composition is the major aspect which influence the NOx emissions.

4.5.1 Influence of O_2 Enrichment in the Oxides of Nitrogen Emissions

Since NOx emissions are highly temperature-dependent, the presence of O_2 plays a crucial role in influencing these emissions. As discussed in Section 4.3.1, enriching the combustion mixture with O_2 results in a higher combustion temperature, which accelerates the formation of nitrogen oxides, particularly NO and NO_2. This temperature increase intensifies the oxidation reactions that convert atmospheric nitrogen into NO_x species, especially under high-temperature conditions as described by the Zel'dovich mechanism. The results in Table 4.8 confirm this relationship as the O_2 content increases across the different fuels, there is a rise in the average NO and NO_2 mole fractions at the outlet.

Table 4.8: Average NO and NO_2 mole fraction in the outlet while burning Biogas 3, Biogas 4 and Biogas 5

Fuel	Average NO mole fraction in the outlet	Average NO_2 mole fraction in the outlet
B_3	6.67E-05	9.87E-07
B_4	1.15E-04	1.42E-06
B_5	1.49E-04	1.72E-06

This trend highlights the direct impact of higher O_2 levels on NOx formation.

Chapter 5 – Conclusion

This study presents a numerical investigation into the combustion simulation of natural gas and biogas with variations in the fuel composition, in a can-type combustor, using ANSYS Fluent 2023 R2. The primary aim was to assess the pollutant emissions, specifically CO, UHC, CO_2, and NOx species. Additionally, to provide further insight into these assessments, the recirculation zone and the static temperature distribution across the combustor were also analysed. In the course of this work, it was essential to delve into several topics to greatly understand and develop this study. These topics included thermodynamics, turbulence, chemistry, and pollutant formation. Furthermore, it was needed to learn how to properly use the ANSYS software (Fluent and Fluent Meshing). to successfully carry out the work.

Regarding the results, in addition to fuel composition, other factors significantly impacted the results, including the quality of the mixture and boundary conditions, specifically the fuel injection velocity and the flue mass flow rate. The result analysis started with the recirculation zone, in which it was observed that variations in the fuel composition do not significantly alter the recirculation patterns. This behaviour is primarily due to the primary air swirl velocity, which remains equal across simulations and is the dominant factor in defining the recirculation zones. The CRZ remains centred and well-defined, while the ERZ's at the combustor edges form due to sudden expansions and are shaped by boundary constraints. To continue the analysis, after examining the recirculation zones, it moved on to assess the static temperature distribution across the combustor. While the recirculation zones play a fundamental role in stabilizing the flame and mixing efficiency, the temperature across the combustor is equally crucial in the pollutant formation. It was observed that fuel composition significantly affects the overall combustion temperature, thereby influencing the peak temperature reached. The presence N_2 and CO_2 in the fuel content is a key factor in this effect. Due to the properties of these species, a portion of the heat released during combustion is absorbed by them, reducing the overall temperature. So, as the content in N_2 and CO_2 increased in the fuels the static temperature across the combustor decreased. Regarding the NOx results, the emissions were observed to decrease across the different fuels. Since NO formation is highly temperature-dependent, the increase in N_2 and CO_2 content led to a reduction in combustion temperature, which lowered the NO emissions. Consequently, NO_2 formation also decreased, as there was less NO available for oxidation in the cooler regions. Once again, the fuel composition played an important role, in this case, on the

mitigation of these emissions. Regarding CO_2 emissions, an increase was observed across the different fuels. Since CO_2 is a common component of biogas, an increase in the CO_2 content of the fuel directly leads to higher CO_2 emission, as it does not directly participate in the combustion reactions. In addition to fuel composition, other factors, such as the fuel mass flow rate, significantly influenced CO_2 emissions. For fuels B_1, B_2, and B_3, which all contain 35% CO_2, the increasing fuel mass flow rate in these configurations resulted in progressively higher CO_2 emissions. Regarding the CO and UHC emissions, the values obtained were virtually zero, but still gave an insight about the behaviour. A decreasing trend was observed across the different fuels analysed. These results highlighted the importance of combustion efficiency, which was highly impacted by the quality of the mixture. The increasing content of N_2 and CO_2 in the fuel delayed the combustion allowing more time for the air and fuel to mix. This extended mixing period resulted in a more homogeneous mixture, leading to a more complete combustion process.

Oxygen can be present in biogas, affecting the formation of pollutant emissions, for that reason, in this study was also included an analysis of the impact of oxygen in the fuel. Starting with the overall temperature across the combustor, the presence of O_2 made the mixture more reactive. This was because part of the oxygen required for combustion was already present in the fuel stream, resulting in a higher combustor temperature and a greater peak temperature. This temperature rise led to an increase in NOx emissions, as this pollutant is highly temperature dependent. Regarding the other pollutants, an interesting pattern was observed. The CO_2 emissions for B_4 and B_5 remained practically similar, indicating that the additional O_2 did not significantly enhance combustion completeness. For CO and UHC emissions, the values were virtually negligible but still provided insight into the process. From B_4 and B_5, the decrease in CO and UHC emissions was minimal, further confirming that the increased O_2 did not notably improve combustion efficiency.

This work led to the conclusion that biogas presents a promising alternative for reducing pollutant emissions, offering significant environmental benefits. While the use of biogas led to an increase in CO_2 emissions and CO levels remained practically unchanged, a remarkable reduction in NOx emissions was observed. This decrease in NOx emissions highlights the potential of biogas as a cleaner fuel option, contributing to improved air quality. Moreover, the production process of biogas is more environmentally friendly compared to that of natural gas, contributing to a lower environmental impact.

Adding O_2 to the biogas resulted in an increase in NOx emissions, while CO_2, CO, and UHC emissions were more influenced by combustion conditions; in this case, all remained largely unchanged. This assessment concludes that adding O_2 to the fuel, does not mitigate the pollutant emissions.

5.1 Future Studies

The research conducted in this work provided valuable insights into the combustion processes of natural gas and biogas and their respective pollutant emissions. This chapter outlines the potential areas and studies of future research that could expand upon the findings presented in this study. Some of those studies are:

- Asses the pollutant emissions of the production process of biogas;
- Study the lifecycle and economic assessments of the biogas implementation in gas turbines;
- Study the optimization of biogas composition;
- Study the influence of the equivalence reason, while burning biogas, in the pollutant emissions.

Bibliography

[1] N. E. Efekemo, N. E. G. Saturday, and N. J. Ofodu, "Gas turbine modification: A review," *International Journal of Frontiers in Engineering and Technology Research*, vol. 6, no. 2, pp. 054–070, May 2024, DOI: 10.53294/ijfetr.2024.6.2.0025

[2] D. Burnes, P. Saxena, and R. Kurz, "Study to adapt industrial gas turbines for significant and viable CO2 emissions reduction," *Journal of Engineering for Gas Turbines and Power*, vol. 145, no. 1, Oct. 2022, DOI: 10.1115/1.4055682

[3] M. Anheden, "Analysis of gas turbine systems for sustainable energy conversion," [PhD's Thesis]. Stochkolm, Sweden: Royal Institute of Technology Stockholm, 2000

[4] E. Cabrera and J. M. De Sousa, "Use of Sustainable Fuels in Aviation—A Review," *Energies*, vol. 15, no. 7, p. 2440, Mar. 2022, DOI: 10.3390/en15072440

[5] United Nations, "Net Zero Coalition | United Nations," *United Nations*. Available at: https://www.un.org/en/climatechange/net-zero-coalition [Accessed: 24 Feb, 2024]

[6] M. J. B. Kabeyi and O. A. Olanrewaju, "Biogas production and applications in the sustainable energy transition," *Journal of Energy*, vol. 2022, pp. 1–43, Jul. 2022, DOI: doi: 10.1155/2022/8750221

[7] M. J. B. Kabeyi and O. A. Olanrewaju, "Technologies for biogas to electricity conversion," *Energy Reports*, vol. 8, pp. 774–786, Dec. 2022, DOI: 10.1016/j.egyr.2022.11.007

[8] H. I. H. Saravanamuttoo, G. F. C. Rogers, H. Cohen, "Gas turbine theory", 4th ed., Harlow: Longman Scientif. Et Techn, 1996

[9] M. Prussi, M. Padella, M. Conton, E. D. Postma, and L. Lonza, "Review of technologies for biomethane production and assessment of Eu transport share in 2030," Journal of Cleaner Production, vol. 222, pp. 565–572, 2019, DOI: DOI: 10.1016/j.jclepro.2019.02.271

[10] A. James and S. Rajagopalan, "Gas turbines: operating conditions, components and material requirements,", Elsevier eBooks, pp. 3–21, 2014, DOI: 10.1533/9780857097552.1.3

[11] Massachusetts Institute of Technology, "3.7 Brayton Cycle," Mit.edu, 2019. Available at: https://web.mit.edu/16.unified/www/SPRING/propulsion/notes/node27.html [Accessed: 26 Feb, 2024]

[12] A. Koopman, “The Gas Turbine Handbook”, National Energy Technology Laboratory and U.S. Department of Energy, 2006

[13] A. H. Lefebvre and D. R. Ballal, “Gas turbine combustion: Alternative Fuels and Emissions”, Third Edition. CRC Press, 2010

[14] M. P. Boyce, “Gas Turbine Engineering Handbook “ , third edition, Oxford, Elsevier, 2006.

[15] S. Sarıkoç, “Fuels of the Diesel-Gasoline Engines and Their Properties,” Diesel and Gasoline Engines, Feb. 2020

[16] R. Chang and J. Overby,” Chemistry”, 13th ed. New York, Ny: Mcgraw-Hill Education, 2019

[17] V. Kvasnicova, “Organic chemistry 1 - Hydrocarbons.”, University of Karlova, [online]. Available at: https://fl.lf3.cuni.cz/studijni/Premedical%20course/Study%20materials/Chemistry/100-Hydrocarbons%20-%20Appendix%20(VK).pdf [Accessed: 5 Mar, 2024]

[18] GE Energy, “Addressing Gas Turbine Fuel Flexibility,” 2011. [Online]. Available at: https://www.gevernova.com/content/dam/gepower-new/global/en_US/downloads/gas-new-site/resources/reference/ger-4601b-addressing-gas-turbine-fuel-flexibility-version-b.pdf [Accessed: 5 Mar, 2024]

[19] M. Lackner, Á. Palotás, and F. Winter, “*Combustion: From Basics to Applications”*. John Wiley & Sons, 2013.

[20] W. A. W. A. Bakar and R. Ali, “Natural gas,” in *Sciyo eBooks*, 2010. Doi: 10.5772/9804

[21] P. Gonzalez and U. Pascual, “Energy use, Human,” in *Elsevier eBooks*, 2024, pp. 484–501. DOI: 10.1016/b978-0-12-822562-2.00369-8.

[22] R. A. Hamdan *et al.*, “Hydrotreating and acidic gas removal for natural gas pretreatment,” in *Elsevier eBooks*, 2024. Doi: 10.1016/b978-0-443-15740-0.00047-1

[23] M. K. Jameel *et al.*, “Biogas: Production, properties, applications, economic and challenges: A review,” *Results in Chemistry*, vol. 7, p. 101549, Jan. 2024, DOI: 10.1016/j.rechem.2024.101549

[24] P. Gupta, C. Kurien, and M. Mittal, “Biogas (a promising bioenergy source): A critical review on the potential of biogas as a sustainable energy source for gaseous fueled spark ignition engines,” *International Journal of Hydrogen Energy*, vol. 48, no. 21, pp. 7747–7769, Mar. 2023, DOI: 10.1016/j.ijhydene.2022.11.195

[25] N. Nwokolo, P. Mukumba, K. Obileke, and M. Enebe, “Waste to Energy: A focus on the impact of substrate type in biogas production,” *Processes*, vol. 8, no. 10, p. 1224, Oct. 2020, Doi: 10.3390/pr8101224

[26] “How does anaerobic digestion work? | US EPA,” *US EPA*, Jan. 20, 2024, Available at: https://www.epa.gov/agstar/how-does-anaerobic-digestion-work [Accessed: 14 Mar, 2024]

[27] “Alternative Fuels Data Center: Renewable natural gas production.” Available at: https://afdc.energy.gov/fuels/natural-gas-renewable [Accessed: 14 Mar, 2024]

[28] Environmental and Energy Study Institute (EESI), “Fact Sheet | Biogas: Converting Waste to Energy | White papers | EESI.” Available at: https://www.eesi.org/papers/view/fact-sheet-biogasconverting-waste-to-energy [Accessed: 14 Mar, 2024]

[29] M. Welch and B. M. Igoe, “Combustion, Fuels and Emissions for Industrial Gas Turbines,” Jan. 01, 2015. DOI: 10.21423/r11m62

[30] A. N. Mustafa, O. M. Ali, and O. R. Alomar, “Effect of heavy fuel combustion in a gas power plant on turbine performance: a review,” *International Journal of Design & Nature and Ecodynamics*, vol. 17, no. 1, pp. 102–111, Feb. 2022, DOI: 10.18280/ijdne.170113

[31] D. A. Carasillo, “Liquid fuels: Types, Properties, and Production”. 2012

[32] “Liquid Fuels: Types, Advantages, and examples,” *Decoding Biosphere*, Aug. 16, 2023. Available at: https://decodingbiosphere.com/2371-2/liquid-fuels-types-advantages-examples/ [Accessed: 15 Mar,2024]

[33] M. Molière, “The Fuel Flexibility of Gas Turbines: A Review and Retrospective outlook,” *Energies*, vol. 16, no. 9, p. 3962, May 2023, DOI: 10.3390/en16093962

[34] S. Thomas, T. A. Nguyen, M. Ahmadi, A. Farmani, and G. Yasin, *Nanosensors for smart manufacturing*. Elsevier, 2021

[35] M. Arbab, H. H. Masjuki, M. Varman, M. A. Kalam, S. Imtenan, and H. Sajjad, “Fuel properties, engine performance and emission characteristic of common biodiesels as a renewable and sustainable source of fuel,” Renewable & Sustainable Energy Reviews, vol. 22, pp. 133–147, Jun. 2013.

[36] “Aviation Fuels Technical Review,” Chevron Products Company, 2004, [Online]. Available at https://www.chevron.com/-

/media/chevron/operations/documents/aviation-tech-review.pdf [Accessed: 12 Mar, 2024]

[37] S. Kuczyński, M. Łaciak, A. Szurlej, and T. Włodek, "Impact of liquefied natural gas composition changes on methane number as a fuel quality requirement," *Energies*, vol. 13, no. 19, p. 5060, Sep. 2020, DOI: 10.3390/en13195060.

[38] G. Palmer, "Mathane number," *Journal of Natural Gas Engineering*, vol. 2, no. 2, pp. 134–142, Dec. 2017, DOI: 10.7569/jnge.2017.692506

[39] *ChemEuropre*. "Wobbe_index," *Chemeuropre*. Available at: https://www.chemeurope.com/en/encyclopedia/Wobbe_index.html [Accessed at: 15 Mar, 2024]

[40] MIT OpenCourseWare "Part 2.C: Introduction to Thermochemistry" [Online]. Available at: https://ocw.mit.edu/courses/16-050-thermal-energy-fall-2002/5f0215e91a0abd3b968b4602a1c4bace_09_part2c.pdf [Accessed: 13 Mar, 2024]

[41] E. H. Smith, "Mechanical engineer's reference book," *Choice Reviews Online*, vol. 32, no. 05, pp. 32–2764, Jan. 1995, DOI: 10.5860/choice.32-2764

[42] N. Marszałek and T. Lis, "The future of sustainable aviation fuels," Combustion Engines, Mar. 2022, DOI: 10.19206/ce-146696

[43] S. Postrzednik, "Combined use of coal mine gases for efficient energy generation," *Archives of Thermodynamics*, vol. 37, no. 4, pp. 37–53, Dec. 2016, DOI: 10.1515/aoter-2016-0026

[44] S. McAllister, J.-Y. Chen, and A. C. Fernandez-Pello, "*Fundamentals of Combustion Processes"*. New York, Springer New York, 2011

[45] M. Bahrami, "Chemical Reactions", Simon Frazer University, [Online]. Available at: https://www.sfu.ca/~mbahrami/ENSC%20461/Notes/Chemical%20Reactions.pdf [Accessed: 2 Apr, 2024]

[46] R. Domingues, "CFD ANALYSIS OF THE COMBUSTION OF HYDROGEN FUEL ON A CFM56-3 COMBUSTOR" [Master's Thesis]. Covilhã, Portugal: University of Beira Interior, 2022

[47] K. K Kuo, "*Principles of combustion"*, Hoboken, New Jersey, John Wiley & Sons, 2005

[48] R. Pavri, G. D. M. Moore, “Gas Turbine Emissions and Control.”,GE Power Systems, [Online]. Available at: https://www.gevernova.com/content/dam/gepower-new/global/en_US/downloads/gas-new-site/resources/reference/ger-4211-gas-turbine-emissions-and-control.pdf [Accessed: 5 Apr, 2024]

[49] C. Martins, M. Ferreira, “CONSIDERAÇÕES SOBRE A FORMAÇÃO DE NOx NA COMBUSTÃO”, VI Congresso de engenharia Mecânica, August, 2010

[50] A. N. Hayhurst and I. M. Vince, “Nitric oxide formation from N2 in flames: The importance of ‘prompt’ NO,” *Progress in Energy and Combustion Science*, vol. 6, no. 1, pp. 35–51, Jan. 1980, DOI: 10.1016/0360-1285(80)90014-3.

[51] C. P. Fenimore, “Formation of nitric oxide in premixed hydrocarbon flames,” *Symposium (International) on Combustion*, vol. 13, no. 1, pp. 373–380, Jan. 1971, doi: 10.1016/s0082-0784(71)80040-1

[52] M. Fischer and X. Jiang, “An investigation of the chemical kinetics of biogas combustion,” *Fuel*, vol. 150, pp. 711–720, Jun. 2015, DOI: 10.1016/j.fuel.2015.01.085

[53] G. Smith et al“GRI-Mech 3.0.”, University of California, Barkeley, Available at: http://combustion.berkeley.edu/gri-mech/version30/text30.html [Accessed: 21 Mar, 2024]

[54] A. Kazakov, M. Frenklach “DRM mechanism”, University of California, Barkeley Available at: http://combustion.berkeley.edu/drm/ [Accessed: 21 Mar, 2024]

[55] C. I. Heghes, “C1-C4 hydrocarbon oxidation mechanism,” 2007. Doi: 10.11588/heidok.00007379

[56] H. Wang and M. Frenklach, “A detailed kinetic modeling study of aromatics formation in laminar premixed acetylene and ethylene flames,” *Combustion and Flame*, vol. 110, no. 1–2, pp. 173–221, Jul. 1997, Doi: 10.1016/s0010-2180(97)00068-0

[57] S. Martinez *et al.*, “An experimental and kinetic modeling study of the ignition delay characteristics of binary blends of ethane/propane and ethylene/propane in multiple shock tubes and rapid compression machines over a wide range of temperature, pressure, equivalence ratio, and dilution,” *Combustion and Flame*, vol. 228, pp. 401–414, Jun. 2021, DOI: 10.1016/j.combustflame.2021.02.009

[58] A. Wresta and A. Saepudin, “Analysis of product and temperature of biogas combustion in various air biogas equivalence ratio and methane content,” *Indonesian Journal of Chemistry*, vol. 18, no. 2, p. 211, May 2018, DOI: 10.22146/ijc.23923

[59] H. Seliger-Ost, P. Kutne, J. Zanger, and M. Aigner, “Experimental investigation of the impact of biogas on a 3 kW micro gas turbine FLOX®-Based combustor,” *Journal of Engineering for Gas Turbines and Power*, vol. 143, no. 8, Mar. 2021, DOI: 10.1115/1.4049927

[60] I. Sivri, H. Yilmaz, O. Cam, and I. Yilmaz, “Combustion and emission characteristics of premixed biogas mixtures: An experimental study,” *International Journal of Hydrogen Energy*, vol. 47, no. 24, pp. 12377–12392, Mar. 2022, DOI: 10.1016/j.ijhydene.2021.08.119

[61] N. Ghenai and N. Janajreh, “Combustion of renewable biogas fuels,” *Journal of Energy and Power Engineering*, vol. 9, no. 10, Oct. 2015, DOI: 10.17265/1934-8975/2015.10.001

[62] X. Chen, W. Zhou, Y. Jia, and J. Tang, “Numerical Analysis of the Combustion in Micro Gas Turbine with Methane/Biogas Fuels,” *Arabian Journal for Science and Engineering*, vol. 46, no. 12, pp. 11897–11907, Jun. 2021, DOI: 10.1007/s13369-021-05731-3

[63] H. K. Versteeg and W. Malalasekera, “*An introduction to computational fluid dynamics : the finite volume method*” 2006.

[64] ANSYS, Inc., “ANSYS Fluent Theory Guide”, Release 2020 R2, July 2020

[65] L. Davidson, “Fluid mechanics, turbulent flow and turbulence modeling”. Mar, 2024

[66] J. Blazek, “*Computational Fluid Dynamics: Principles and Applications” Ed. 3*. 2015

[67] K. Hami, “Turbulence modeling a review for different used methods,” *International Journal of Heat and Technology*, vol. 39, no. 1, pp. 227–234, Feb. 2021, DOI: 10.18280/ijht.390125

[68] J. He, W. Wang, W. Zhao, and D. Wan, “Hybrid turbulence models for flows around a stationary smooth circular cylinder,” *Ocean Engineering*, vol. 262, p. 112312, Oct. 2022, DOI: 10.1016/j.oceaneng.2022.112312

[69] O. A. Marzoukand and E. D. Huckaby, “Simulation of a Swirling Gas-Particle Flow Using Different k-epsilon Models and Particle-Parcel Relationships,” *Engineering Letters*, Jan. 2010

[70] A. R. Norwazan and M. N. M. Jaafar, “Studies of isothermal swirling flows with different RANS models in unconfined burner,” Dec. 01, 2014. DOI: 10.1109/wcst.2014.7030095

[71] J. M. P. Oliveira, “CFD analysis of the combustion of Bio-Derived fuels in the CFM56-3 combustor,” Master's Thesis, Covilhã, Portugal: University of Beira Interior, 2016

[72] “Damkohler number - CFD-Wiki”, Available at: https://www.cfd-online.com/Wiki/Damkohler_number [Accessed: 30 Mar, 2024]

[73] P. Chatterjee, “A computational fluid dynamics investigation of thermoacoustic instabilities in premixed laminar and turbulent combustion systems,” Ph.D. dissertation, Virginia Polytechnic Institute and State University, 2004

[74] A. A. A. Gamil, T. Nikolaidis, I. Lelaj, and P. Laskaridis, “Assessment of numerical radiation models on the heat transfer of an aero-engine combustion chamber,” *Case Studies in Thermal Engineering*, vol. 22, p. 100772, Dec. 2020, DOI: 10.1016/j.csite.2020.100772

[75] S. B. Pope, “PDF methods for turbulent reactive flows,” *Progress in Energy and Combustion Science*, vol. 11, no. 2, pp. 119–192, Jan. 1985, DOI: 10.1016/0360-1285(85)90002-4

[76] M. Hafeez, “Computational Fluid Dynamics modelling of non-premixed Hydrogen Combustion in O2-H2O mixtures using ANSYS Fluent,” Master's Thesis, Lisbon, Portugal: Instituto Superior Técnico, 2022

[77] H. Pitsch and N. Peters, “A consistent flamelet formulation for non-premixed combustion considering differential diffusion effects,” *Combustion and Flame*, vol. 114, no. 1–2, pp. 26–40, Jul. 1998, DOI: 10.1016/s0010-2180(97)00278-2

[78] ANSYS, Inc., “Ansys Fluent Meshing with Watertight Geometry Workflow.” Available at: https://www.ansys.com/training-center/course-catalog/fluids/ansys-fluent-meshing-with-watertight-geometry-workflow [Accessed: 28 Apr, 2024]

[79] ANSYS Inc., “5 Best Practices for Gas Turbine Combustor Meshing,” Mar. 2022. Available at: https://www.ansys.com/blog/5-best-practices-for-gas-turbine-combustor-meshing [Accessed: 28 Apr, 2024]

[80] ANSYS, Inc. “Lecture 7: Mesh Quality & Advanced Topics” Release 15.0 Germany. February 12, 2015

[81] S. Rasi, A. Veijanen, and J. Rintala, “Trace compounds of biogas from different biogas production plants,” *Energy*, vol. 32, no. 8, pp. 1375–1380, Aug. 2007, DOI: 10.1016/j.energy.2006.10.0187

[82] A. Guessab, A. Aris, M. Cheikh, and T. Baki, “Combustion of methane and biogas fuels in gas turbine can-type combustor model,” *Journal of Applied Fluid Mechanics*, vol. 9, no. 7, pp. 2229–2238, Jul. 2016, DOI: 10.18869/acadpub.jafm.68.236.24289.

[83] *US EPA*, “Overview of greenhouse gases | US EPA,” Apr. 11, 2024. Available at: https://www.epa.gov/ghgemissions/overview-greenhouse-gases [Accessed 25 Aug, 2024]

Appendix A – Can Type Combustor Views

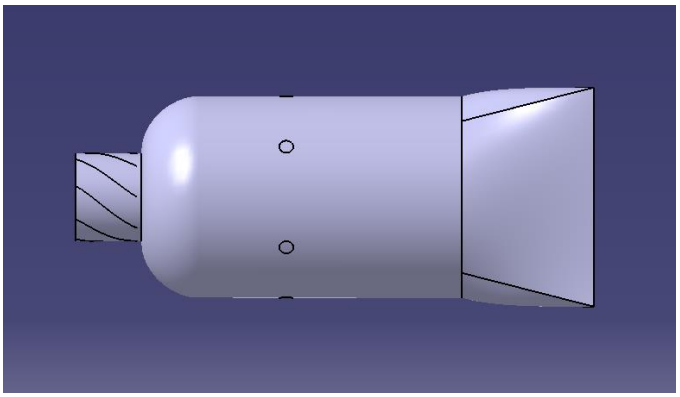

Figure A.1: Side view of the can-type combustor

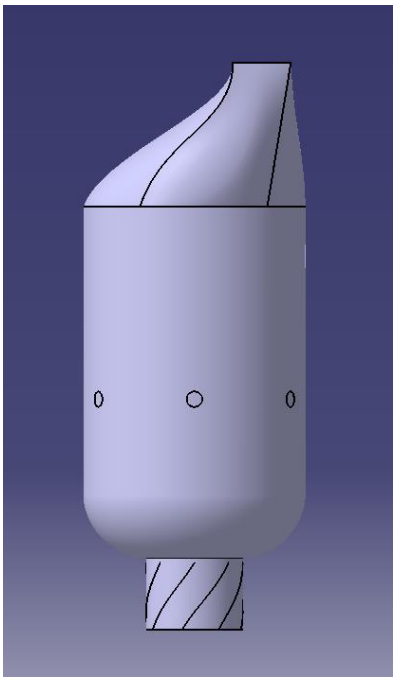

Figure A.2: Top view of the can-type combustor

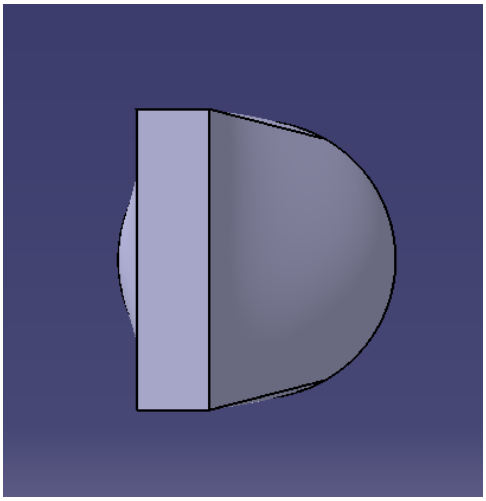

Figure A.3: Rear view of the can-type combustor

Appendix B – Mesh Refinement Parameters

This appendix outlines the process undertaken in this study to generate the meshes used.

In this software, the first step is to choose the Workflow type desired to create the mesh, which in this case, the *Watertight Geometry* was selected. Once the workflow is selected, a series of tasks must be completed. The first task involved importing the geometry of the combustor. To do this, the CAD file is uploaded into the ANSYS *Fluent Meshing* software. Before uploading, the CAD file must be converted to a compatible file format, which to this purpose, the IGS file format was used. The next task was when it was possible to make the refinement or coarsening of the surface mesh, through the option Add Local Sizing. In this option, it was selected the mesh size parameters for specific regions of the geometry, such as the walls, the outlet, the primary air inlet, the secondary air inlet and the fuel inlet. For the final meshes created, the parameters used in these features are presented in Table B.1 and Table B.2.

Table B.1: Mesh refinement parameters used in the intermediate and fine mesh through the "Add Local Sizing" option with the “Size Functions” of “Curvature”

Mesh	Parameters	Size Control Type	Local Min Size	Max Size	Growth Rate	Curvature Normal Angle
Intermediate	Secondary Air Inlet	Curvature	0.35	0.9	1.2	18
	Fuel Inlet	Curvature	0.35	0.9	1.2	18
	Wall	Curvature	0.9	6	1.2	18
Fine	Secondary Air Inlet	Curvature	0.25	0.8	1.2	18
	Fuel Inlet	Curvature	0.25	0.8	1.2	18
	Wall	Curvature	0.8	5	1.2	18

Table B.2: Mesh refinement parameters used in the intermediate and fine mesh through the "Add Local Sizing" option with the “Size Functions” of “Proximity”

Mesh	Parameters	Size Control Type	Local Min Size	Max Size	Growth Rate	Cell per Gap
Intermediate	Primary Air Inlet	Proximity	0.9	3	1.2	1
	Outlet	Proximity	0.9	4	1.2	1
Fine	Primary Air Inlet	Proximity	0.8	2	1.2	1
	Outlet	Proximity	0.8	3	1.2	1

After configuring all the local sizing settings, the surface mesh was finally generated. The following task consisted on describing the geometry (as solid, fluid, or both) and defining the boundary condition type for each of the geometry features. In this case, the geometry was described as consisted only of fluid regions with no voids and the assigned boundary conditions are presented in Table B.3.

Table B.3: Boundary Labels and respective Boundary Types used in the mesh generation process

Boundary Label	Boundary Type
Primary Air Inlet	Velocity Inlet
Secondary Air Inlet	Velocity Inlet
Fuel Inlet	Mass flow Inlet
Outlet	Pressure Outlet
Swirler Vanes	Wall
Wall	Wall

With the surface mesh generated and the geometry defined, the final task was to configure the parameters for the volume mesh generation. Firstly, was defined the setting Add Boundary layer where boundary layers will be added to various portions of the model. It was defined 3 layers with the first aspect ratio of 1.5 and a growth ratio of 0.4. These settings were used in order to fulfil the Y^+ requirement for fully turbulent flow. Lastly, it was specified and adjust various global properties of the volume itself to ensure a comprehensive mesh for the entire flow volume. The parameters used are presented in Table B.4.

Table B.4: Parameters used for volume mesh generation used in the coarse, intermediate and finer mesh

Mesh	Cell Geometry	Buffer Layers	Peel Layers	Min. Cell Length [mm]	Max. Cell Length [mm]
Coarser	Poly Hexacore	2	1	0.41	6.56
Intermediate	Poly Hexacore	2	1	0.3	4.8
Finer	Poly Hexacore	2	1	0.235	3.76

Additionally, it was also used an Improve Volume Mesh command, in order to assure that the minimum orthogonal quality of the cells was 0.25.

Appendix C – Mesh Quality Analysis and Independence Test

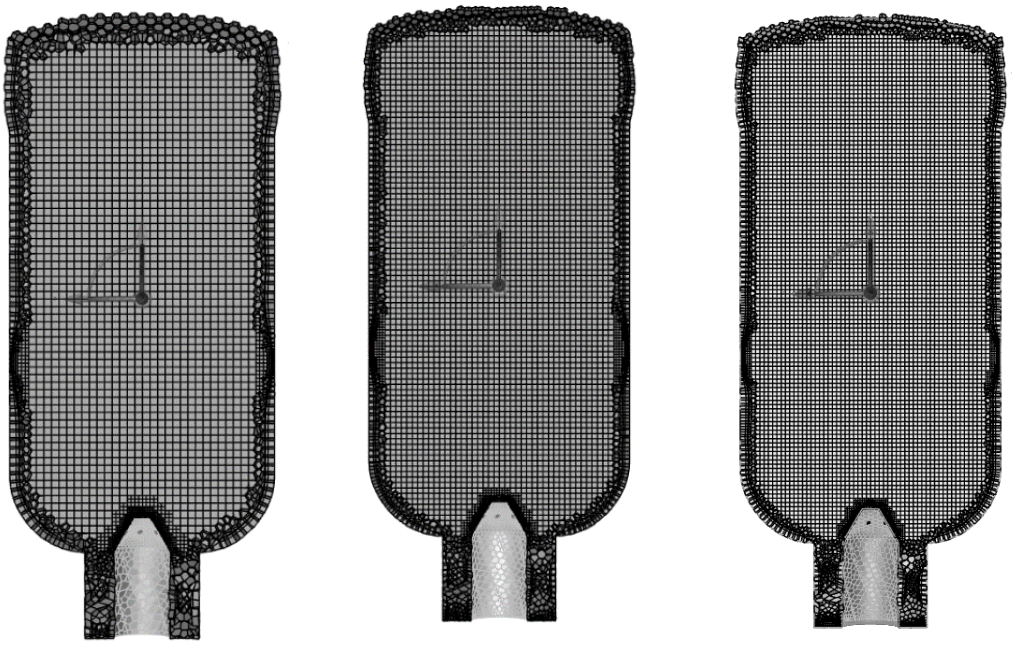

Figure C.1: Structure of the meshes in the view plane XZ Y=0, in the left, the coarse mesh; in the middle, the intermediate mesh (used in this work); and in the right, the refined mesh, obtained with the Fluent Meshing software

```
Mesh Quality:

Minimum Orthogonal Quality =  2.50036e-01 cell 11725 on zone 409 (ID: 20462 on partition: 0) at location
(-8.80828e-02,  1.90601e-02, -4.76066e-05)


Maximum Aspect Ratio =  3.35715e+01 cell 35715 on zone 409 (ID: 60761 on partition: 0) at location (-5.60741e-02,
-2.78240e-02, -1.99449e-02)

 Domain Extents:
   x-coordinate: min (m) = -5.900000e-01, max (m) = 0.000000e+00
   y-coordinate: min (m) = -1.149797e-01, max (m) = 1.149682e-01
   z-coordinate: min (m) = -1.251368e-01, max (m) = 1.251290e-01
 Volume statistics:
   minimum volume (m3): 7.678826e-12
   maximum volume (m3): 2.425390e-07
     total volume (m3): 1.926954e-02
 Face area statistics:
   minimum face area (m2): 8.349550e-10
   maximum face area (m2): 4.922292e-05
 Checking mesh.....................................
Done.
```

Figure C.2: Command window of ANSYS Fluent with the reports of Mesh Quality and Mesh Check

Appendix D – Solution Methods and Solution Controls

Table D.1: Schemes selected in Solution Methods Task Page in the simulations using the First and Second Order Approach

Parameters	First Order Approach	Second Order Approach
Pressure-Velocity Coupling	SIMPLE	SIMPLE
Gradient	Green-Gauss Node Based	Green-Gauss Node Based
Pressure	PRESTO!	PRESTO!
Momentum	First Order Upwind	Second Order Upwind
Turbulent Kinetic Energy	First Order Upwind	Second Order Upwind
Turbulent Dissipation Rate	First Order Upwind	Second Order Upwind
Energy	First Order Upwind	Second Order Upwind
Mean Mixture Fraction	First Order Upwind	Second Order Upwind
Mixture Fraction Variance	First Order Upwind	Second Order Upwind

Table D.2: Under Relaxation Factors used in the Solution Control parameters for the First and Second Order Approach

Parameters	First Order Approach	Second Order Approach
Pressure	0.3	0.2
Density	1	0.8
Body Forces	1	1
Momentum	0.7	0.3
Turbulent Kinetic Energy	0.8	0.6
Turbulent Dissipation Rate	0.8	0.6
Turbulent Viscosity	1	1
Energy	1	1
Temperature	1	1
P1	1	1
Mean Mixture Fraction	1	1
Mixture Fraction Variance	0.9	0.9

Appendix E – Velocity Streamline Contours

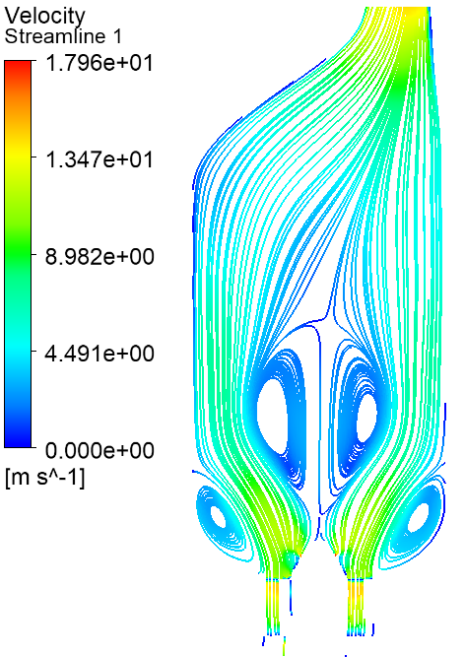

Figure E.1: Velocity streamline contour, in the view plane XY Z=0, while burning 50% Natural Gas + 50% Biogas 1

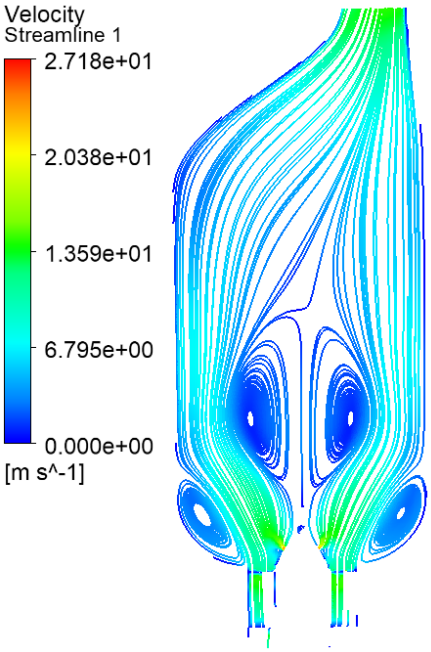

Figure E.2: Velocity streamline contour, in the view plane XY Z=0, while burning Biogas 2

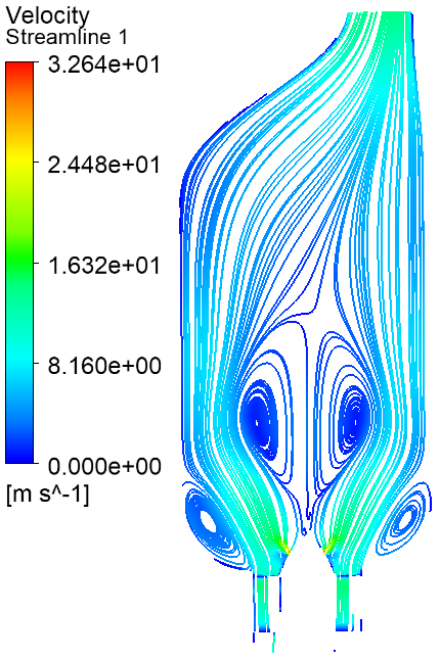

Figure E.3: Velocity streamline contour, in the view plane XY Z=0, while burning Biogas 3

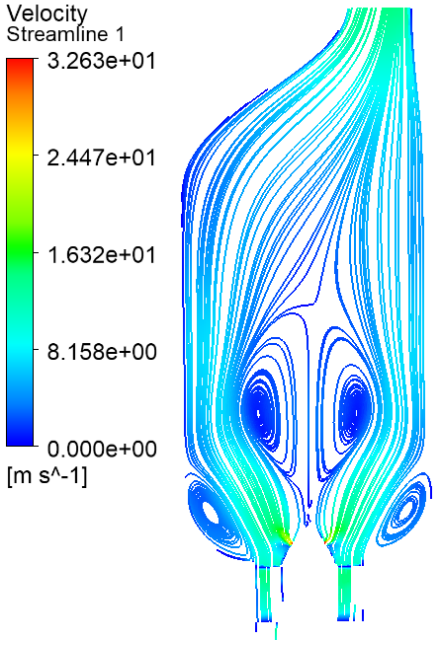

Figure E.4: Velocity streamline contour, in the view plane XY Z=0, while burning Biogas 4

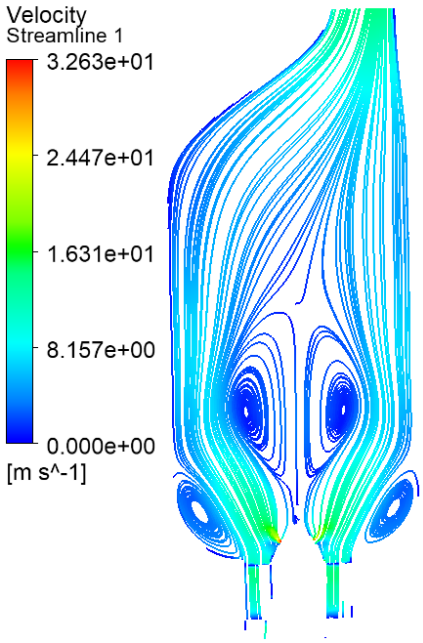

Figure E.5: Velocity streamline contour, in the view plane XY Z=0, while burning Biogas 5

Appendix F – Static Temperature Contours

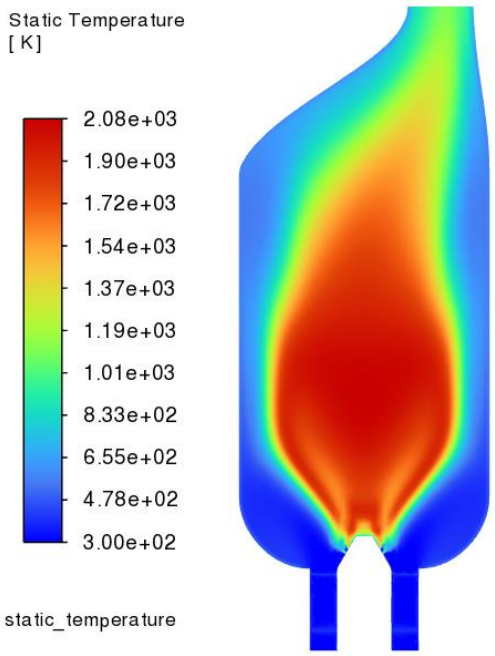

Figure F.1: Contour of static temperature, in the view plane XY Z=0, while burning 50% Natural Gas and 50% Biogas 1

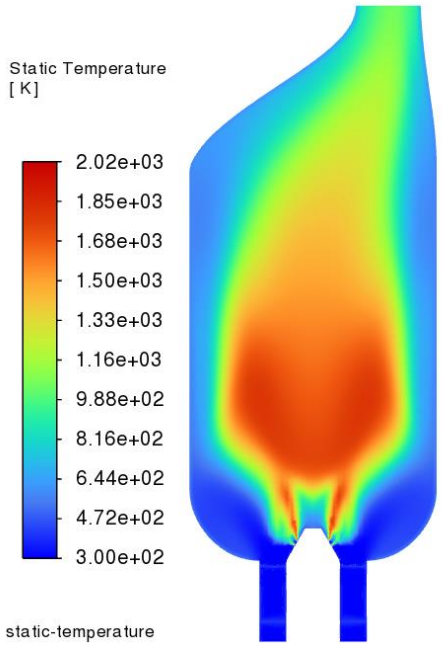

Figure F.2: Contour of static temperature, in the view plane XY Z=0, while burning Biogas 4

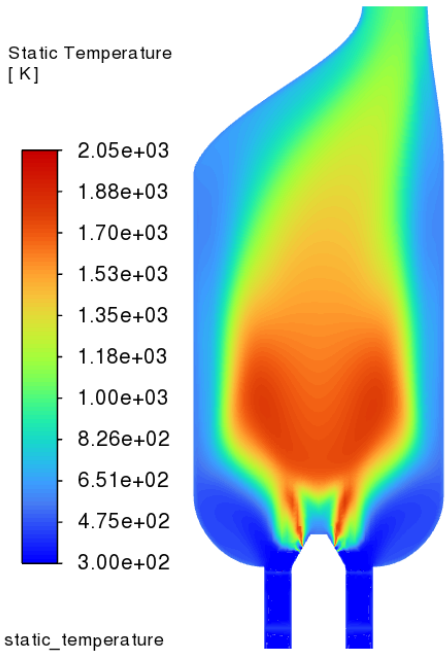

Figure F.3: Contour of static temperature, in the view plane XY Z=0, while burning Biogas 5

Appendix G – Nitric Oxide Contours

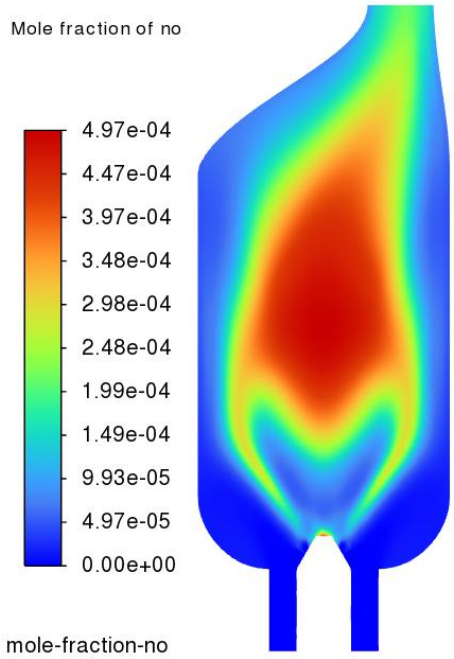

Figure G.1: Contour of NO mole fraction, in the view plane XY Z=0, while burning Natural Gas

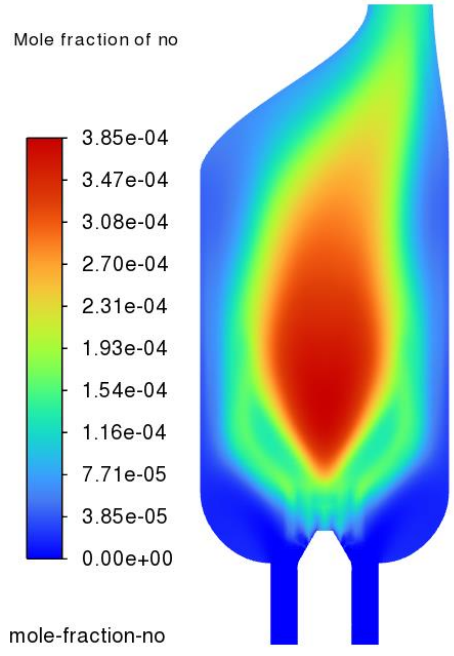

Figure G.2: Contour of NO mole fraction, in the view plane XY Z=0, while burning Biogas 1

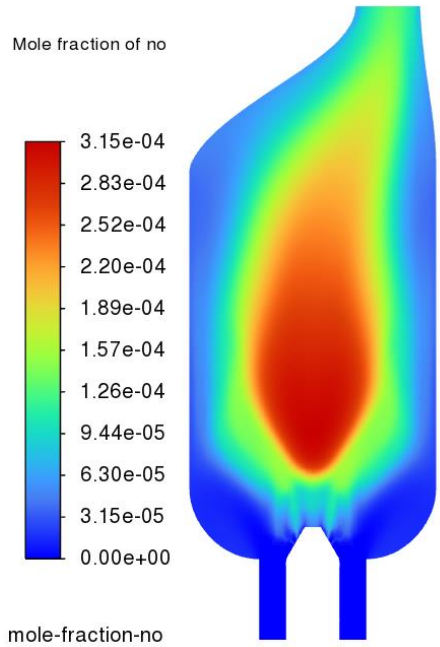

Figure G.3: Contour of NO mole fraction, in the view plane XY Z=0, while burning Biogas 2

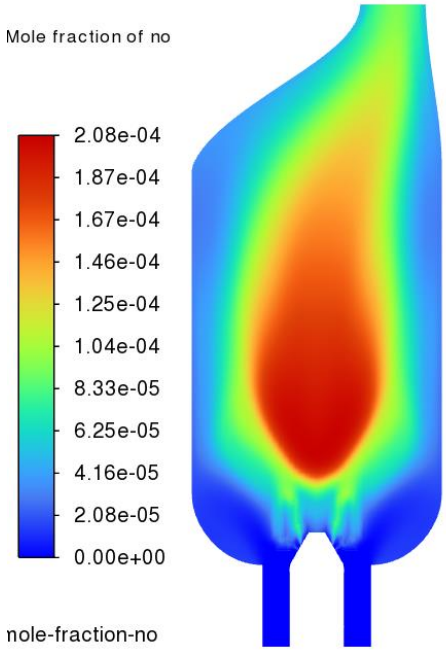

Figure G.4: Contour of NO mole fraction, in the view plane XY Z=0, while burning Biogas 3

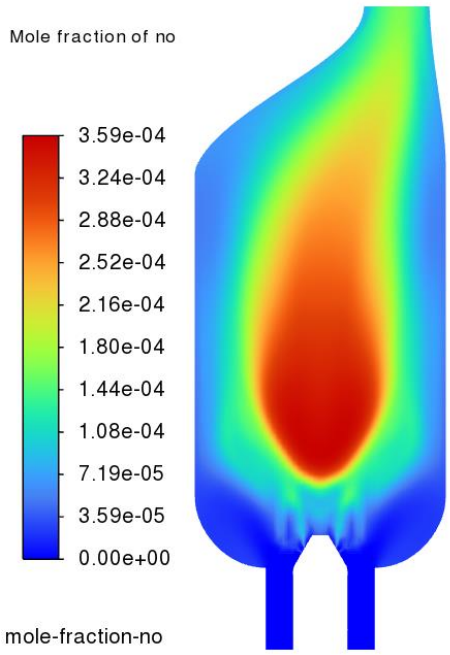

Figure G.5: Contour of NO mole fraction, in the view plane XY Z=0, while burning Biogas 4

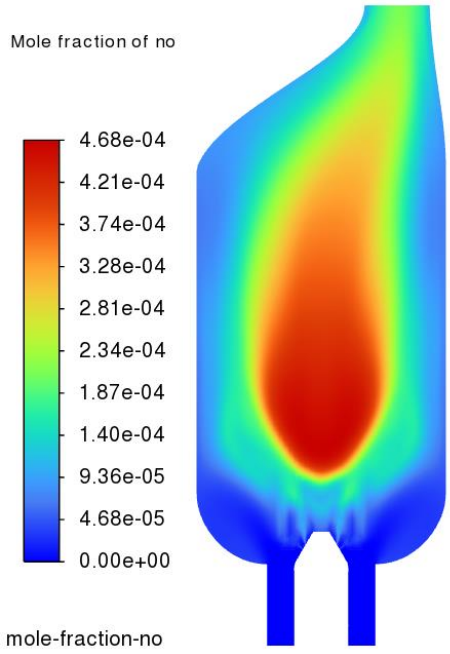

Figure G.6: Contour of NO mole fraction, in the view plane XY Z=0, while burning Biogas 5

Appendix H – Nitrogen Dioxide Contours

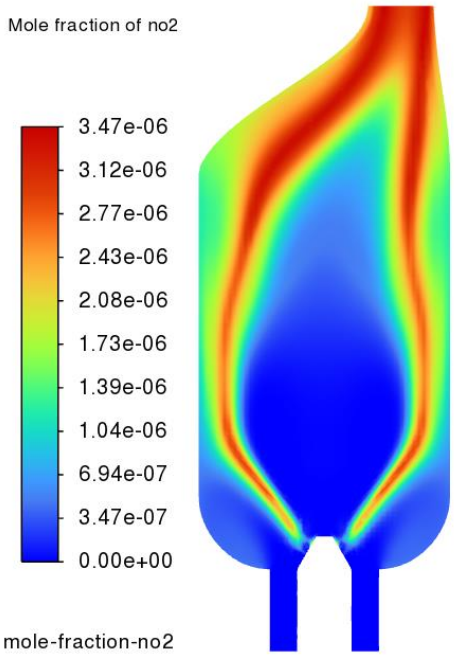

Figure H.1: Contour of NO_2 mole fraction, in the view plane XY Z=0, while burning Natural Gas

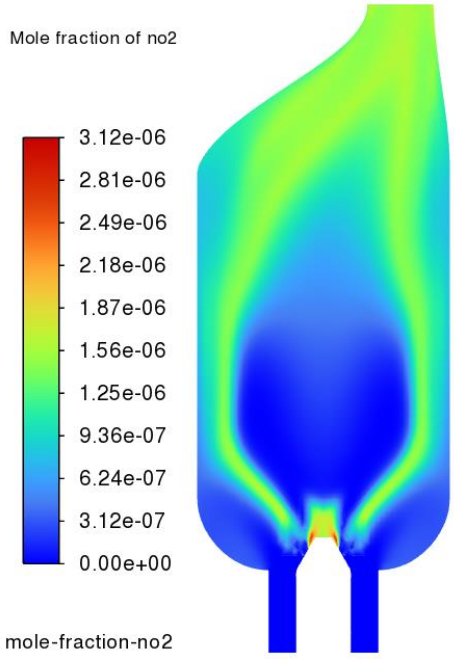

Figure H.2: Contour of NO_2 mole fraction, in the view plane XY Z=0, while burning Biogas 1

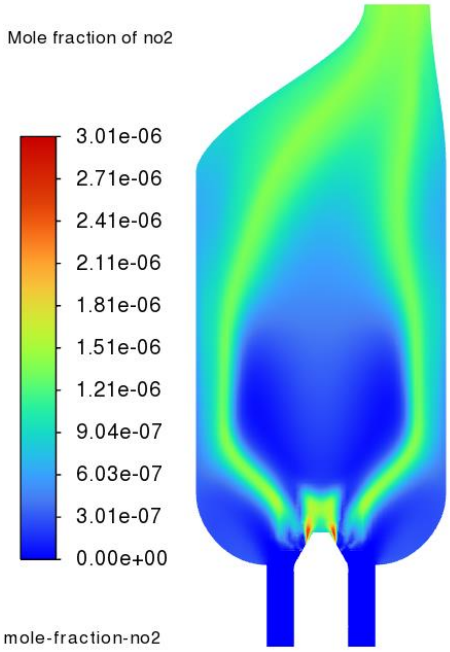

Figure H.3: Contour of NO_2 mole fraction, in the view plane XY Z=0, while burning Biogas 2

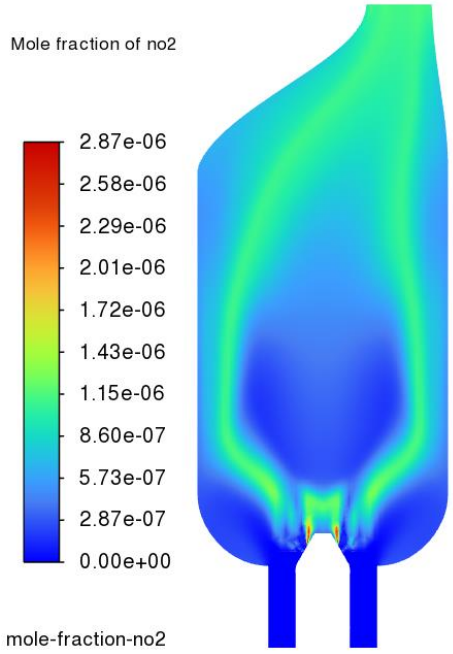

Figure H.4: Contour of NO_2 mole fraction, in the view plane XY Z=0, while burning Biogas 3

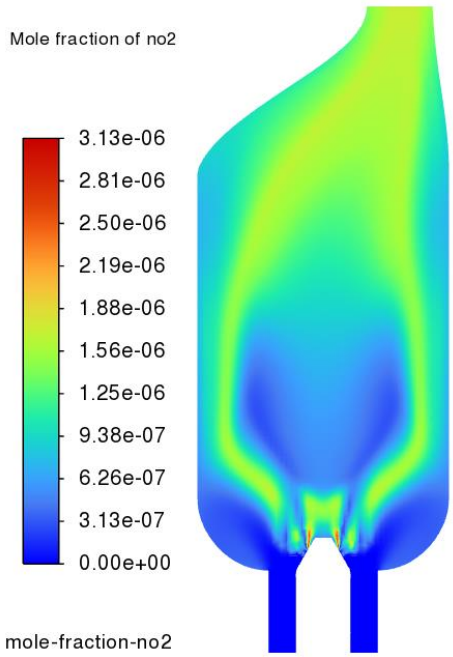

Figure H.5: Contour of NO_2 mole fraction, in the view plane XY Z=0, while burning Biogas 4

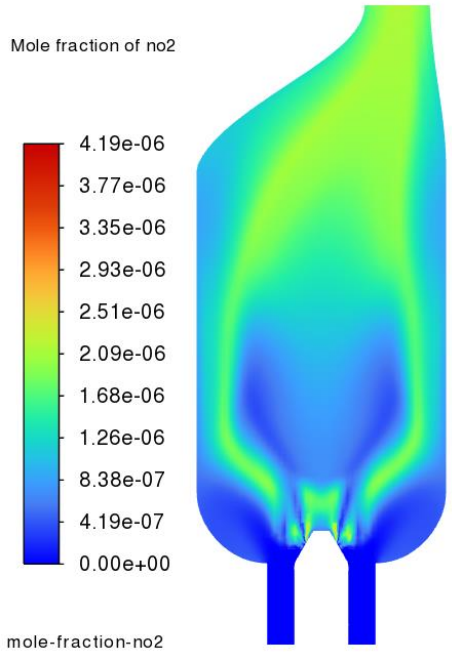

Figure H.6: Contour of NO_2 mole fraction, in the view plane XY Z=0, while burning Biogas 5